NUREG/CR-3805
Vol. 2

Engineering Characterization of Ground Motion

Task II: Effects of Ground Motion Characteristics on Structural Response Considering Localized Structural Nonlinearities and Soil-Structure Interaction Effects

Prepared by R. P. Kennedy, R. H. Kincaid, S. A. Short/SMAI

Structural Mechanics Associates, Inc.

Woodward-Clyde Consultants

Prepared for
U.S. Nuclear Regulatory Commission

GPO Printed copy price: $5.50

DISCLAIMER

NUREG/CR--3805-Vol.2

TI85 901169

Engineering Characterization of Ground Motion

Task II: Effects of Ground Motion Characteristics on Structural Response Considering Localized Structural Nonlinearities and Soil-Structure Interaction Effects

Manuscript Completed: December 1984
Date Published: March 1985

Prepared by
R. P. Kennedy, R. H. Kincaid, S. A. Short, Structural Mechanics Associates, Inc.

Structural Mechanics Associates, Inc.
Newport Beach, CA 92660

Woodward-Clyde Consultants
Walnut Creek, CA 94596

Prepared for
Division of Engineering Technology
Office of Nuclear Regulatory Research
U.S. Nuclear Regulatory Commission
Washington, D.C. 20555
NRC FIN B6680

GPO Printed copy price $5.50

FOREWORD

This report presents the results of part of a two-task study on the engineering characterization of earthquake ground motion for nuclear power plant design. The overall objective of this research program sponsored by the U.S. Nuclear Regulatory Commission (USNRC) is to develop recommendations for methods for selecting design response spectra or acceleration time histories to be used to characterize motion at the foundation level of nuclear power plants.

Task I of the study, which is presented in Vol. 1 of NUREG/CR-3805, developed a basis for selecting design response spectra taking into account the characteristics of free-field ground motion found to be significant in causing structural damage. Task II incorporates additional considerations of effects of spatial variations of ground motions and soil-structure interaction on foundation motions and structural response. The results of Task II are presented in Vols. 2 through 5 of NUREG/CR-3805 as, follows: Vol. 2, effects of ground motion characteristics on structural response considering localized structural nonlinearities and soil-structure interaction effects; Vol. 3, empirical data on spatial variations of earthquake ground motions; Vol. 4, soil-structure interaction effects on structural response; and Vol. 5, summary of conclusions and recommendations based on Tasks I and II studies. This report presents the results of the Vol. 2 studies.

This study is being conducted under Contract No. NRC 04-80-192 with the USNRC. Woodward-Clyde Consultants (WCC) is the prime contractor for the project. The studies described in this report have been carried out primarily by Structural Mechanics Associates (SMA) as a subcontractor to WCC.

Technical review of draft versions of this report was provided by I. M. Idriss, M. S. Power, and C.-Y. Chang of WCC; by Project Consultants, W. J. Hall of the University of Illinois, Champaign, J. E. Luco of the University of California, San Diego, J. M. Roesset of the University of Texas, Austin, and N. C. Tsai of NCT Engineering, Inc. Lafayette, California; and by J. F. Costello, technical representative of the USNRC for this research project.

TABLE OF CONTENTS

TABLE OF CONTENTS (Continued)

1. INTRODUCTION

This report presents the results obtained during Task II of an investigative study with the objective of providing guidance and the development of procedures for the characterization of earthquake ground motion used for design of nuclear power plant structures. The overall study effort was divided into two separate tasks:

I: The development of a basis for selecting design response spectra based on free-field motion.

II: The development of recommendations for methods for selecting design response spectra and time histories to be used as input motions at the foundation level.

Reference 1 presents the results of all work conducted for Task I. A brief review of Task I objectives and summary of all important conclusions is presented in Section 1.2. Task II results presented in this report extend Task I findings to multi-degree-of-freedom systems with localized nonlinearities. Guidance is provided for determining the relative importance of factors such as structural nonlinearities, depth of embedment, wave scattering, and soil-structure interaction on overall system response for a typical reactor building excited by selected earthquake ground motions having significantly different engineering characterizations.

1.1 PURPOSE AND SCOPE OF WORK

Ground motion input for the seismic evaluation and design of nuclear power plants is generally defined in terms of a design response spectrum for which the structure is expected to remain elastic. The design response spectrum is generally a broadbanded spectrum with broad frequency content. It expresses the peak linear response of a whole

series of single-degree-of-freedom oscillators at a specified damping level. Either site-independent or site-dependent spectra are specified. A site-independent spectrum such as the U.S. Nuclear Regulatory Guide 1.60 spectrum uses a broad standard spectrum shape while a site dependent spectrum may be less broadbanded as it depends at least in part on particular local site conditions.

Task I results demonstrated that both the elastic and inelastic response of stiff structures to free-field ground motion can be adequately approximated by the U.S. Nuclear Regulatory Guide 1.60 response spectra anchored to an "effective" peak acceleration for earthquake ground motion of relatively long duration. However, actual plant site conditions often are significantly different from free-field assumptions and use of design spectra based on free-field motion may be inappropriate. For example, variations in the site soil shear moduli may cause significant impedance mismatches resulting in reflection of radiation energy dissipated by the structure. In addition, kinematic interaction of the foundation with the surrounding soil for a deeply embedded structure results in wave scattering of the ground motion. For these reasons, a consistent approach to the development of foundation level input design motion should consider the importance of effects such as: kinematic and inertial interaction of the structure and soil, structure embedment, soil layering and high strain nonlinearity, earthquake duration and frequency content, and structural nonlinearities on overall response.

Task II evaluates the seismic response of a typical PWR reactor building designed according to common practice for low to moderate seismic risk areas subjected to ground motion 2.5 times larger than the design ground motion. Previous studies presented in References 2 and 3 demonstrated that at this ground motion level significant inelastic behavior of the PWR internal structure would be expected. Both linear and nonlinear analyses of the PWR reactor building are conducted for fixed base

conditions. Additional analyses are also conducted considering the effects of soil-structure interaction on PWR behavior for both stiff and intermediate soil sites. By comparing the results of these analyses, the relative importance of the soil-structure interaction considerations presented above on stuctural response may be determined.

For both the fixed base and soil-structure interaction analyses, the PWR dynamic model is excited by four different ground motions with significantly different engineering characterizations. Two of the ground motions correspond to relatively long duration earthquake records which are adequately represented by a broadbanded design response spectrum such as the U.S. Regulatory Guide 1.60. The remaining two earthquake records correspond to a nearby moderate magnitude event. Earthquakes of this type can have high peak acceleration values within a limited frequency band but are of short duration with limited energy content. It has been observed that although near field, moderate magnitude earthquakes generate very large accelerations, the damage is much less than would have occurred had these accelerations been generated by a large magnitude earthquake from a more distant source. Comparisons of results from these four different ground motions gives insight into the effect of earthquake duration and frequency content on the damage capability of the ground motion.

The final phase of this study involved determining the applicabilities of Task I methodology to Task II work. Procedures are developed for predicting the nonlinear response of multi-degree-of-freedom systems based on the engineering characteristics of the input ground motion. Predicted nonlinear responses determined from equivalent elastic systems are compared to actual nonlinear results in order to demonstrate the Task I methodology provides an adequate engineering characterization of ground motion for multi-degree-of-freedom systems with localized nonlinearities.

1.2 Summary of Task I

The objective of Task I was to develop recommendations for choosing translational design response spectra or time histories based on free-field motion which consider the response and performance of nuclear power plant structures. Many studies have concluded that neither instrumental peak acceleration nor elastic response spectra are good measures of potential seismic damage. It has been noted, particularly in connection with near-source motions due to low-to-moderate magnitude earthquakes, that structures have performed much better than would be predicted considering the instrumental peak acceleration to which the structures were subjected.

The problem with a simple characterization of earthquake ground motion based on instrumental peak acceleration is twofold. First, a limited number of high frequency spikes of high acceleration but of very short duration have little effect on the elastic response spectra within the frequency range of primary interest for nuclear plants of 1.8 to 10 Hz. This problem can be corrected by anchoring the design response spectra to a design ground acceleration value defined as the "effective peak acceleration" which considers the duration of strong shaking, frequency content, and the energy content of the earthquake. However, the second problem is that an elastic response spectrum anchored to a design acceleration value does not provide a good measure of damage to structures. Elastic response spectra describe elastic response while structure damage is related to the number of strong nonlinear cycles of response a structure experiences. One of the primary objectives of Task I was to develop a method for accurately predicting inelastic structural response for a given level of damage as measured by displacement ductility, μ.

Ground motion characteristics were studied by conducting seismic response analysis for a single-degree-of-freedom (SDOF) model representing degrading stiffness structures such as those found in nuclear power plants. The SDOF shear wall models were used to conduct both elastic and

inelastic analyses for 12 different earthquake motions. Ductility factors of 1.0, 1.9 and 4.3 were studied which represented elastic behavior, low levels of structural damage and the onset of significant structural damage, respectively. The study concentrated on stiff structures considered representative of nuclear plant construction (i.e., 1.8 to 10 Hz) considering models at 2.1, 3.2, 5.3 and 8.5 Hz.

1.2.1 Engineering Characterization of Ground Motion

Study results demonstrated both the elastic and inelastic response of stiff structures can be adequately approximated by the U.S. NRC Regulatory Guide 1.60 response spectra anchored to an "effective" peak acceleration for earthquake ground motion of relatively long duration. In the case of inelastic response, the regulatory guide spectrum must be converted to an inelastic spectrum. The definition of "effective" peak acceleration which resulted in the closest agreement with actual earthquake response was:

$$A_{DE} = \left(\sqrt{2\ell n\ (2.8T_D'\Omega')}\right) a_{rms} \qquad (1\text{-}1)$$

where a_{rms} is the rms acceleration. The best correlation was achieved by defining strong motion duration, T_D', as the time associated with the first zero crossing of the accelerogram following the maximum acceleration or the time associated with 75% of the total cumulative energy, whichever is greater, minus the time associated with 5% of the total cumulative energy. The central or mean frequency, Ω', is defined in terms of the power spectral density function. The breadth of the record frequency content is defined by the frequency range from f_{10} to f_{90} where 10 percent and 90 percent of the cumulative power lies at frequencies below f_{10} and f_{90}, respectively.

For earthquake records examined which had a local magnitude, M_L of 6.4 or greater, strong duration T_D' of 3.4 seconds or greater and frequency content breadth f_{10} to f_{90} of at least 1.2 to 5.5 Hz,

the Regulatory Guide 1.60 spectrum provided an adequate engineering characterization when anchored to A_{DE}. For earthquakes with M_L of 5.7 or less and T'_D of 3.0 seconds or less the Regulatory Guide 1.60 spectrum did not adequately represent the actual elastic or inelastic structural response. Based on a limited number of records, it appears that earthquakes with M_L less than 6.0 do not have sufficient energy content to be capable of producing high acceleration, long duration and broad frequency content spectra. For small earthquakes, a narrowbanded design response spectrum obtained by averaging only records with similar central frequencies and frequency bands seems more realistic.

1.2.2 Prediction of Inelastic Response Spectra

Inelastic analyses of single-degree-of-freedom shear wall type models of several elastic frequencies were performed for the 12 ground motion records considered. The model was designed to be at the onset of yielding for the actual ground motion input and this input was scaled by a factor F_μ such that various ductility levels were achieved. In this manner, the required factors F_μ to reach ductility levels, μ, of 1.9 and 4.3 were determined for each earthquake ground motion record. The input scale factor F_μ is equal to the inelastic spectral deamplification factor by which elastic spectra must be divided to obtain inelastic spectral based accelerations.

Analysis results demonstrated inelastic reponse spectra could be accurately predicted by either of two methods from the elastic response spectrum and an approximate knowledge of the duration of strong shaking, T'_D. By the point estimate approach, the inelastic spectral deamplification factor, F_μ, is given by:

$$F_\mu = \mu(f'_e/f)^2 \left\{ \frac{S_a(f,\beta)}{S_a(f'_e,\beta'_e)} \right\} \qquad (1\text{-}2)$$

where f and β are the elastic frequency and damping and f_e' and β_e' are the effective linear frequency and damping which account for frequency lowering and damping increase during inelastic response. The point estimate approach which used single values of the effective frequency f_e', and damping β_e' can be improved slightly by using a spectral averaging approach based upon average spectral acceleration and damping over the region to the soft side of the elastic frequency. The additional effort required for the spectral averaging approach was not warranted for the small level of improvement obtained over the point estimate approach.

The recommended approach has been compared to estimated F_μ values based on the Sozen and Iwan methods for predicting effective frequency and damping and from the Newmark and Riddell methods for directly estimating F_μ. It is concluded that either the point estimate or spectral averaging approach provide significantly more accurate estimates for F_μ than do other commonly used approaches for the shear wall type resistance functions considered in this study.

1.3 REPORT OUTLINE

The analytical approach used in this study is presented in Chapter 2. The typical PWR reactor building evaluated in Task II has localized nonlinearities represented by the degrading stiffness, degrading strength, shear wall model developed in Task I. Analytical models are developed appropriate for both fixed base and soil-structure interaction analyses. The four earthquake ground motions used in the evaluation are presented and discussed.

Fixed base analysis results for the PWR structure excited by the free-field ground motion are presented in Chapter 3. Linear and nonlinear time history analysis results are compared to determine the effects of inelastic energy absorption on earthquake damage capability.

Chapter 4 examines the effects of soil-structure interaction on PWR response. Using the results of linear and nonlinear analyses, conclusions are developed concerning the relative importance of factors such as kinematic and inertial interaction between the structure and soil, structure embedment, earthquake duration and frequency content, and structural nonlinearities on overall building response.

The applicability of Task I methodology to Task II is discussed in Chapter 5. A procedure for predicting the nonlinear response of multi-degree-of-freedom structures with localized nonlinearities based on the engineering characteristics of the ground motion is presented. Predicted results based on an equivalent elastic model with reduced frequency and higher effective damping are compared to actual nonlinear time history results to demonstrate the Task I methodology provides an adequate engineering characterization of ground motion for complex structures with localized nonlinearities.

Lastly, important conclusions from the analytical studies are summarized in Chapter 6.

2. ANALYTICAL APPROACH

2.1 CHARACTERIZATION OF STRUCTURAL DAMAGE

This study concentrates on predicting nonlinear response of a typical PWR structure with localized stiffness degrading shear walls and minor bond slip nonlinearities with fundamental frequencies in the amplified spectral acceleration region from 1.8 to 10 Hz. Both fixed base and soil-structure interaction analyses of the PWR structure are conducted. The structure and fundamental frequencies studied are considered representative of conditions encountered at nuclear power plants.

A representative shear force versus deformation diagram for shear walls undergoing multiple cycles of deformation is shown in Figure 2-1. The structural element retains its initial stiffness and strength characteristics up to the first nonlinear cycle. After the first nonlinear cycle, the structure loses stiffness and strength. Thus, each subsequent nonlinear cycle ratchets the structure to greater total nonlinear deformations. A short duration ground motion is likely to result in only one nonlinear cycle. With a long duration record, multiple nonlinear cycles occur and each subsequent cycle results in greater deformation. Thus, one effect of a longer duration ground motion is to result in greater total deformation than occurs from a short duration ground motion for a stiffness and strength degrading structure. The force deformation diagram shown in Figure 2-1 also indicates significant energy absorption capacity in the large hysteretic loops. This capacity is very significant when considering limited energy loadings such as earthquakes.

Task I used displacement ductility as a measure of damage for degrading stiffness and strength shear wall structures. Displacement ductility is defined as the ratio of the maximum deformation to yield deformation. The displacement ductility also partially describes cumulative damage because each nonlinear cycle results in increased deformation

or displacement ductility over the previous nonlinear cycle as shown by Figure 2-1. Thus, the maximum displacement ductility reached provides one possible measure of the cumulative damage up to that point. A study of multiple cycle force-deformation diagrams such as the one presented in Figure 2-1 tends to indicate that strength degradation is minor until a certain displacement ductility is reached. Beyond the displacement ductility, strength degradation increases rapidly with additional nonlinear cycles. This displacement ductility at which strength degradation tends to increase rapidly with subsequent cycles can be considered to represent the onset of significant structural damage. Thus, if the onset of significant structural damage is considered to represent the limit of acceptable structural performance, the displacement ductility probably represents a good descriptor of permissible damage. Collapse would generally require additional nonlinear cycles resulting in substantial strength degradation after the permissible displacement ductility is reached.

The use of permissible displacement ductility as the descriptor of structural performance introduces some conservative bias to the study for short duration records. A short duration ground motion could result in the permissible displacement ductility being reached without the ground motion time history having sufficient remaining strong motion duration to lead to the rapid strength degradation from subsequent nonlinear cycles necessary for collapse. On the other hand, for a long duration record, reaching the permissible displacement ductility would indicate the structure was at the onset of collapse from rapid strength degradation during subsequent nonlinear cycles.

For a multi-degree-of-freedom structure, the displacement ductility may be defined in terms of either a system ductility factor or a story drift ductility factor. The system ductility factor accounts for the ratio of the total inelastic energy absorption capacity spread

throughout the structure to the total elastic energy absorption capability of the structure. The story drift ductility factor is the ratio of maximum lateral relative drift to the elastic relative drift at yield for any given story. The system ductility factor and story drift ductility factors are only identical if the inelastic energy absorption is equally spread throughout the structure (i.e., if the story drift ductility factors are the same for all stories). Otherwise, the system ductility factor underestimates the maximum story drift ductility factor.

In this study, structure damage is predicted on shear story drift ductility since this factor is directly correlatible to the Task I results. A schematic representation of the shear story drift factor, μ_S, is presented in Figure 2-2 and is defined as:

$$\mu_S = \frac{\delta_S}{\delta_{Y_S}} \tag{2-1}$$

where δ_{Y_S} is the inter-story shear deformation at the onset of shear yielding for the story and δ_S is the portion of the total inter-story inelastic deformation due to shear only. In this report, shear story drift ductility is of primary interest and is used interchangeably with story drift ductility.

Story drift ductility may also be defined in terms of a total story drift ductility factor, μ_T, dependent on both shear and flexural deformations as shown in Figure 2-2. The total story drift ductility factor, μ_T, is defined as:

$$\mu_T = \frac{\delta_T}{\delta_{Y_T}} \tag{2-2}$$

where δ_{Y_T} is the total elastic inter-story drift including both shear and flexural deformations associated with the onset of shear yielding for the story and δ_T is the total inter-story deformation determined from inelastic time history analysis.

2.2 TYPICAL PWR REACTOR BUILDING

2.2.1 Description of Structure Dynamic Model

A schematic representation of the PWR reactor building used in Task II is presented in Figure 2-3. PWR structural properties are based upon a reactor building model presented in References 2 and 3. This structure is designed to an approximately 0.2g maximum ground acceleration, regulatory guide-type response spectra applicable to structures on a stiff soil site. This design is consistent with current practice for nuclear facilities in low-to-moderate seismic risk areas subjected to a nearby moderate magnitude earthquake.

The building consists of a reinforced concrete internal structure supporting the reactor vessel and steam generators and a prestressed concrete containment with hemispherical head supported by a reinforced concrete raft foundation. The raft foundation is circular with a radius of 63.6 feet and a thickness of 11.5 feet at the center which thickens to 16.4 feet around the circumference to allow space for tendon galleries. A polar crane is located approximately 143 feet above the top of the basemat.

The reactor building dynamic lumped mass model is presented in Figure 2-4 and is also superimposed on the PWR structure shown in Figure 2-3 for reference. The dynamic model includes two lumped mass, vertical sticks to represent the containment vessel shell and concrete internals. All lumped mass are located at major floor locations and includes the mass of all concrete and steel. Because the structure is symmetric, a planar model was used and the center of mass for each floor coincides with the structure geometric centroid.

Beam elements define the stiffness characteristics of the structural stiffnesses between floor levels. All structural stiffnesses are considered to be symmetric about the reactor building centerline and coincide with center of mass locations.

Because of the lower design capacity of the radial shear walls at the base of the internal structure, nonlinear shear yielding occurs in the bottom two shear wall elements of the internal structure between Elevation 0' and Elevation 25'-4" when the PWR is excited by 0.5g earthquake ground motion. Nonlinear shear behavior for these members was represented by elements 18 and 20. Elements 17 and 19 were used to maintain the correct geometric relationship for these members and represent wall flexural stiffness only. Similarly, element 21 was used to represent nonlinear bond-slip which may occur at the base of the internal structure. The behavior of these nonlinear elements is discussed in Section 2.2.2. Note that in elastic time history analyses, nonlinear behavior of these elements was precluded from occurring by artificially increasing the yield levels.

Both fixed base and soil-structure interaction linear and nonlinear time history analyses of the PWR were conducted. In the fixed base analyses, the structure was considered to be unembedded. The free-field ground motion discussed in Section 2.3 was applied as base excitation at the top of slab, node 22, with all nodal locations below this point restrained from deforming relative to the ground. In the soil-structure interaction analyses, the structure was embedded at a depth of 42 feet and soil springs and dashpots were used to represent the stiffness and damping of the underlying soil. The soil-structure interaction model of the PWR building was excited by the foundation input motion which was derived from the free-field motion by incorporating kinematic interaction. Section 2.4.2 presents the soil impedances and earthquake ground motions used in the soil-structure interaction analyses.

2.2.2 Localized Structural Nonlinearities

In general, inelastic structural behavior may occur in both the prestressed containment and the reinforced concrete internal structure due to moment yielding, shear yielding, and bond slip. Because of the large initial prestress loads required in the concrete containment structure to protect against possible overpressurization due to steam line rupture, seismic response moments were shown in all cases to be

below the cracking moment required to overcome initial prestress and structure dead weight such that linear behavior of the containment occurs. Similarly, moments in the reinforced concrete internal structure were demonstrated to be lower than the yield moment at all critical locations and a linear moment representation of the internal stucture was adequate. However, significant inelastic behavior at the bottom of the internal structure does occur due to shear yielding. Some minor additional non-linearity also occurs due to bond slip of the vertical reinforcement at the junction between the internal structure and foundation raft. A discussion of the inelastic properties of critical internal structure elements is presented in the following section.

2.2.2.1 Inelastic Shear Behavior of Reinforced Concrete Elements

Inelastic shear behavior occurs when the concrete load capacity is exceeded and the concrete cracks but the steel behaves elastically. Initially, the wall behaves elastically and shear resistance is developed according to elastic beam theory. Inclined shear cracks develop when the principal tensile stresses exceed the concrete tensile strength. Once shear cracks open, the shear force is resisted primarily by the reinforcing bars and aggregate interlock. The opening and closing of cracks under load reversals causes the pinching behavior noted in the hysteresis loops for a shear wall under load reversals shown by test results in Figure 2-1. As shear cracks open wider and damage to the concrete increases, the contribution of the concrete, through aggregate interlock, to shear resistance decreases. This effect causes strength degradation under large displacement cycles.

The shear element representing the shear wall behavior of the reinforced concrete internal structure is presented in Figure 2-5. This element was used in Task I to represent inelastic behavior of low-rise shear walls. The slope of the first segment, K, is equal to the shear stiffness of the reinforced concrete internal structure and is appropriate for shear being carried totally by the concrete. At the yield shear force, V_Y, the concrete is unable to carry additional shear and all added shear beyond this point is carried by the reinforcing steel. A

softer slope of 0.1K is used to represent the effective stiffness of the reinforcing steel once concrete cracking has occurred. The unloading stiffness parameter, α, and strength degradation parameter, γ, were taken to be identical to the Task I values of 0.35 and 0.95, respectively. The interested reader is referred to the Task I report (Reference 1) for a complete discussion of the hysteresis behavior of the shear wall element shown in Figure 2-5.

The reinforced concrete internal structure presented in Figure 2-3 consists of two concentric concrete rings supporting the reactor vessel and auxiliary equipment. At higher elevations, large radial shear walls emanate outward from the center ring with resultant large yield shear capacities as presented in Table 2-1. However, between Elevations 0' and 25'-4" these walls are missing to allow for passage of the main coolant lines. The absence of these walls at lower elevations results in a "weak link" in the PWR structure as evidenced by the low yield shear capacities presented for elements 18 and 20. Chapters 3 and 4 of this report will show only these lower two elements respond inelastically for the earthquake ground motions considered. Above this region, the structure responds elastically with seismic response loads below the shear yield load, V_Y, in all cases.

2.2.2.2 Internal Structure Bond Slip

A special inelastic hinge element is located at the base of the internal structure connecting the bottom shear element to the base slab, as shown in Figure 2-4. This element represents the added flexibility due to bond slip at the base of the internal structure which may occur during seismic excitation. Bond slip occurs when the tensile stress due to the internal structure overturning moment exceeds the compressive stress from the internal structure dead weight. All load beyond this point must be carried by vertical reinforcing steel which is tied into the foundation basemat. As the steel picks up load, movement of the rebar relative to the surrounding aggregate occurs until sufficient steel-to-aggregate interlock has occurred to carry the additional load. Movement of the steel relative to the concrete matrix results in some

minor additional rotational flexibility of the internal structure which is represented in this study by a nonlinear bond slip element.

Figure 2-6 presents the moment-rotation relationships used for the inelastic bond slip hinge element as given by References 2 and 3. Initially, the element is rigid with no rotation occurring due to bond slip. Once the seismic overturning moments have exceeded the moment, M_{bond}, bond slip takes place as shown, which is valid up to the steel yield moment. Unloading occurs along the same path so long as steel stresses remain below yield which is the case for this study.

2.3 EARTHQUAKE GROUND MOTION

Because the intent of the Task II is to realistically evaluate response of a typical PWR structure at a ground motion 2.5 times the design motion of 0.2g, the three real earthquake records selected for this study all had recorded peak instrumental accelerations close to 0.5g. In addition to these three real earthquake records, one artificial time history was used which approximates, at low damping, the NRC Regulatory Guide 1.60 response spectrum anchored to 0.5g maximum ground acceleration. It is typical of some of the more realistic time histories used in nuclear power plant dynamic analyses. The earthquake records chosen were based on Task I results and are identified as follows: Artificial Earthquake; El Centro Array No. 5, 140° Component, of the 1979 Imperial Valley Earthquake; Cholame Array No. 2, N65E Component, of the 1966 Parkfield Earthquake; and Melendy Ranch Barn, N29W Component, of the 1972 Bear Valley Earthquake. Note that throughout this report, when a particular earthquake is referred to, such as the Parkfield Earthquake, this reference really implies the specific recording station and component presented above.

The 7 percent damped elastic response spectra, scaled to a 1g peak ground acceleration, corresponding to these time histories are presented in Figure 2-7. These free-field ground motions were scaled to 0.5g peak ground acceleration for all Task II studies.

The Artificial earthquake record is classified as a long duration earthquake with an effective strong motion duration, T_D', of 9.4 seconds exhibiting substantial amplified response in the 1.8 to 10 Hz range of interest for stiff, shear wall structures. The f_{10} to f_{90} frequency range for this time history is 0.60 Hz to 6.55 Hz. Task I demonstrated ground motions with a f_{10} to f_{90} breadth of frequency of at least 1.2 to 5.5 Hz may be classified as broad frequency content record which is adequately approximated by a single broad frequency content design spectrum such as Reg. Guide 1.60 anchored to an "effective" acceleration.

El Centro #5 is a moderate duration earthquake record with an effective strong motion duration of 3.4 seconds and peak instrumental acceleration of 0.53g. This local magnitude 6.6 earthquake has an f_{10} to f_{90} frequency content of 0.80 to 6.75 Hz and is shown in Task I to be reasonably approximated by a Regulatory Guide 1.60 response spectra anchored to an effective acceleration, A_{DE} = 0.471g.

In contrast to these earthquakes, both Parkfield and Melendy Ranch are representative of short duration earthquakes with only limited frequency content and damage capability. Parkfield is a local magnitude 5.6 earthquake with an effective strong motion duration of only 1.4 seconds and peak instrumental acceleration of 0.490g. The f_{10} to f_{90} frequency range for Parkfield was determined in Task I to be 1.20 to 2.75 Hz. The narrow breadth of frequency content for this ground motion may be seen from the elastic response spectra presented in Figure 2-7 which exhibits peak spectral amplification between 1.7 to 2.3 Hz and little amplification above 2.6 Hz. Because of this narrow frequency content, the Parkfield response spectrum is not adequately represented by the Reg. Guide 1.60 spectrum anchored to any effective acceleration.

Similarly, Melendy Ranch is a local magnitude 4.7 earthquake with a very short effective strong motion duration of only 0.8 seconds and peak ground acceleration of 0.52g. The Melendy Ranch spectrum shows

peak spectral response at 5.7 Hz which rapidly drops off outside the range of 5.2 Hz to 6.2 Hz. This narrow frequency content is shown in Task I by the f_{10} to f_{90} frequency content which is 3.55 to 8.20 Hz. Like Parkfield, Melendy Ranch is not adequately represented by the U.S. Regulatory Guide 1.60 response spectra. These four earthquake records represent a wide range of possible ground motion which cause substantially different linear and nonlinear structural response of the PWR building.

2.4 PWR DYNAMIC ANALYSES

Both linear and nonlinear time history analyses were conducted for the PWR structure. Initially, the structure was considered to be fixed base excited by free-field ground motion scaled to a 0.5g maximum ground acceleration. Linear analyses were conducted for each of the four ground motions discussed above to determine peak moments, shear, and displacements and selected in-structure response spectra throughout the PWR building. Next, nonlinear time history analyses were conducted allowing inelastic shear and bond-slip of the lower walls in the internal structure as previously discussed. Results from these two analyses were compared to determine the effect of local inelastic behavior on earthquake damage capability of the fixed base PWR structure.

Additional analyses were also conducted assuming the structure was embedded 40 feet in the surrounding soil. For this case, two soil profiles were studied corresponding to a stiff site and an intermediate site representation of soil conditions typically encountered at nuclear power plants. Linear and nonlinear analyses were conducted for the PWR structure for the 0.5g free-field ground motions. Complete kinematic interaction of the foundation and soil was considered resulting in both translational and rotational input time histories being included in the time history analyses. Peak moments, shears, and displacements were compared to evaluate the effects of soil-structure interaction of PWR seismic response. Section 2.4.2 presents a complete discussion of the soil profiles and input ground motions used in the soil-structure interaction evaluation.

The PWR mathematical model previously presented in Section 2.2.1 was used in all analyses. Time history analyses were conducted using an SMA version of computer program DRAIN (Reference 4). A time step size of 0.0025 seconds was used in all linear and nonlinear analyses to ensure accurate results.

2.4.1 Fixed Base Analyses

Mode shapes and frequencies for the first 4 linear fixed base vibration modes are presented in Figure 2-8. Modes 1 and 4 correspond to containment structure response while Modes 2 and 3 are internal structure modes. The percentage of translational mass participating in each mode is presented in Table 2-2. The modal masses demonstrate internal structure response is essentially single mode with 82 percent of total internal structure mass participating in the 5.22 Hz fundamental mode. The fundamental containment mode has a frequency of 4.47 Hz with a 70 percent of the containment mass participating in this mode.

Damping for the prestressed containment structure was assumed to be 5 percent of critical corresponding to U.S. Regulatory Guide 1.61 damping for members exceeding one-half the yield stress. Internal structure damping was taken as 6 percent of critical damping which is slightly lower than the 7 percent of critical damping allowed by nuclear regulatory commission guidelines. Dynamic analyses of the fixed base structure used a Rayleigh definition of the structure damping given by:

$$\lambda_i = \frac{\alpha T_i}{4\pi} + \frac{\beta\pi}{T_i} \qquad (2\text{-}3)$$

where λ_i is the critical damping ratio at structure period, T_i. The coefficients α and β were selected on a best fit of damping for important fixed base modes for the frequency range of interest. In nonlinear runs, Equation 2-3 still applies but the stiffness proportional damping term β was set proportional to the structure tangent stiffness rather than the

initial elastic stiffness to avoid double-counting hysteretic energy dissipation within the inelastic range. A discussion of the reasons for setting structural damping proportional to the tangent stiffness is presented in Reference 1.

2.4.2 Soil-Structure Interaction Analyses

2.4.2.1 Site Conditions and Ground Motion Input

The PWR structure shown in Figure 2-3 was assumed embedded 40 feet in the surrounding soil in all soil-structure interaction analyses. Two soil profiles with significantly different layer configurations and shear wave velocities were studied. These profiles were developed by Woodward-Clyde Consultants. The shear wave velocities and material damping ratios for these profiles are presented in Figures 2-9 through 2-12.

The intermediate soil profile presented in Figures 2-9 and 2-10 corresponds to an intermediate stiffness site. The top, 250-foot deep soil layer has an approximately uniform shear wave velocity of 900 fps. At 250 feet, a sharp impedance mismatch exists, with the deeper material having a shear wave velocity of 3600 fps. Soil material damping for the upper layer is approximately 6.5 percent of critical damping while damping for the deeper layer was taken as a constant 2 percent of critical damping.

The stiff soil profile presented in Figures 2-11 and 2-12 is representative of stiff site conditions with significant impedance mismatches occurring at 40 feet and 250 feet. The top 40 feet has a shear wave velocity of 850 fps and soil material damping varying between 2.5 and 6.5 percent. Between 40 feet and 250 feet, the soil shear wave velocity varies linearly from 1750 fps to 1900 fps. A soil material damping of about 4 percent was used for this layer. Below 250 feet the soil was assumed to have a shear wave velocity of 3600 fps and a soil material damping of 2 percent.

Soil impedances representing stiffness and damping characteristics of these profiles were supplied to SMA by Woodward-Clyde Consultants. In addition, Woodward-Clyde Consultants also supplied to SMA translational and rotational time histories for the ground motions discussed previously which had been deconvoluted to the foundation basemat accounting for soil kinematic interaction only and ignoring inertial feedback from the PWR structure.

In general, soil impedances representing the stiffness and damping of the underlying soil are frequency dependent. However, computer program DRAIN, which was used to conduct the linear and nonlinear time history analyses, requires unique soil springs and dashpots representing the soil characteristics. Therefore, a step by step procedure was developed to estimate soil spring and dashpot properties for use in program DRAIN consistent with the frequency dependent impedances supplied by Woodward-Clyde. This procedure is presented in Appendix A along with the soil spring and dashpot properties used to represent the stiff and intermediate site soil profiles.

A summary of the procedure for evaluating the earthquake ground motions and soil spring and dashpots used to conduct soil-structure interaction analyses of the PWR reactor building is as follows:

A. Work conducted by other consultants and supplied to SMA

1. Determine frequency dependent soil impedances for the embedded reactor building for both soil profiles.

2. Deconvolute the free-field ground motions scaled to 0.5g to the foundation basemat accounting for wave-scattering due to kinematic interaction only.

B. Work conducted by SMA

3. Using the procedure presented in Appendix A with the soil impedances supplied in 1 above, determine soil springs and dashpots for both the intermediate and stiff site soil profiles.

4. Using the appropriate ground motions from step 2 and soil springs and dashpots from step 3, conduct linear and nonlinear time history analyses of the PWR structure for both the intermediate and stiff site profile for all four ground motions.

For both the linear and nonlinear seismic response analyses of the PWR structure, the soil springs and dashpots used were developed based on linear structure characteristics. This approximation of the soil impedances for the nonlinear response cases is justifiable for the following reasons. First, the fundamental response mode of the combined system is a rigid body soil-structure translation or rotation. Large changes is the structure stiffness as a result of nonlinear behavior have only minor effects on the fundamental soil-structure frequency. In addition, the soil impedances presented in Appendix A are relatively smooth functions of frequency for the range of interest and do not exhibit large breaks or discontinuities which could cause significant changes in the impedances value for small shifts in frequency. Thus, using a linear approximation of the structure to approximate structural dynamic response when estimating soil impedances for the nonlinear cases studied appears reasonable.

2.4.2.2 Flexible Base Structure Mode Shapes and Frequencies

Mode shapes and frequencies for the first 4 linear flexible base vibration modes are presented in Figures 2-13 and 2-14 for the stiff and intermediate soil profiles, respectively. Including the flexibility of the underlying soil for the stiff soil profile reduces the fundamental structure first mode frequency from 4.47 Hz determined for the fixed base case to 2.62 Hz. Higher important modes of the system correspond to a

translational internal structure mode at 4.84 Hz and a soil translation mode at 8.48 Hz. Approximately 98 percent of the total structure mass participates in the first 3 modes of the structure.

Results for the softer intermediate soil profile show an even further reduction in the fundamental structure frequency. For this case, the fundamental soil-structure rocking mode occurs at a frequency of 1.78 Hz. Higher important modes correspond to a combined soil translation, internal structure response mode at 4.26 Hz and a combined soil translation and rocking mode at 6.15 Hz. Essentially 100 percent of the structure translational mass responds in these first three modes.

TABLE 2-1

PWR INTERNAL STRUCTURE SHEAR CAPACITIES*

Element	Yield Shear V_y (lbs.)
13	1.66×10^7
14	3.48×10^7
15	4.01×10^7
16	3.12×10^7
18	1.73×10^7
20	1.73×10^7

*All shear capacities are from Reference 2

(see Figure 2-4 for element location)

TABLE 2-2

FIXED BASE MODAL CHARACTERISTICS

Structure	Mode	Frequency	Percentage of Total Mass Participating
Internal	2	5.22	81.6
	3	13.09	15.2
			Σ = 96.8
Containment	1	4.47	70.1
	4	15.23	16.8
			Σ = 86.9

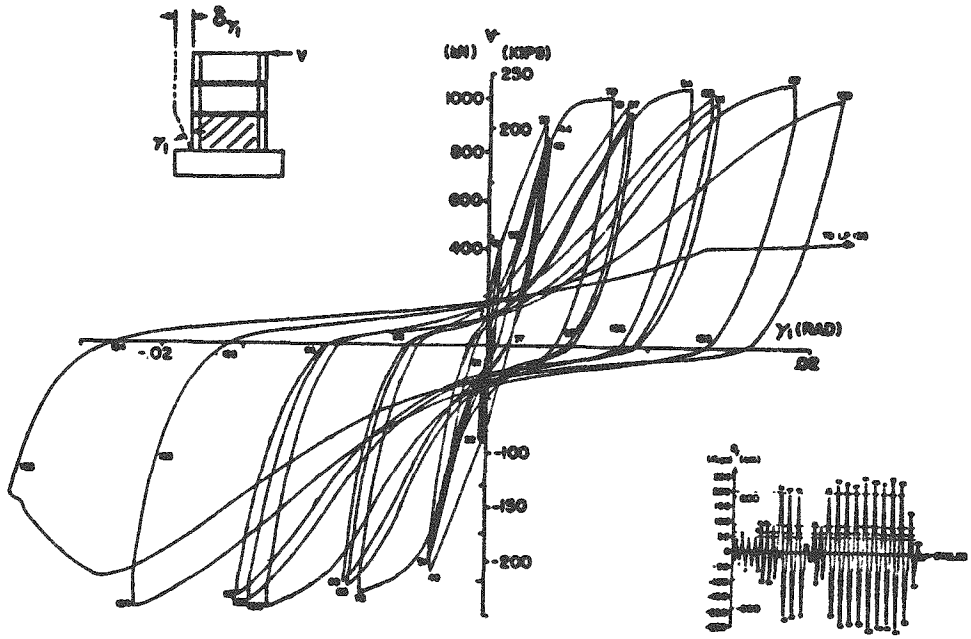

(a) Shear force-shear distortion diagram for structural concrete wall test (Wang, Bertero, Popov; 1975)

FIGURE 2-1. CYCLIC LOAD-DEFLECTION BEHAVIOR OF CONCRETE SHEAR WALLS (From Reference 1)

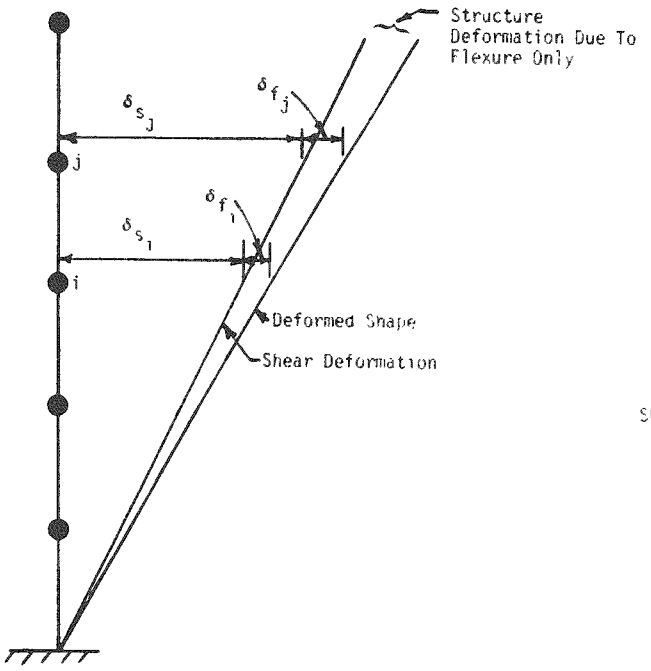

a) Deformed Structure

δ_{s_i} = Shear Deformation of Node i

δ_{f_i} = Flexural Deformation of Node i

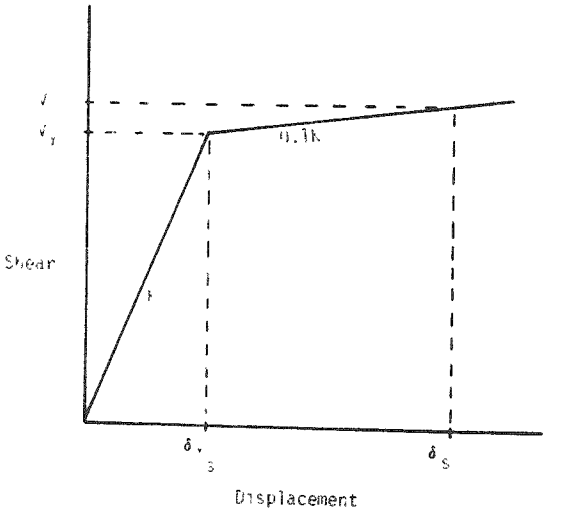

b) Shear-Displacement Relationship For Story i-j

c) Shear Story Drift Ductility

$$\delta_s = \delta_{s_j} - \delta_{s_i}$$

$$\mu_s = \frac{\delta_s}{\delta_{y_s}}$$

d) Total Story Drift Ductility

$$\delta_{y_T} = \delta_{y_s} + \delta_{y_f}$$

where: δ_{y_f} = inter-story flexural deformation associated with shear yield deformation, δ_{y_s}

$$\delta_T = \delta_s + \delta_{f_j} - \delta_{f_i}$$

$$\mu_T = \frac{\delta_T}{\delta_{y_T}}$$

FIGURE 2-2. STORY DRIFT DUCTILITY DEFINITION

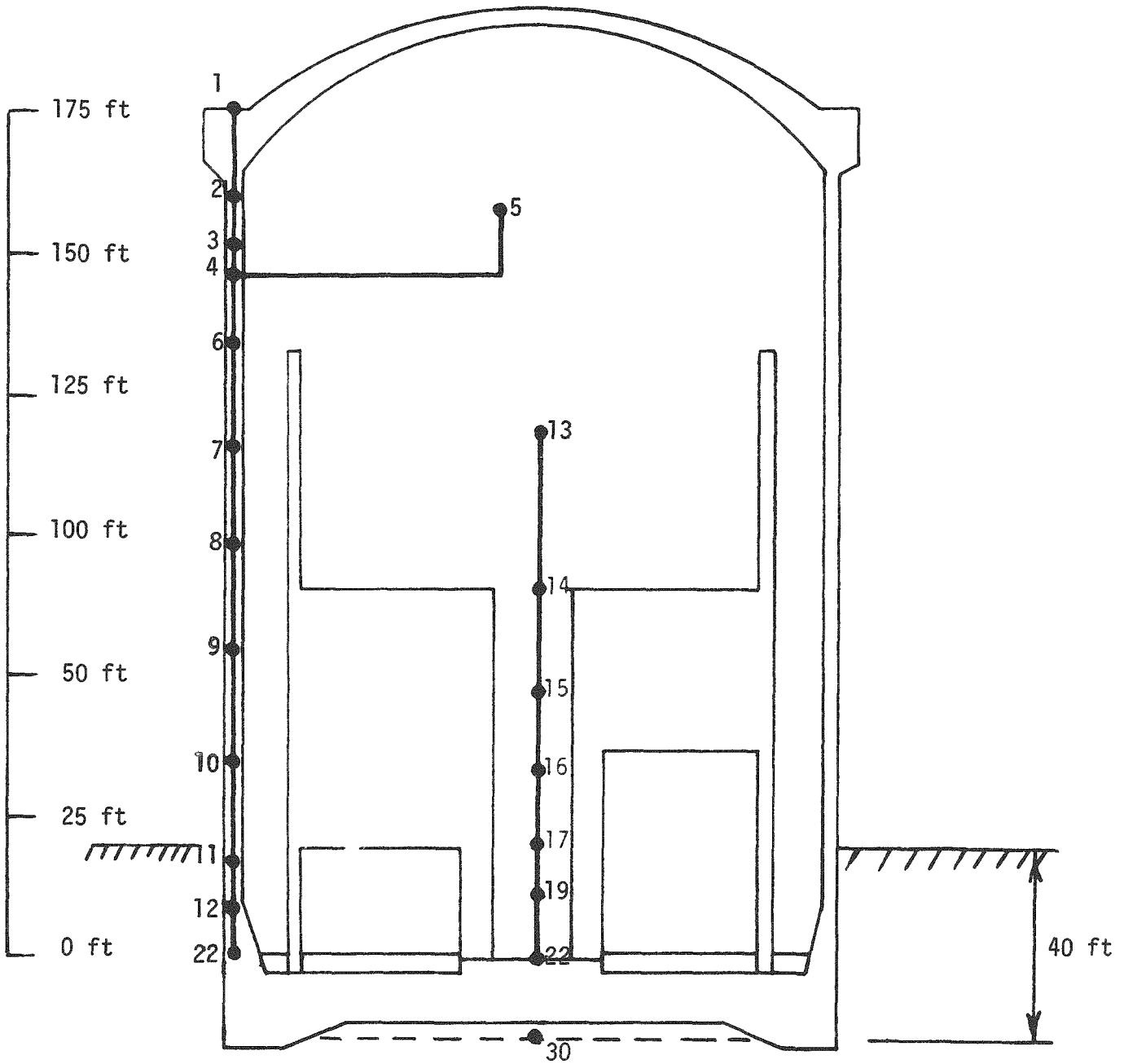

NOTE: 1) Soil springs and dashpots used in SSI analyses are not shown

2) Structure was unembedded for fixed base analyses

FIGURE 2-3. PWR REACTOR BUILDING AND ANALYTICAL MODEL

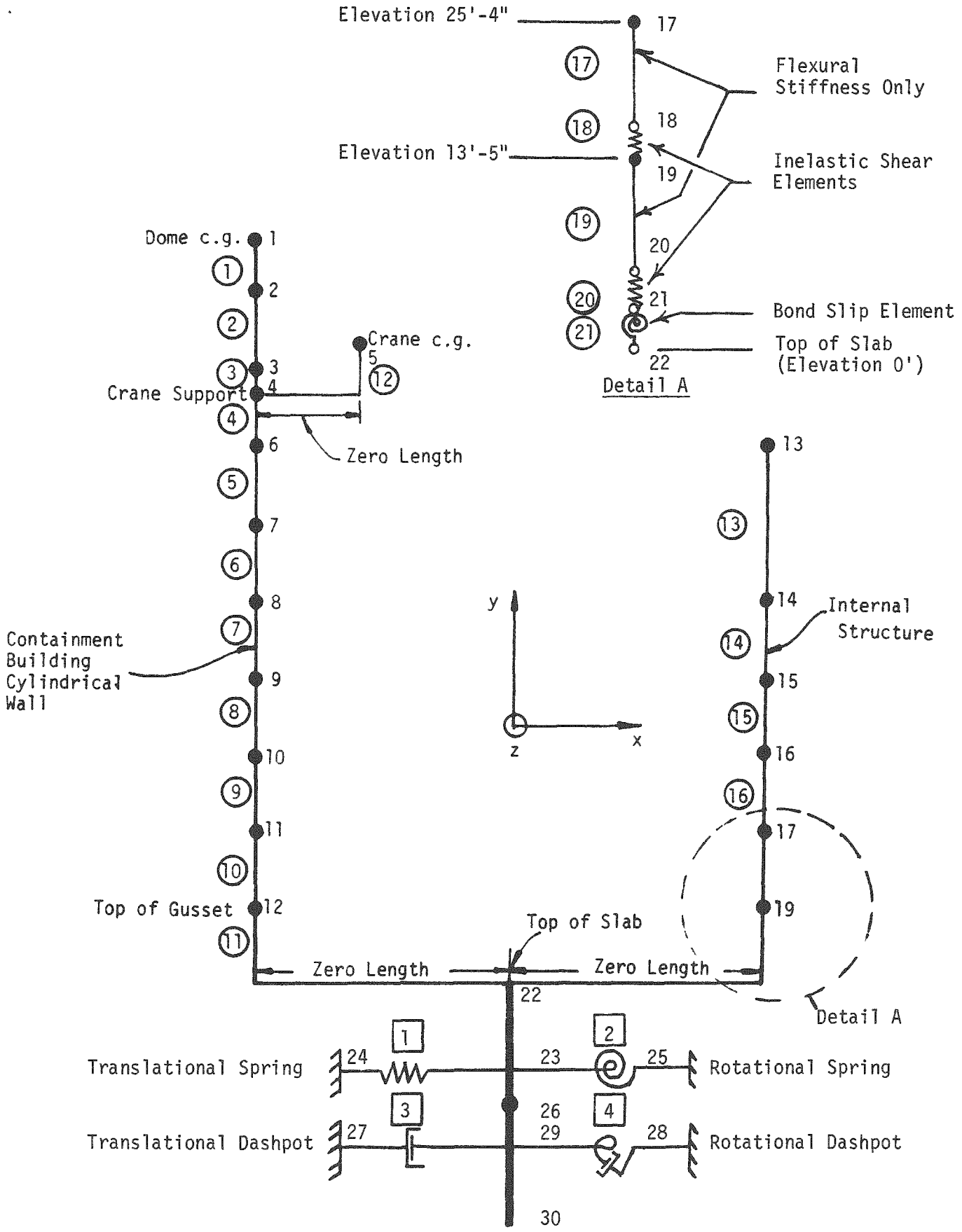

FIGURE 2-4. MATHEMATICAL MODEL OF PWR REACTOR BUILDING

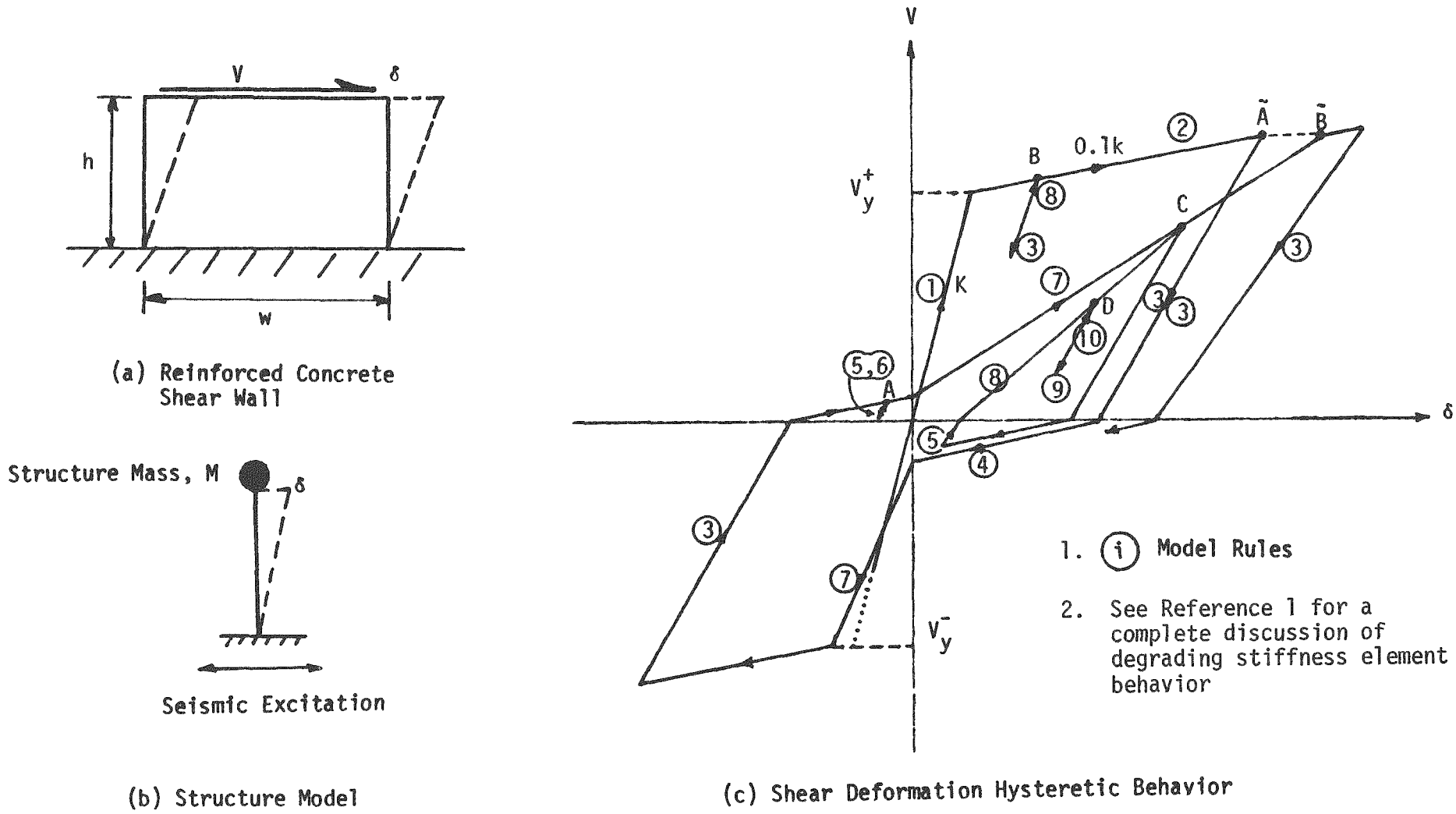

FIGURE 2-5. SHEAR WALL STRUCTURE MODEL AND CORRESPONDING HYSTERETIC DEFORMATION BEHAVIOR (From Reference 1)

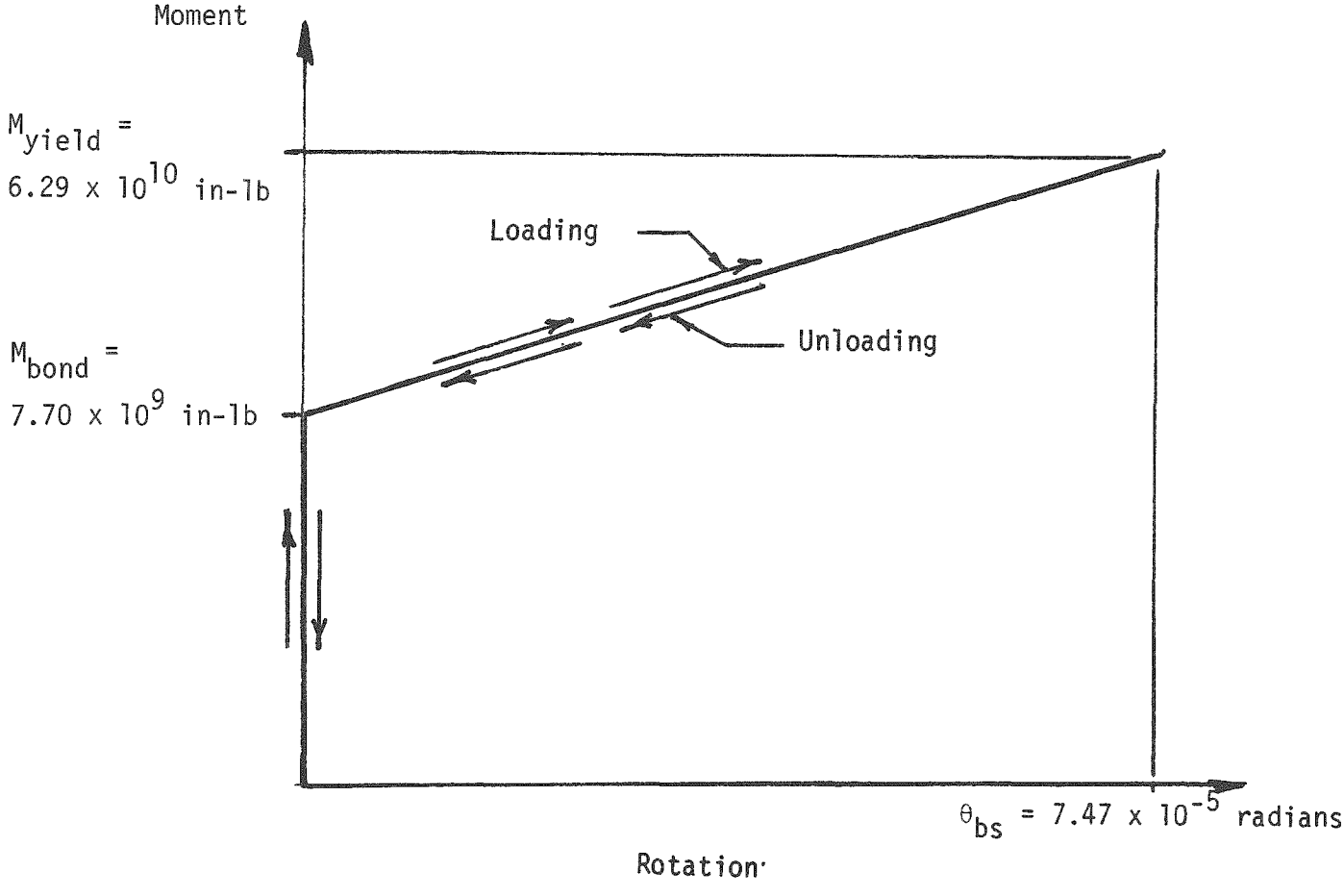

FIGURE 2-6. MOMENT-ROTATION RELATION FOR INELASTIC BOND-SLIP HINGE ELEMENT (From Reference 2)

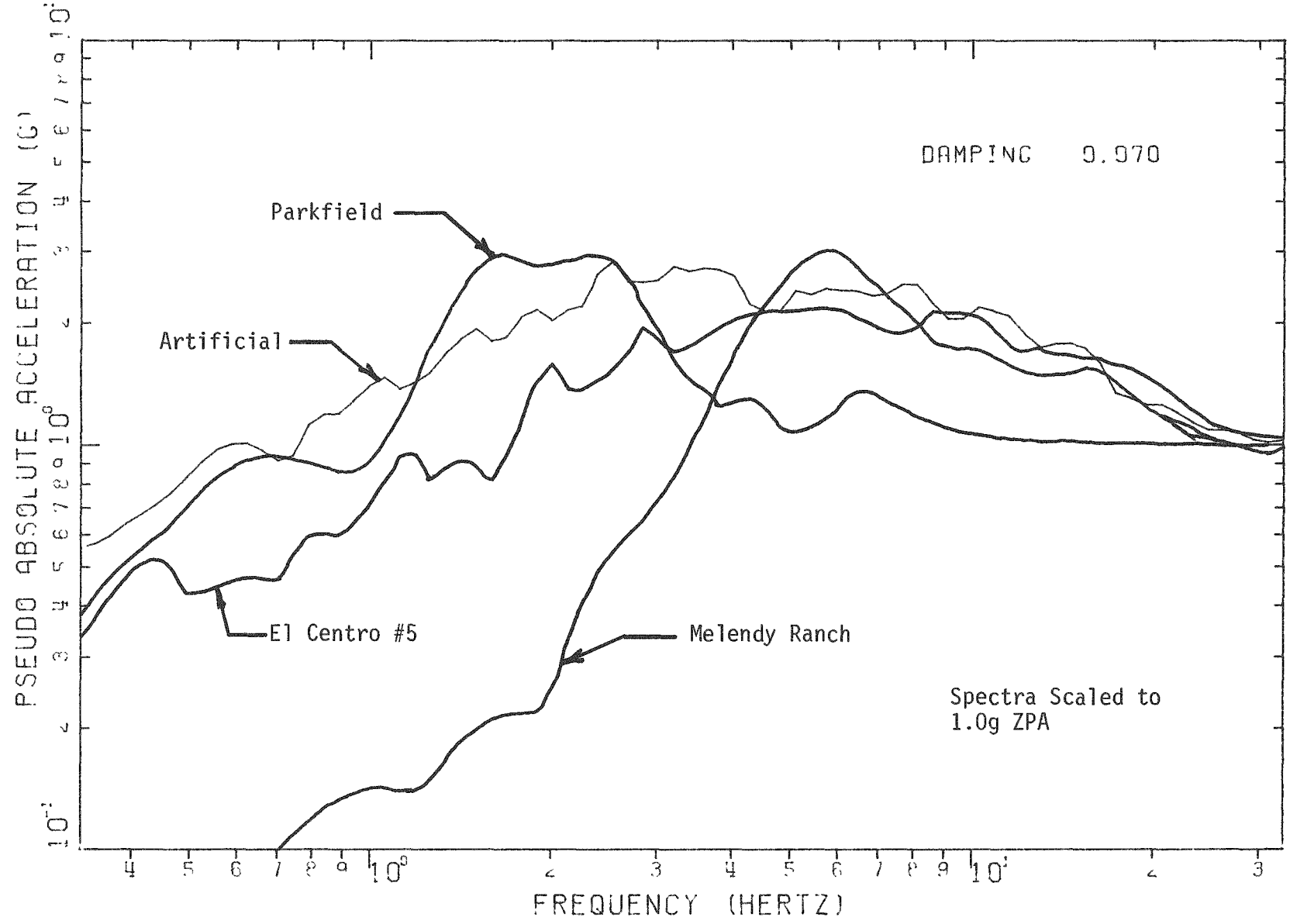

FIGURE 2-7. COMPARISON OF ELASTIC RESPONSE SPECTRUM FOR ARTIFICIAL, EL CENTRO #5, PARKFIELD, AND MELENDY RANCH EARTHQUAKES

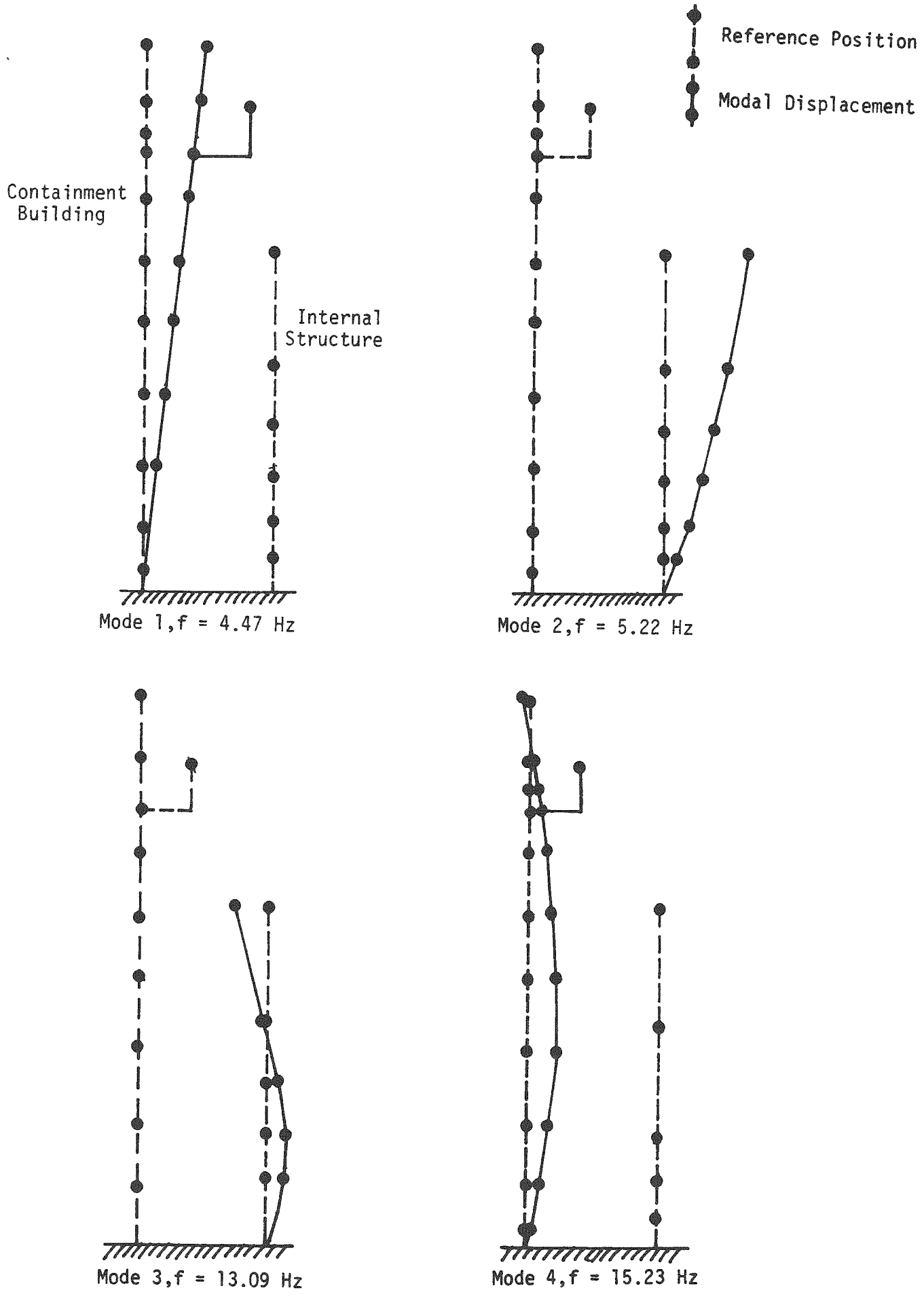

FIGURE 2-8. MODE SHAPES AND FREQUENCIES, FIXED BASE

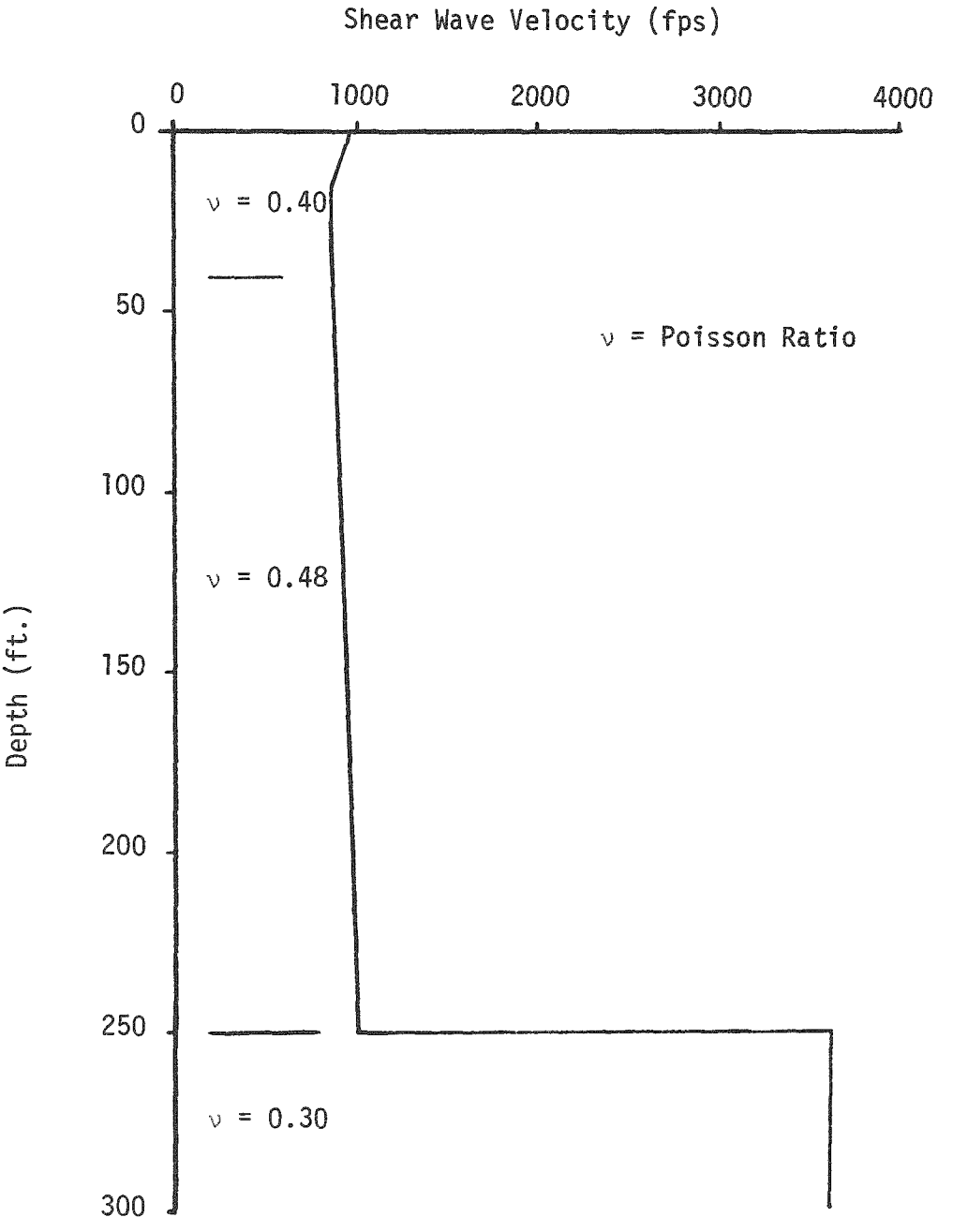

FIGURE 2-9. STRAIN-COMPATIBLE SHEAR WAVE VELOCITY PROFILE FOR INTERMEDIATE SOIL CASE

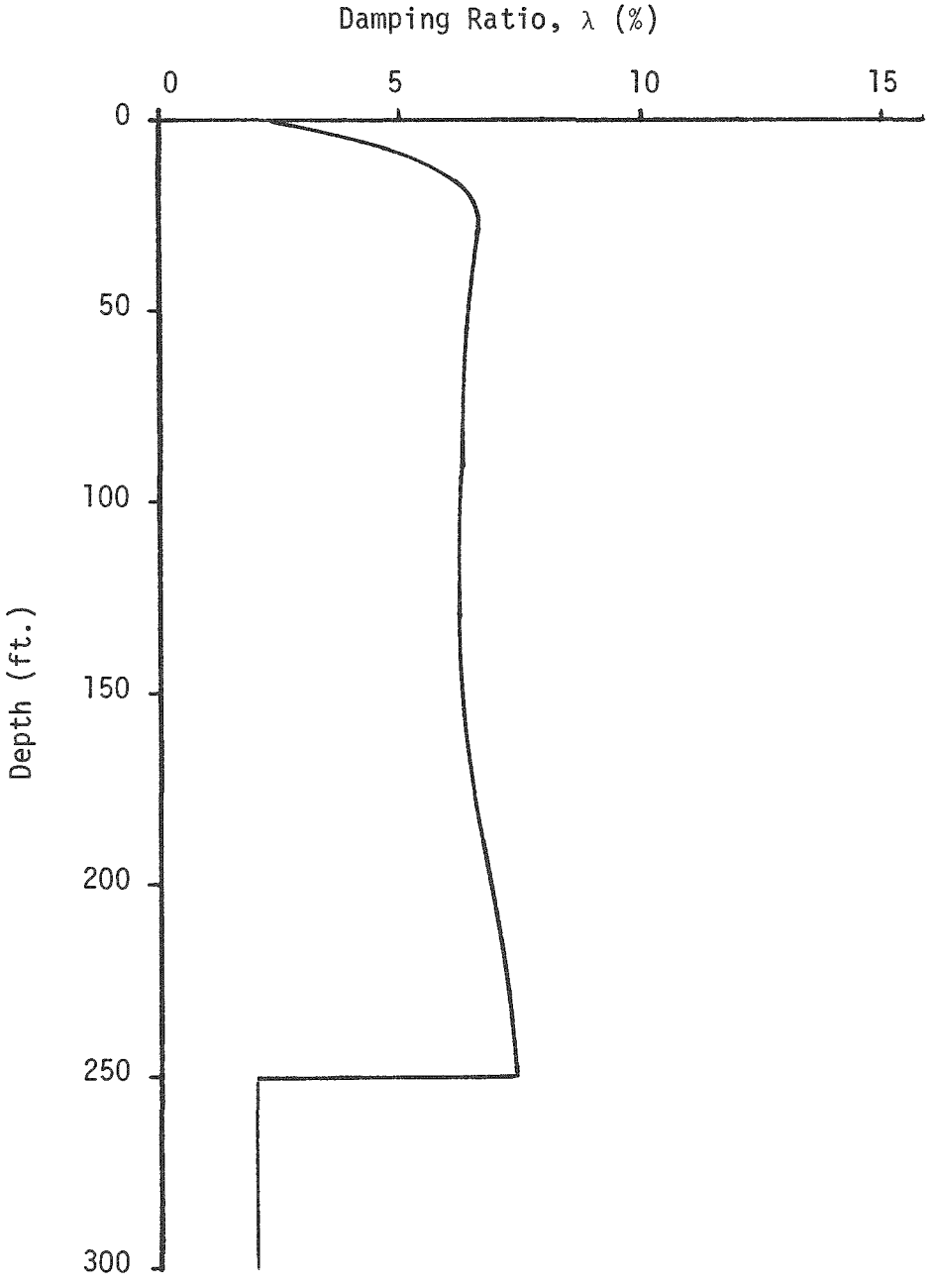

FIGURE 2-10. SOIL DAMPING RATIO FOR INTERMEDIATE SOIL PROFILE

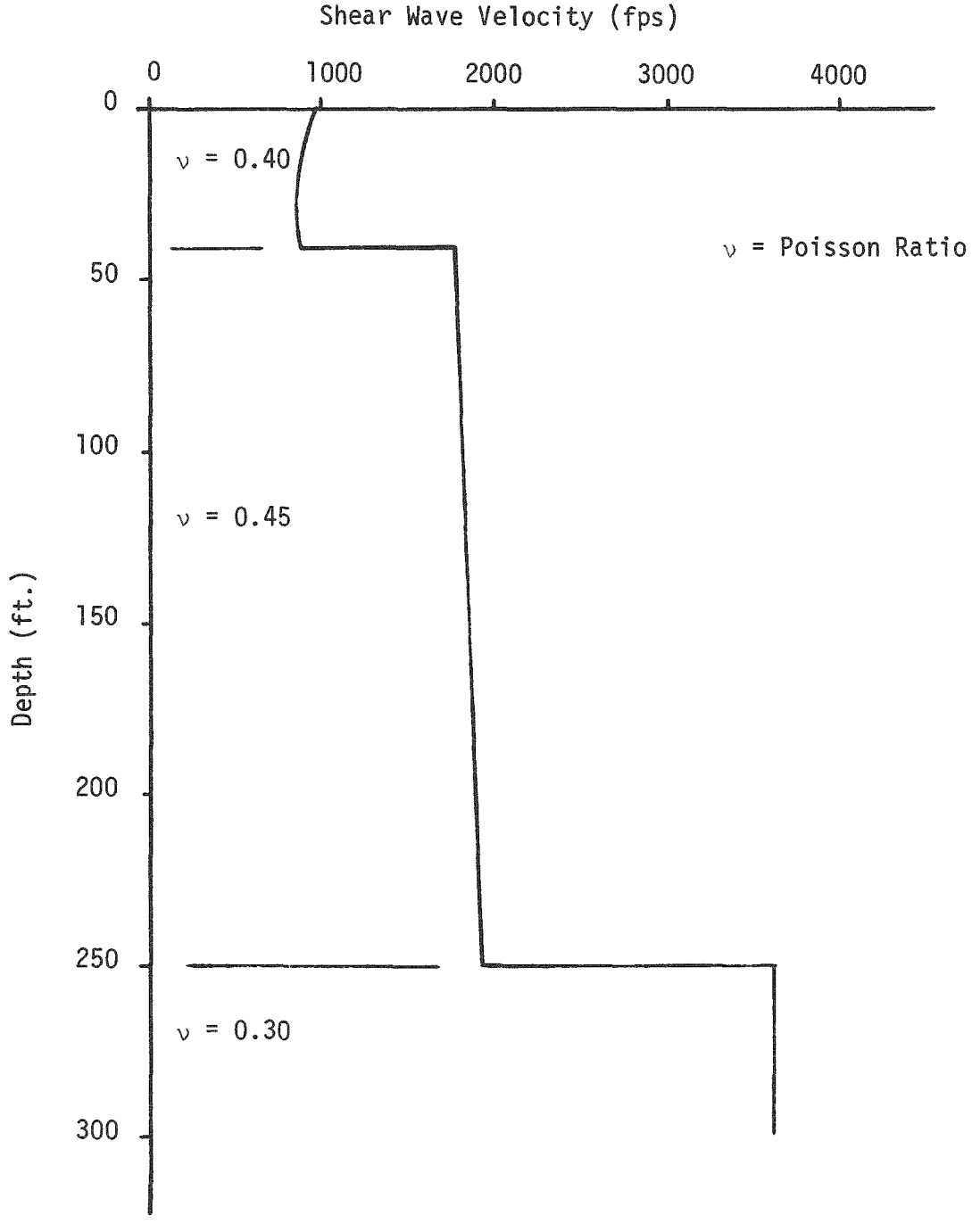

FIGURE 2-11. STRAIN-COMPATIBLE SHEAR WAVE VELOCITY PROFILE FOR STIFF SOIL CASE

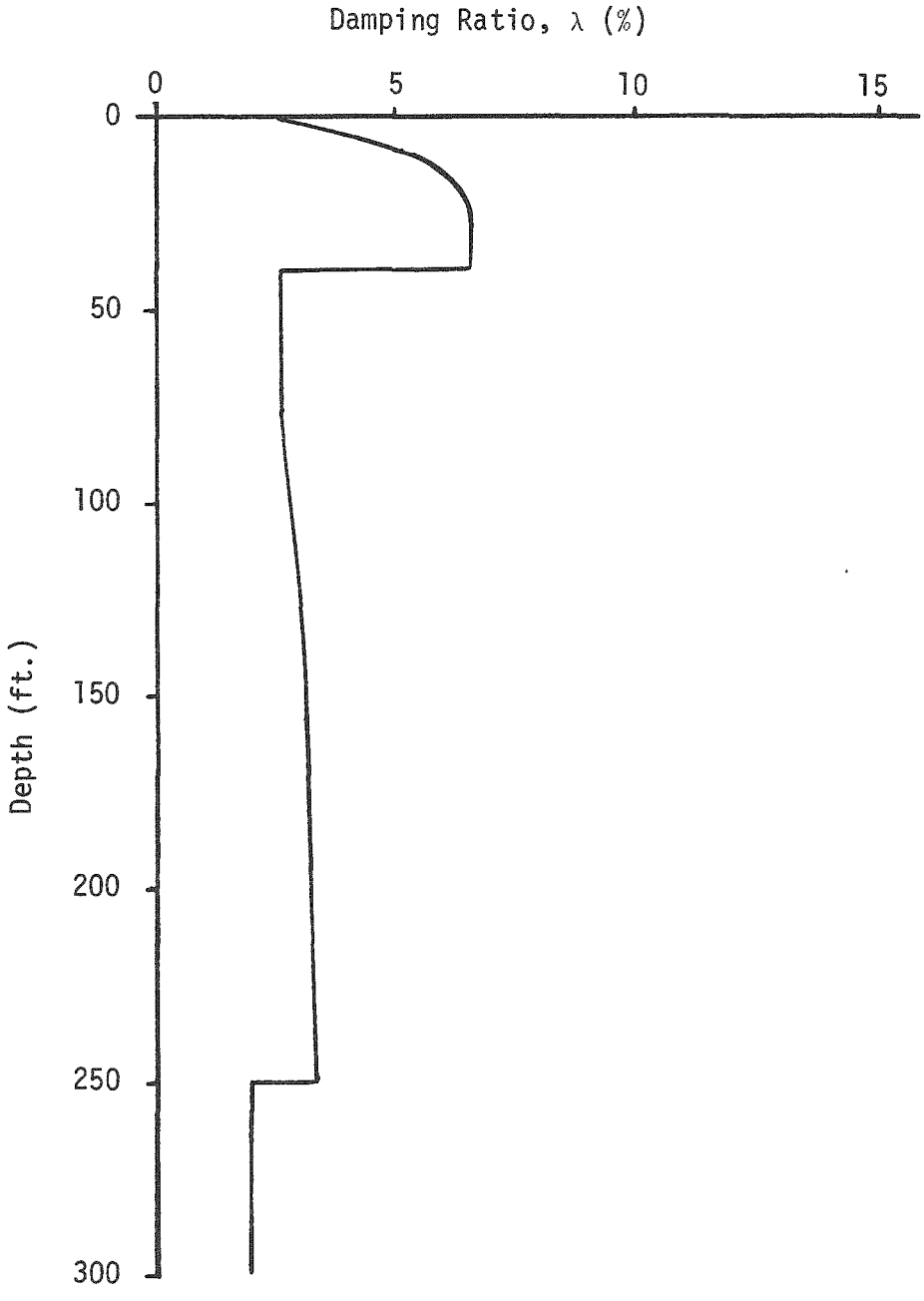

FIGURE 2-12. SOIL DAMPING RATIO FOR STIFF SOIL PROFILE

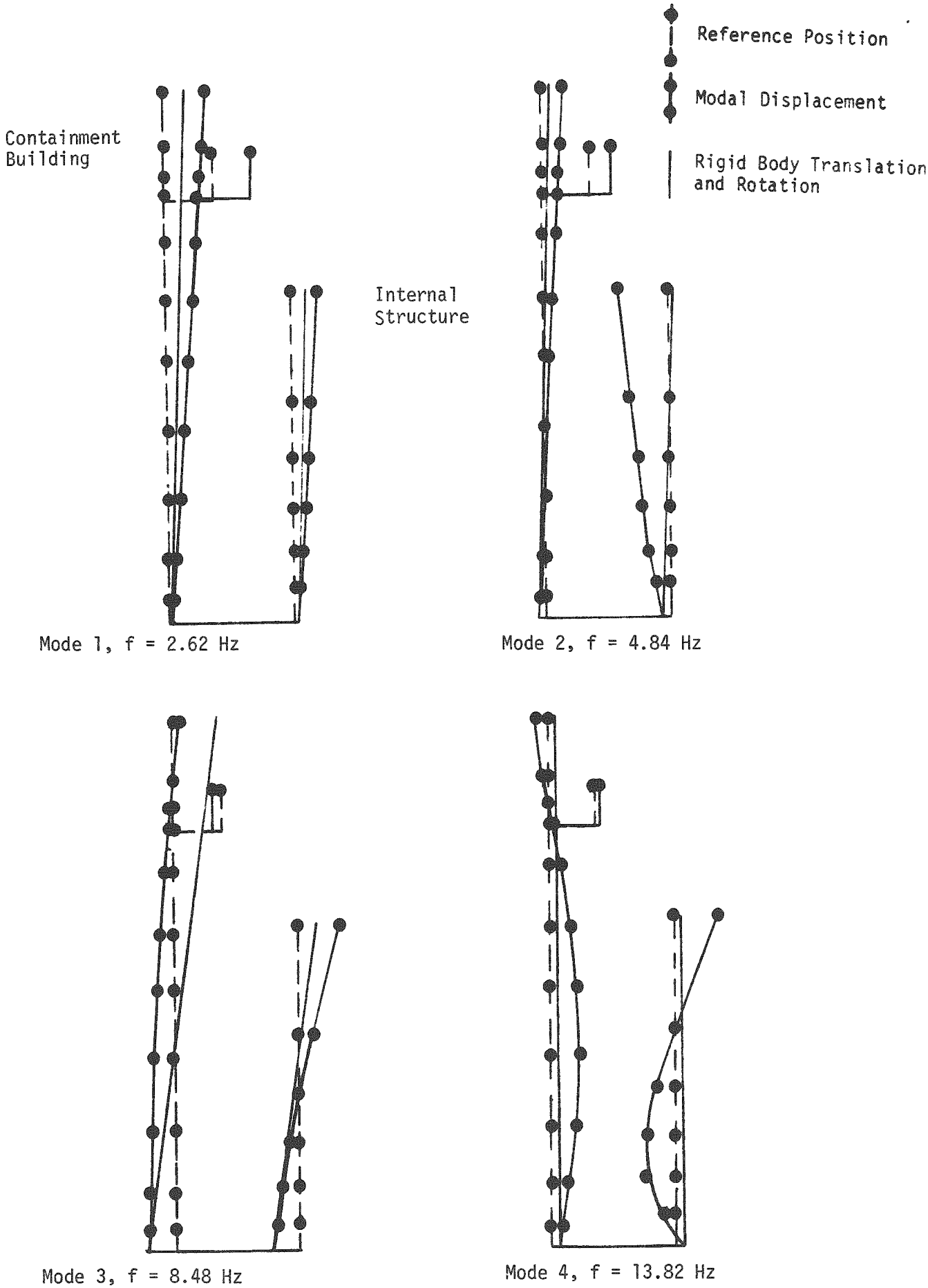

FIGURE 2-13. MODE SHAPES AND FREQUENCIES, STIFF SOIL PROFILE

3. FIXED BASE TIME HISTORY ANALYSES

3.1 LINEAR SEISMIC RESPONSE

Maximum internal structure displacements and shears as determined from elastic time history analyses for a 0.5g peak ground acceleration are presented in Figures 3-1 through 3-8 for each of the four earthquakes studied. The corresponding in-structure response spectra at node 14, Elevation 75', are presented in Figures 3-9 through 3-12. Selected elastic seismic response moments for the PWR structure are presented in Table 3-1.

A comparison of seismic response loads and displacements indicates maximum elastic internal structure response occurs when the PWR structure is excited by Melendy Ranch ground motion. Results for the Artificial and El Centro #5 ground motions are between 10 to 25 percent lower than response calculated for Melendy Ranch. Seismic response loads are even lower for Parkfield with peak shears 55 to 65 percent below Melendy Ranch results. A comparison of the elastic response spectra presented in Figure 2-7 for these earthquakes illustrate the reason for these differences.

At the fundamental internal structure frequency of 5.22 Hz, the structure natural frequency is aligned with the peak of the Melendy Ranch spectrum and high elastic response occurs. Both the Artificial and El Centro #5 spectra are between 17 to 25 percent lower than Melendy Ranch at this frequency and the seismic response loads should be lower than Melendy Ranch. Parkfield shows little spectral amplification in this frequency range, and seismic response loads 60 percent below Melendy Ranch results would be expected.

Similar trends are noted in the in-structure response spectra presented in Figure 3-9 through 3-12. In-structure response spectra for the Artificial, El Centro #5, and Melendy Ranch ground motions all exhibit

large amplification at the structure natural frequency of 5.22 Hz. Little amplification occurs for Parkfield because of the lack of earthquake frequency content in this region.

Peak overturning moments and the cracking moment at the base of the containment structure are presented in Table 3-1a. The cracking moment was determined in References 2 and 3 and is the moment which must be exceeded at the base of the containment to overcome structure deadweight and prestress forces such that cracking of the prestressed concrete shell occurs. Linear response of the containment is expected so long as seismic response moments do not exceed the cracking moment. Time history analysis results presented in Table 3-1a are lower than the cracking moment in all cases. Because the primary purpose of this study is to evaluate the effect of localized nonlinearities on overall response, the linear results determined for the containment structure are of little interest and will not be presented for the fixed base analyses.

In Table 3-2, a comparison of elastic internal structure seismic shear loads to the element yield shears, V_y, and Shear Demand/Capacity Ratios (i.e., ratio of elastic computed shear load to yield strength) are presented. These comparisons indicate that based on elastic analyses, nonlinear response of elements 16, 18 and 20 representing the bottom 3 shear walls of the internal structure would be expected for the Artificial, El Centro #5, and Melendy Ranch ground motions. Only minor yielding of the bottom two shear walls is indicated for Parkfield because of the much lower seismic response determined for this earthquake. In addition, elastic results indicate bond slip at the base of the internal structure occurs for all four earthquakes since the seismic response moment at the base of the internal structure presented in Table 3-1b exceeds the moment required to initiate bond slip, M_{bond}. However, no flexural inelastic behavior is expected because the flexural yield moments are not exceeded in any of the cases.

Based on elastic results, one would conclude Melendy Ranch is the most damaging of the four earthquakes studied since seismic response loads are highest for this case and substantially exceed the yield shear capacity. Relatively, severe damage would also be expected for both the Artificial and El Centro #5 ground motions based on similar comparisons. Because the seismic response loads for Parkfield are only slightly larger than the shear wall yield capacity, little inelasticity would be expected for this case. However, as discussed in the following section, these tentative conclusions based on elastic results are incorrect or misleading. Unless damage predictions adequately consider engineering characteristics of the ground motion such as earthquake duration, frequency content, and number of strong nonlinear response cycles, damage estimates developed based on elastic results can severely over-estimate the damage capability of the ground motion.

3.2 COMPARISON OF LINEAR AND NONLINEAR SEISMIC RESPONSE

3.2.1 Seismic Response Loads

Maximum nonlinear displacements and shears throughout the internal structure as determined from nonlinear time history analyses are presented in Figure 3-1 through 3-8. Shear story drift ductilities in the bottom two internal structure shear walls are tabulated in Table 3-3. In addition, total story drift ductilities based on both shear and flexural deformations are presented in this table for comparison. Seismic response moments are not shown since moment response for a cantilever type structure follows the shear loads and any conclusions developed based on the shear loads are also valid for the moments.

Results for the Artificial earthquake show large inelastic deformations occurring in the bottom two shear walls. These inelastic displacements shown is Figures 3-1, 3-3 etc., are almost entirely the result of inelastic shear wall behavior with little inelastic displacement response resulting from inelastic bond slip. Peak inelastic displacements at the top of the structure are about 65 percent larger

than elastic results. Shear story drift ductilities in the bottom two shear walls ranged from 10.8 to 11.9. Story drift ductilities calculated based on both shear and flexural deformations were slightly lower ranging from 8.7 to 10.9. Inelastic shears throughout the internal structure were reduced by 25 to 35 percent below elastic results due to yielding of the bottom shear walls protecting the remainder of the structure. Note that this beneficial protection due to shear wall inelasticity resulted in no nonlinear behavior in element 16 in contrast to the prediction of nonlinear behavior in this element from the elastic analysis results (Table 3-2). Very severe damage and probably collapse of the PWR internal structure is clearly indicated based on the large ductilities determined for the Artificial ground motion.

Results for the El Centro #5 earthquake indicate better performance of the structure is expected for this ground motion. Relatively large inelastic deformations occur in the lower shear walls resulting in shear story drift ductilities of 5.6 and 5.1 for the lower and upper yielding walls, respectively. Inelastic and elastic displacements at the top of the internal structure are about the same. Inelastic shears at the base of the internal structure are 34 percent lower than the corresponding elastic results. Story drift ductilities in the range of 4 to 6 indicate the structure is in the range of the onset of serious structural strength degradation and possible collapse after multiple nonlinear response cycles. For moderate duration ground motions such as El Centro #5 which ratchet the structure to these ductility levels through only 2 or 3 strong nonlinear response cycles collapse would be unlikely. However, for a longer duration record, rapid strength degradation of the shear walls would be expected under additional duration of ground motion.

Results for Parkfield indicate minor inelastic behavior of internal structure shear walls as evidenced by shear story drift ductilities of 3.2 and 2.0 for the lower and upper yielding walls, respectively. Total story drift ductilities determined for these members were approximately the same. Inelastic displacements at the top of the structure

were 40 percent larger than the linear results. Only slight damage of the PWR structure is expected at these low ductility levels.

Seismic response loads determined for Parkfield indicate little benefit occurs due to yielding of lower stories protecting the remainder of the structure. In the upper portion of the structure, inelastic shears slightly exceed elastic response while at the bottom of the internals, inelastic shears are 93 percent of elastic results. As the structure goes nonlinear, the fundamental internal structure frequency lowers and response is shifted upward on the Parkfield response spectrum (see Figure 2-7) resulting in increased seismic response. This effect negates beneficial hysteretic energy dissipation and protection of upper stories obtained through yielding of the lower shear walls.

Results for Melendy Ranch illustrate the opposite effect. In this case, the original structure frequency of 5.22 Hz is tuned to the peak of the elastic spectra. As nonlinear deformation occurs, the effective structure natural frequency is shifted off the spectrum peak to a region of low spectral amplification. Seismic response loads are greatly reduced as a result of this frequency shift.

Melendy Ranch results presented in Figures 3-7 and 3-8 demonstrate this effect. Significant inelastic displacements occur in the lowest two shear walls resulting in shear story drift ductilities ranging from 4.7 to 4.5. However, inelastic displacements at the top of the structure are only 75 percent of elastic results and inelastic shear loads only 45 to 50 percent of elastic results. The large reduction in inelastic shear loads and displacements is a combined result of yielding shear walls protecting the structure and shifting of structure response off the spectral peak.

The story drift ductilities of 4.7 and 4.5 determined for Melendy Ranch indicate the PWR internal structure is within the range of the onset of serious structural strength degradation. However, because

Melendy Ranch is a short duration earthquake with only one strong nonlinear response cycle, significant strength degradation of the shear walls would not be expected at this ductility level for the reasons discussed in Section 2.1 and additional capacity to resist seismic loads should be present.

A comparison of the inelastic time history analysis results for all four earthquake records studied indicated that providing the inelastic hinge element to account for additional rotation due to bond slip of reinforcing bars between the internal structure and foundation raft introduces only an additional 18 percent of rotation at the base of the internal structure in the worst case. This relatively small amount of additional flexibility is unimportant since shear is the significant response mode rather than flexure. As a result, inelastic bond slip does not contribute heavily to the maximum ductilities reached during seismic response and will not be further discussed.

3.2.2 In-Structure Response Spectra

Comparisons of linear and nonlinear in-structure response spectra at node 14 in the internal structure are presented in Figure 3-9 through 3-12. In general, large beneficial suppression of peak response occurs at the fundamental internal structure frequency of 5.22 Hz. Inelastic spectral peaks at this frequency typically are only 15 to 30 percent of elastic response. Below 4 Hz, some minor increased response occurs as the structure softens. However, except for the Artifical Earthquake between the 1.7 to 3.5 Hz frequency range, this increased response would generally be enveloped by the elastic results broadened by $\pm$ 15 percent on frequency at all locations. For the Artifical record, between 1.7 and 3.5 Hz, the inelastic spectra exceed the elastic results by a factor of 1.7 at the most and the elastic spectrum generally underpredicts inelastic spectral response by about 40 to 50 percent in this narrow frequency band. At higher frequencies, inelastic spectral response is generally below elastic results. Little spectral amplification at the structure fundamental frequency is noted for Parkfield due to the lack of frequency content of the input time history in this region.

3.3 CONCLUSIONS

Results for the Artificial earthquake clearly indicated that unacceptable structural performance is anticipated based on the high story drift ductilities determined for this earthquake. Shear story drift ductilities of between 10.5 and 11.9 for the Artificial record demonstrates that this ground motion contains sufficient energy content, duration, and number of strong nonlinear response cycles to ratchet the PWR internal structure to failure. It can be concluded that this low rise shear wall structure designed to a broadbanded, regulatory guide type response spectrum scaled to 0.2g maximum ground acceleration, is unlikely to survive an artificial time history in the 0.5g range which approximates the Reg. Guide 1.60 response spectrum.

Results for the three real earthquakes (i.e., El Centro #5, Parkfield, and Melendy Ranch) indicate damage in the structure would be in the permissible range or less as evidenced by the story drift ductilities determined for these ground motions. Marginally acceptable behavior of the PWR structure is expected for both El Centro #5 and Melendy Ranch scaled to 2.5 times the design ground motion of 0.2g. Good behavior of the internal structure is expected for Parkfield. Based on these results, it is concluded the Artificial earthquake approximating the Regulatory Guide 1.60 design spectrum is clearly more damaging than the three real earthquakes studied for this 5.2 Hz structure.

Seismic response loads in the PWR structure were reduced by nonlinear behavior for all ground motions studied except Parkfield. For this earthquake, as the structure softened due to shear wall yielding, the system response was shifted onto highly amplified regions of the response spectra negating beneficial reductions in seismic response loads due to localized inelasticity. This demonstrates that when a structure is located on the stiff side of the elastic spectral peak, local nonlinear yielding may not reduce responses and loadings elsewhere in the structure.

In the case of Melendy Ranch excitation, the internal structure was tuned to the elastic spectral peak. As the structure softened due to inelastic shear yielding, seismic response loads rapidly decreased as the structure shifted onto a region of greatly reduced spectral amplification. Damage capability predictions based on elastic response would have estimated that the Melendy Ranch record was the most severe of the four earthquakes studied, when in fact, it is one of the least damaging. Thus, an accurate engineering characterization of short duration records such as Parkfield or Melendy Ranch must retain the frequency content of the record. Damage predictions based on a broad-banded, regulatory guide type response spectra will generally result in substantial overprediction of the damage capability of short duration earthquakes.

Based on limited comparison of inelastic and elastic in-structure response spectra high in the internal structure, inelastic shear wall behavior results in large reductions of the elastic spectral peak at 5.22 Hz. Appropriate consideration of inelastic structure behavior should be used to determine realistic in-structure response spectra when higher than designed for ground motions are evaluated.

TABLE 3-1

FIXED BASE ANALYSIS PWR PEAK OVERTURNING MOMENTS

a) Moments At Base Of Containment Structure

Earthquake	Seismic Moment (in-lb)	Cracking Moment[1] (in-lb)
Artificial	6.32×10^{10}	9.38×10^{10}
El Centro #5	6.45×10^{10}	9.38×10^{10}
Parkfield	3.92×10^{10}	9.38×10^{10}
Melendy Ranch	6.72×10^{10}	9.38×10^{10}

(1) From Reference 2

b) Moments At Base Of Internal Structure

Earthquake	Seismic Moment (in-lb)	M_{bond}[2] (in-lb)	Yield Moment[3] (in-lb)
Artificial	3.82×10^{10}	7.70×10^{9}	6.29×10^{10}
El Centro #5	3.13×10^{10}	7.70×10^{9}	6.29×10^{10}
Parkfield	1.50×10^{10}	7.70×10^{9}	6.29×10^{10}
Melendy Ranch	4.32×10^{10}	7.70×10^{9}	6.29×10^{10}

(2) See Figure 2-6

(3) From Reference 2

TABLE 3-2

ELASTIC FIXED BASE ANALYSIS INTERNAL STRUCTURE RESULTS FOR EARTHQUAKE EXCITATION SCALED TO 0.5g PEAK GROUND ACCELERATION

a) Shear Loads

Element	Yield Shear V_y (lbs.)	Seismic Response Shears (lbs.)			
		Artificial	El Centro #5	Parkfield	Melendy Ranch
13	1.66×10^7	3.05×10^6	2.51×10^6	9.50×10^5	3.55×10^6
14	3.48×10^7	2.17×10^7	1.79×10^7	8.19×10^6	2.48×10^7
15	4.01×10^7	3.30×10^7	2.71×10^7	1.35×10^7	3.72×10^7
16	3.12×10^7	4.02×10^7	3.30×10^7	1.77×10^7	4.51×10^7
18	1.73×10^7	4.47×10^7	3.67×10^7	2.09×10^7	4.98×10^7
20	1.73×10^7	4.62×10^7	3.79×10^7	2.24×10^7	5.13×10^7

b) Demand to Capacity Ratios

Element	Story Demand/Capacity Ratio			
	Artificial	El Centro #5	Parkfield	Melendy Ranch
13	0.18	0.15	0.06	0.21
14	0.62	0.51	0.24	0.71
15	0.82	0.68	0.34	0.93
16	1.29	1.06	0.57	1.45
18	2.58	2.12	1.21	2.88
20	2.67	2.19	1.29	2.97

[ ] = Walls for which inelastic response is expected based on elastic results

TABLE 3-3

FIXED BASE ANALYSIS STORY DRIFT DUCTILITIES FOR
EARTHQUAKE EXCITATION SCALED TO 0.5g PEAK GROUND ACCELERATION

a) Shear Story Drift Ductility

Shear Wall Location	Shear Story Drift Ductility			
	Artificial	El Centro #5	Parkfield	Melendy Ranch
Elevation 0' to Elevation 13' - 5"	11.9	5.6	3.2	4.7
Elevation 13' - 5" to Elevation 25' - 4"	10.8	5.1	2.0	4.5

b) Total Story Drift Ductility

Shear Wall Location	Total Story Drift Ductility			
	Artificial	El Centro #5	Parkfield	Melendy Ranch
Elevation 0' to Elevation 13' - 5"	10.9	5.1	3.1	4.4
Elevation 13' - 5" to Elevation 25' - 4"	8.7	4.0	1.8	3.2

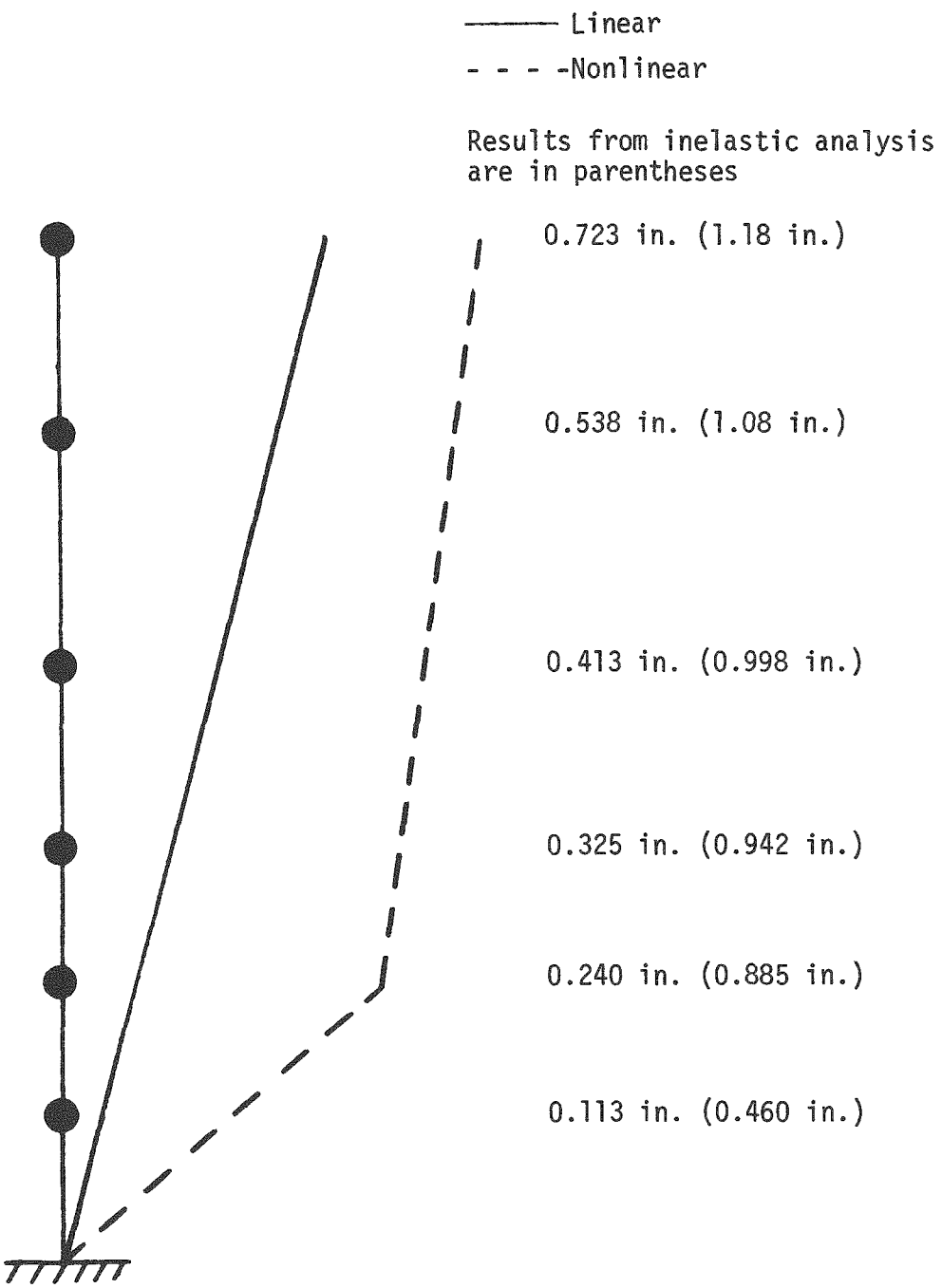

FIGURE 3-1. COMPARISON OF MAXIMUM ELASTIC AND INELASTIC INTERNAL STRUCTURE DISPLACEMENTS FOR THE ARTIFICIAL EARTHQUAKE (0.5g)

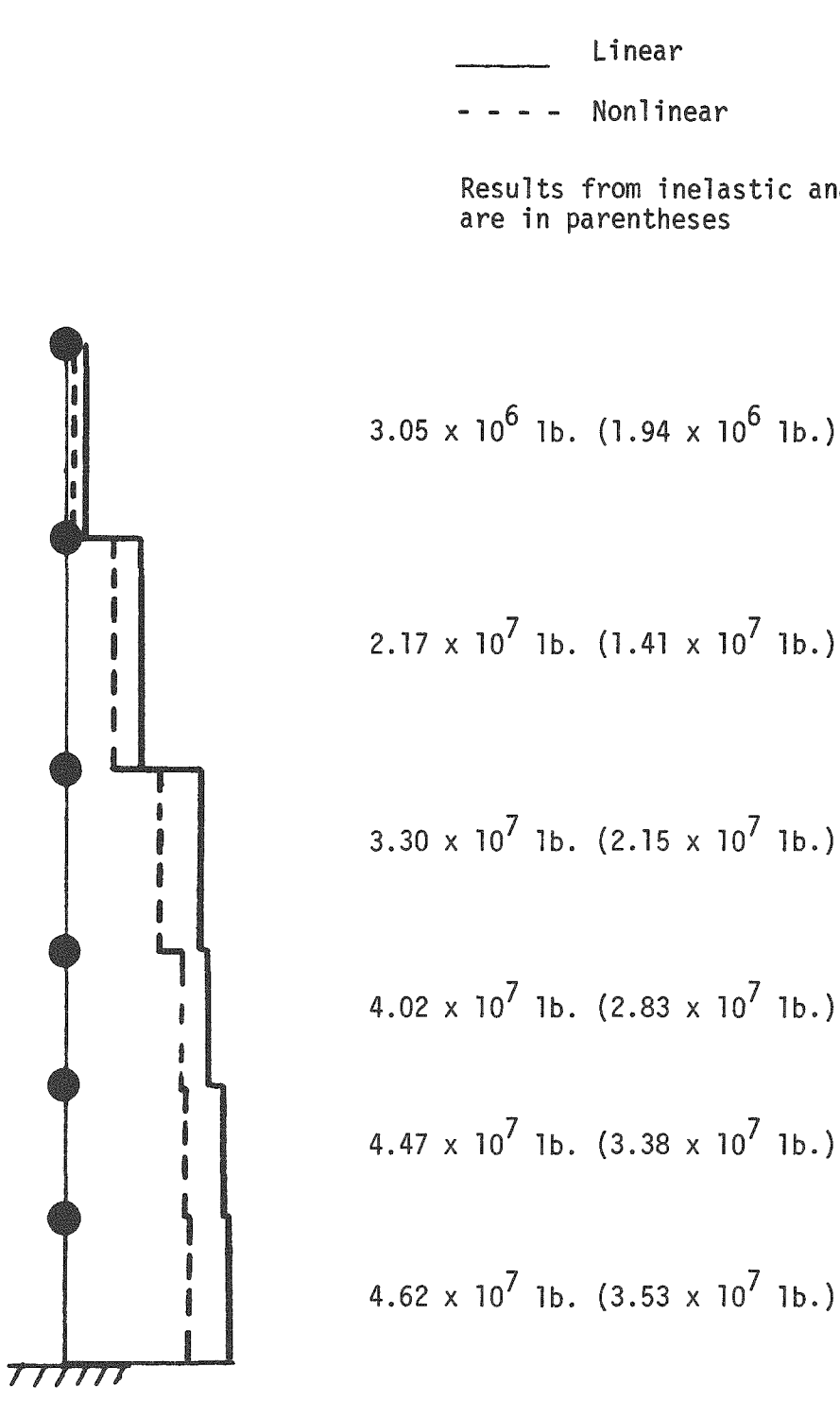

FIGURE 3-2. COMPARISON OF MAXIMUM ELASTIC AND INELASTIC INTERNAL STRUCTURE SHEARS FOR THE ARTIFICIAL EARTHQUAKE (0.5g)

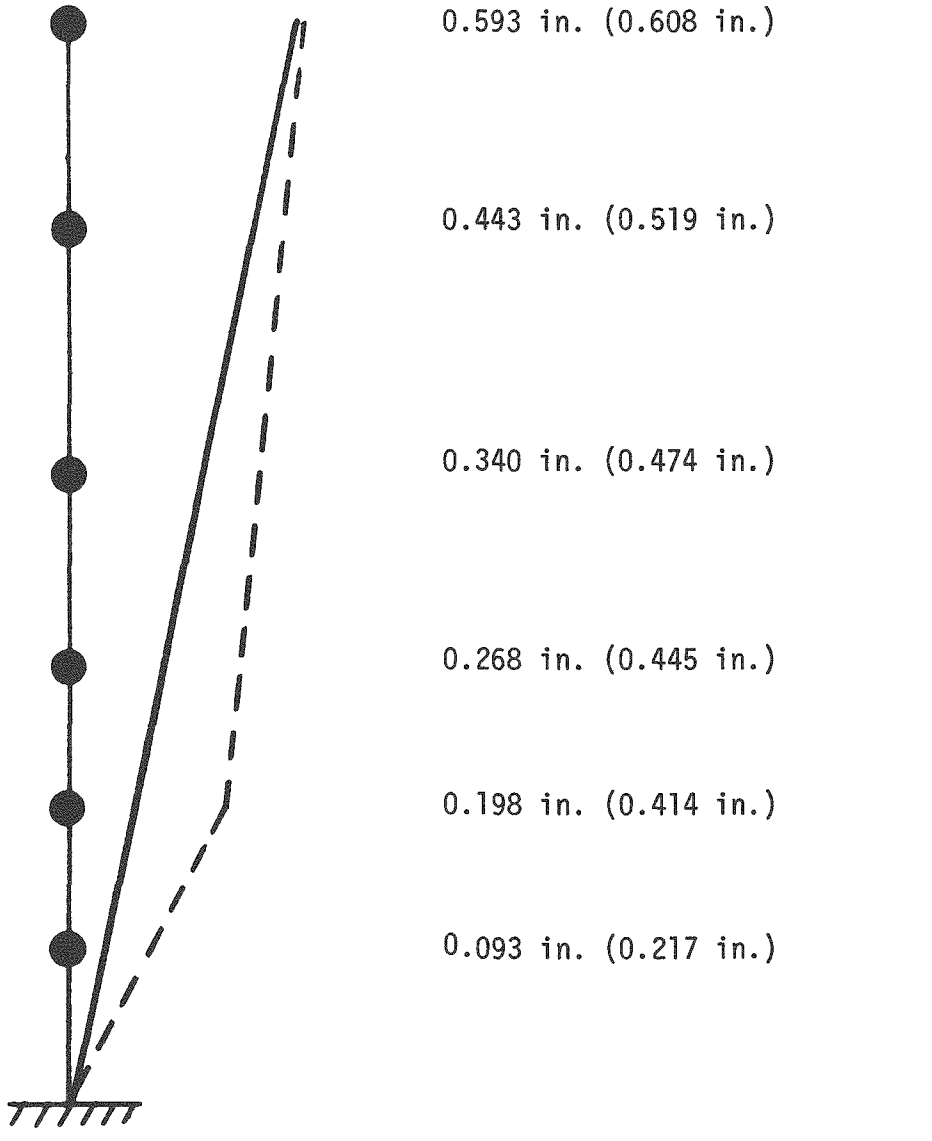

FIGURE 3-3. COMPARISON OF MAXIMUM ELASTIC AND INELASTIC INTERNAL STRUCTURE DISPLACEMENTS FOR THE EL CENTRO #5 EARTHQUAKE (0.5g)

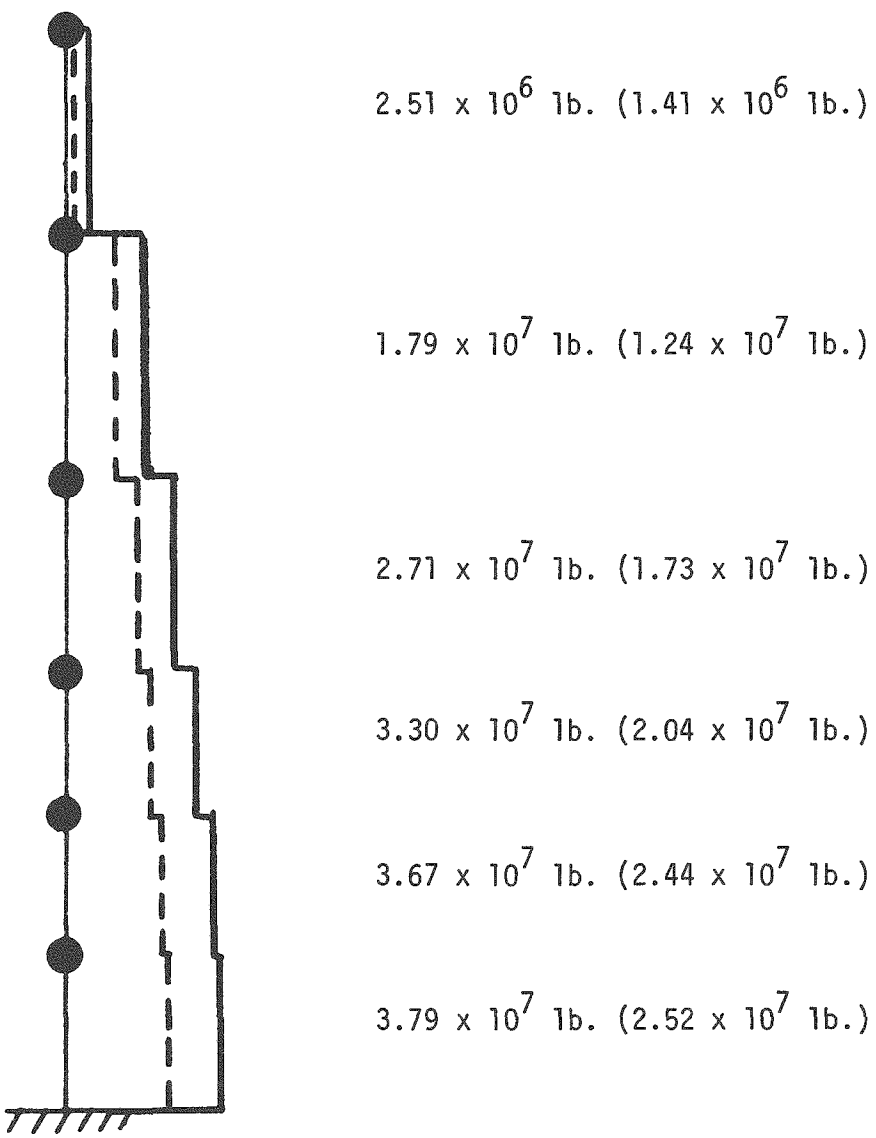

FIGURE 3-4. COMPARISON OF MAXIMUM ELASTIC AND INELASTIC INTERNAL STRUCTURE SHEARS FOR THE EL CENTRO #5 EARTHQUAKE (0.5g)

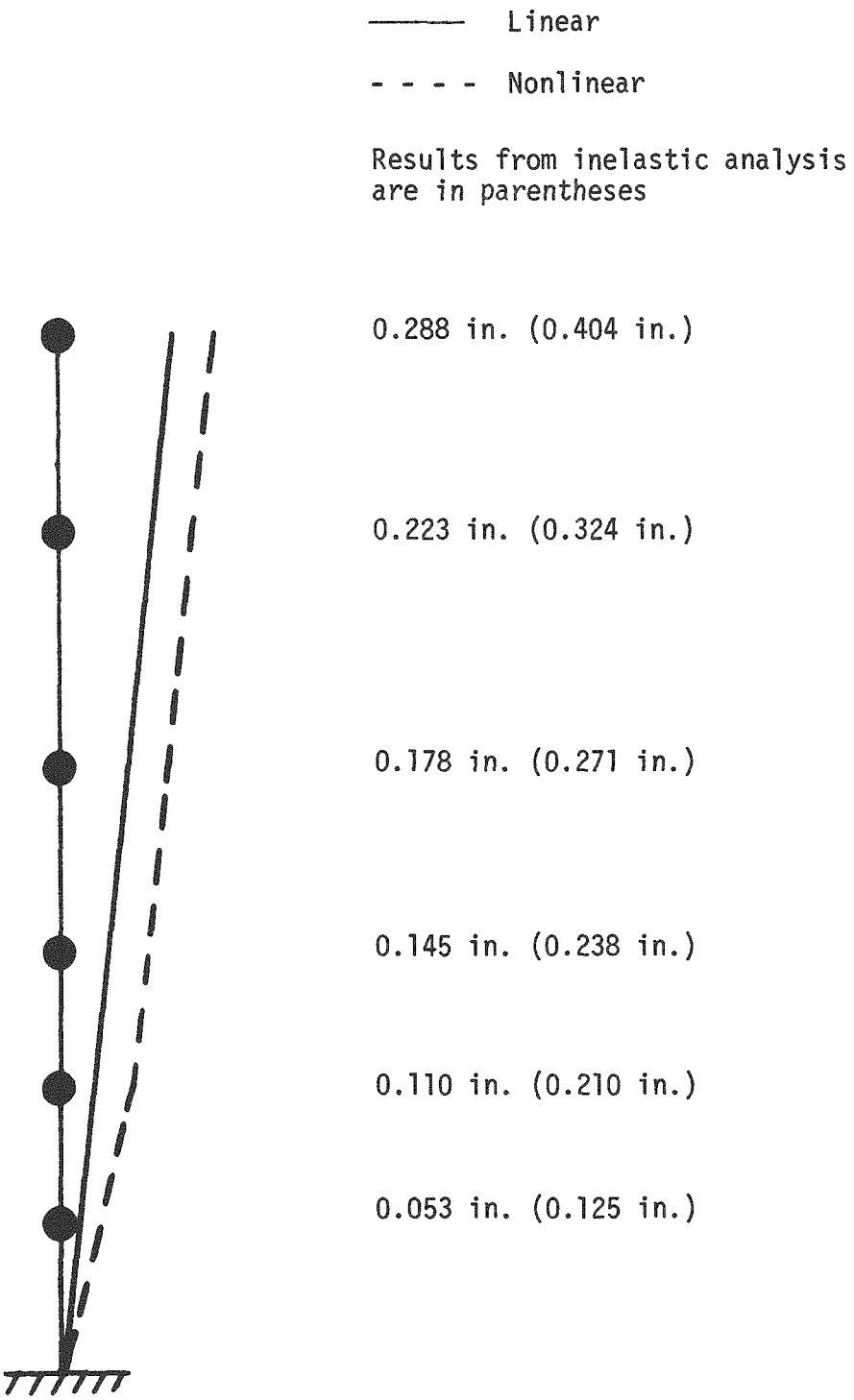

FIGURE 3-5. COMPARISON OF MAXIMUM ELASTIC AND INELASTIC INTERNAL STRUCTURE DISPLACEMENTS FOR THE PARKFIELD EARTHQUAKE (0.5g)

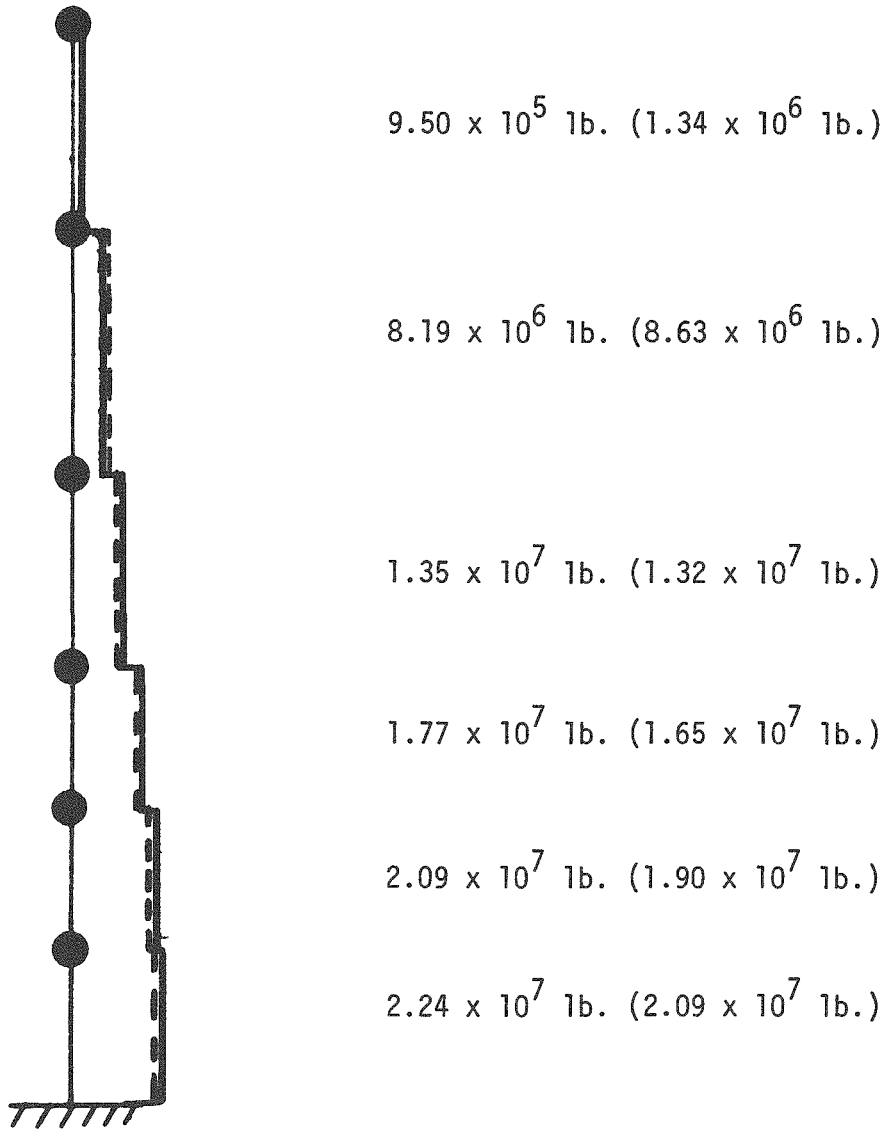

FIGURE 3-6. COMPARISON OF MAXIMUM ELASTIC AND INELASTIC INTERNAL STRUCTURE SHEARS FOR THE PARKFIELD EARTHQUAKE (0.5g)

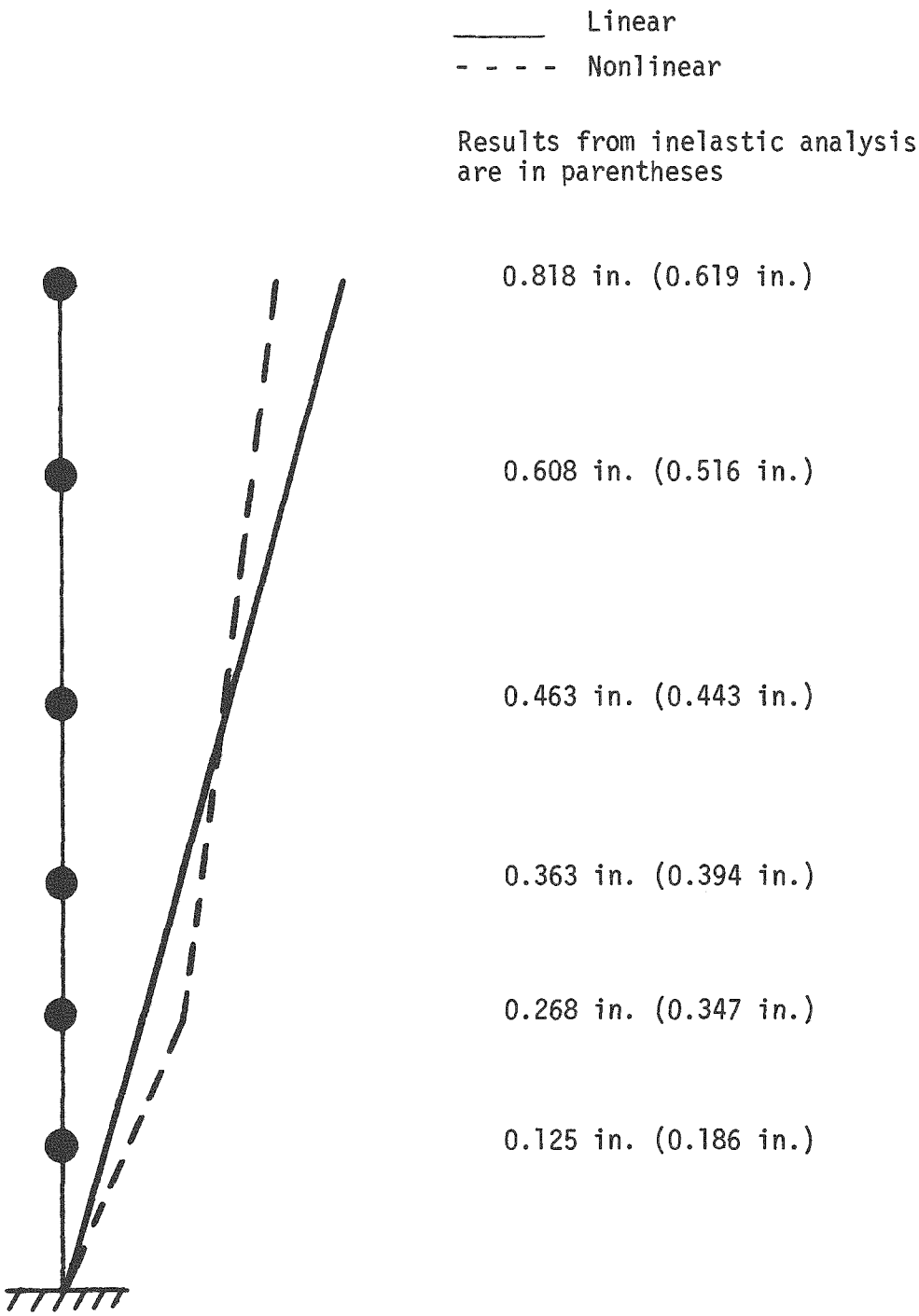

FIGURE 3-7. COMPARISON OF MAXIMUM ELASTIC AND INELASTIC INTERNAL STRUCTURE DISPLACEMENTS FOR THE MELENDY RANCH EARTHQUAKE (0.5g)

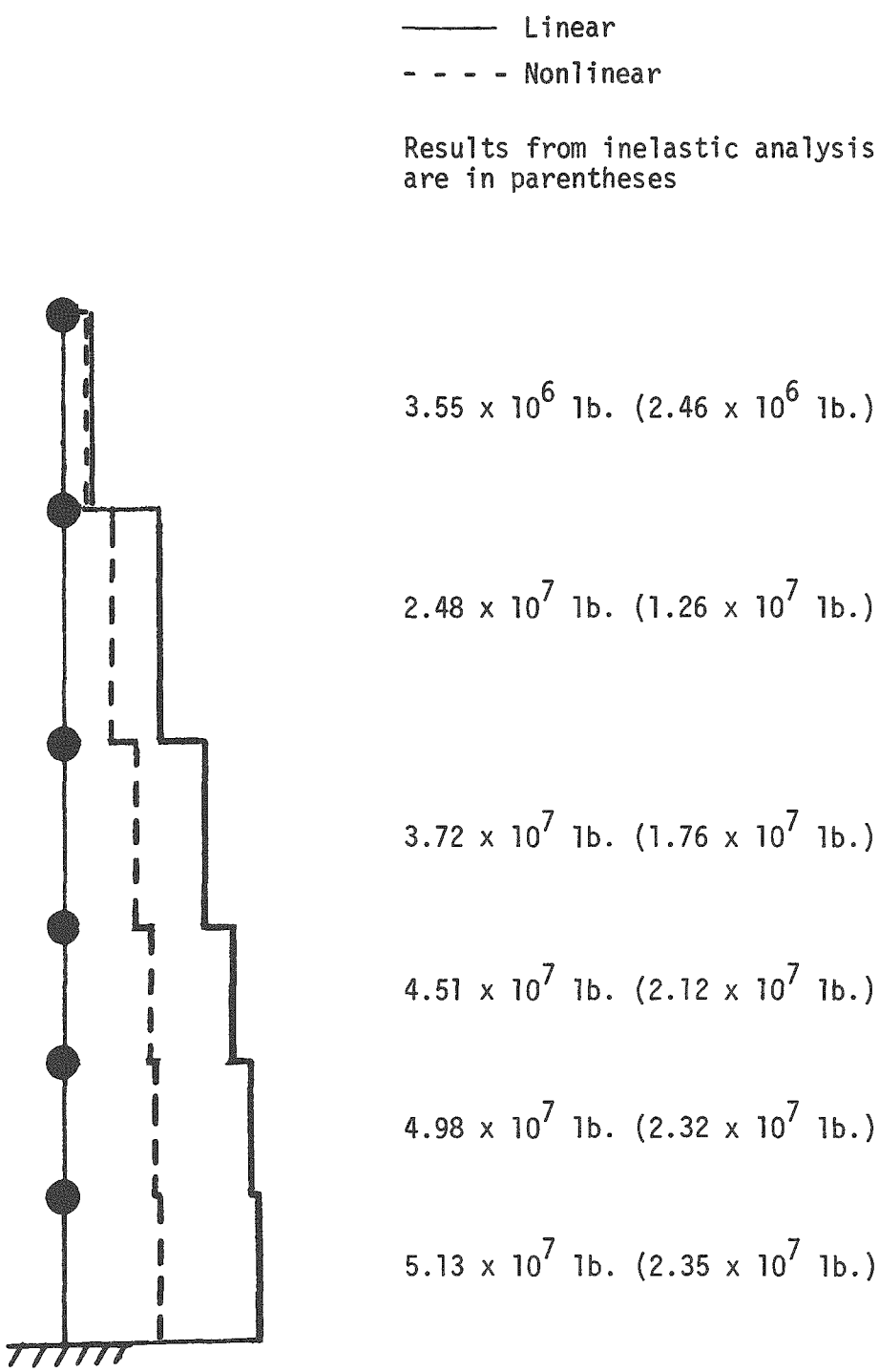

FIGURE 3-8. COMPARISON OF MAXIMUM ELASTIC AND INELASTIC INTERNAL STRUCTURE SHEARS FOR THE MELENDY RANCH EARTHQUAKE (0.5g)

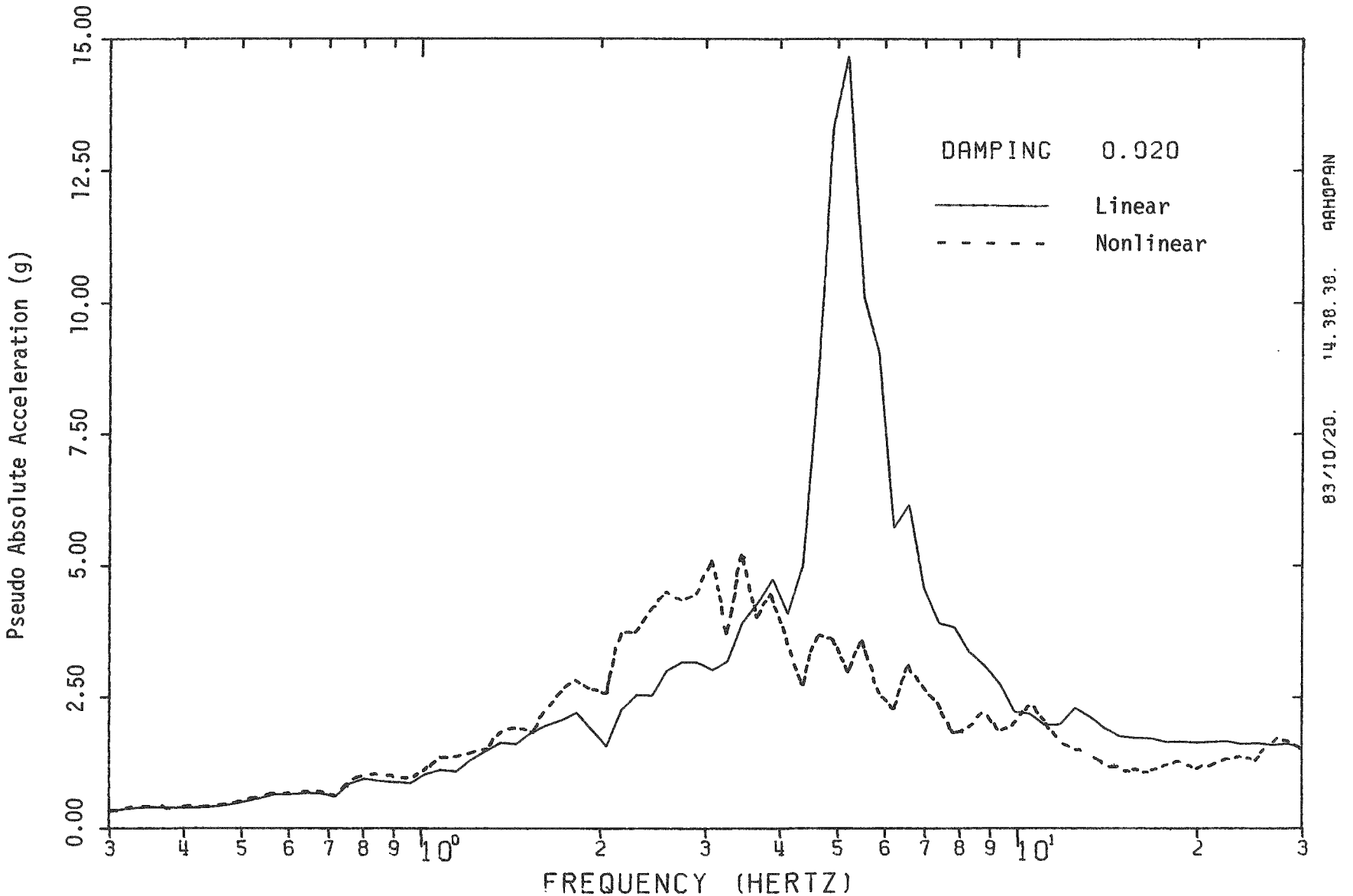

FIGURE 3-9. COMPARISON OF ELASTIC AND INELASTIC IN-STRUCTURE RESPONSE SPECTRA AT NODE 14 IN INTERNAL STRUCTURE FOR ARTIFICIAL EARTHQUAKE (0.5g), FIXED BASE MODEL

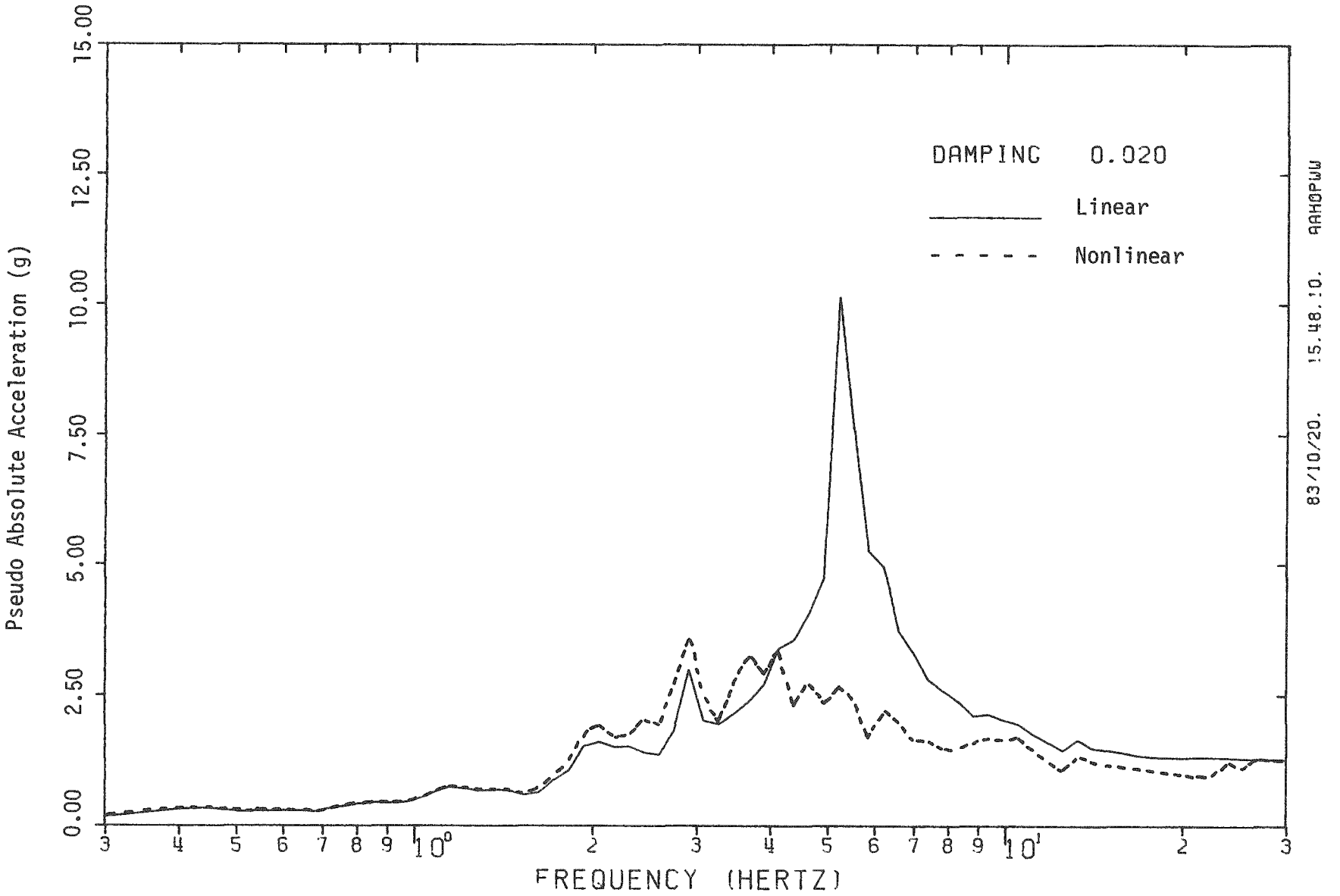

FIGURE 3-10. COMPARISON OF ELASTIC AND INELASTIC IN-STRUCTURE RESPONSE SPECTRA AT NODE 14 IN INTERNAL STRUCTURE FOR EL CENTRO #5 EARTHQUAKE (0.5g), FIXED BASE MODEL

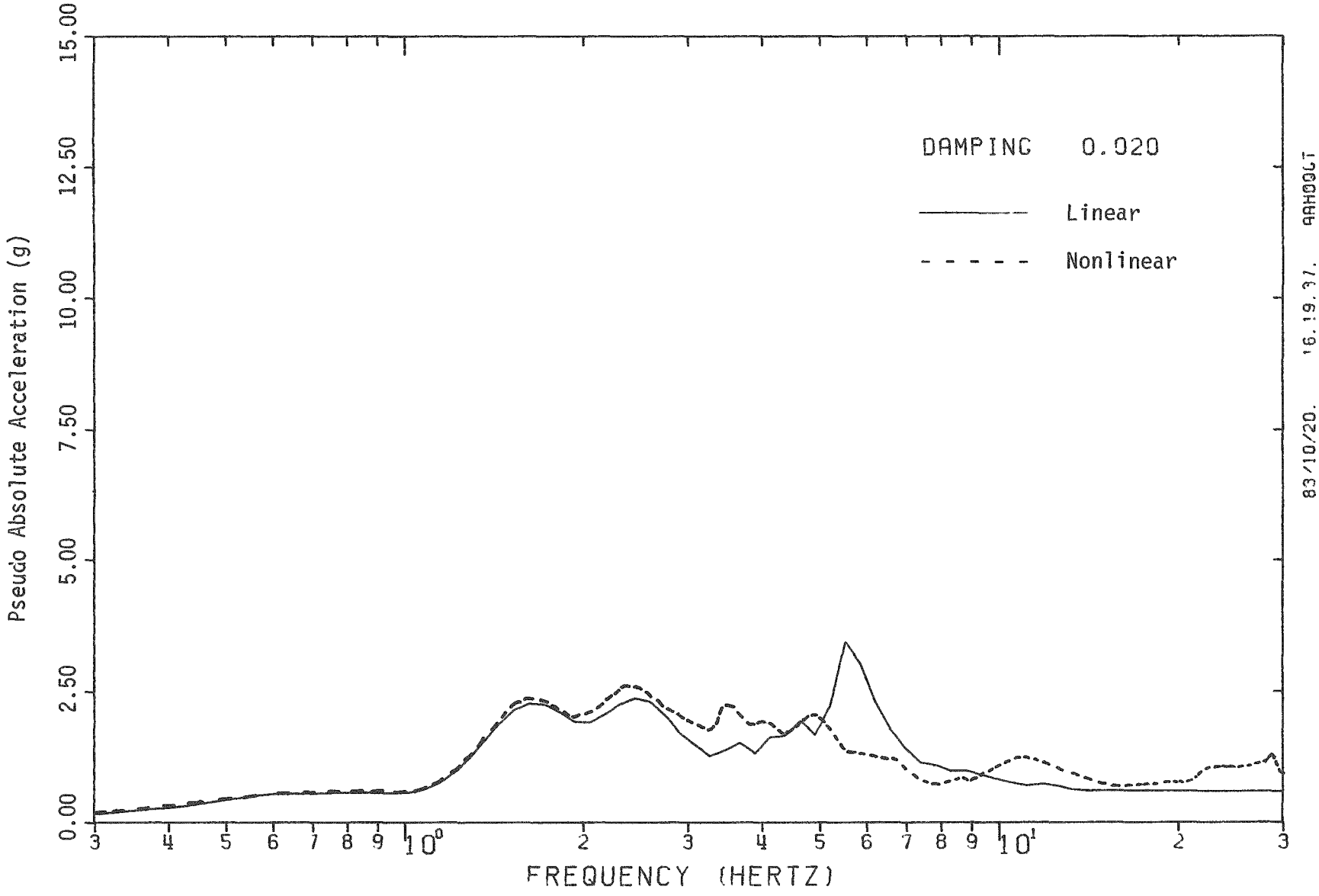

FIGURE 3-11. COMPARISON OF ELASTIC AND INELASTIC IN-STRUCTURE RESPONSE SPECTRA AT NODE 14 IN INTERNAL STRUCTURE FOR PARKFIELD EARTHQUAKE (0.5g), FIXED BASE MODEL

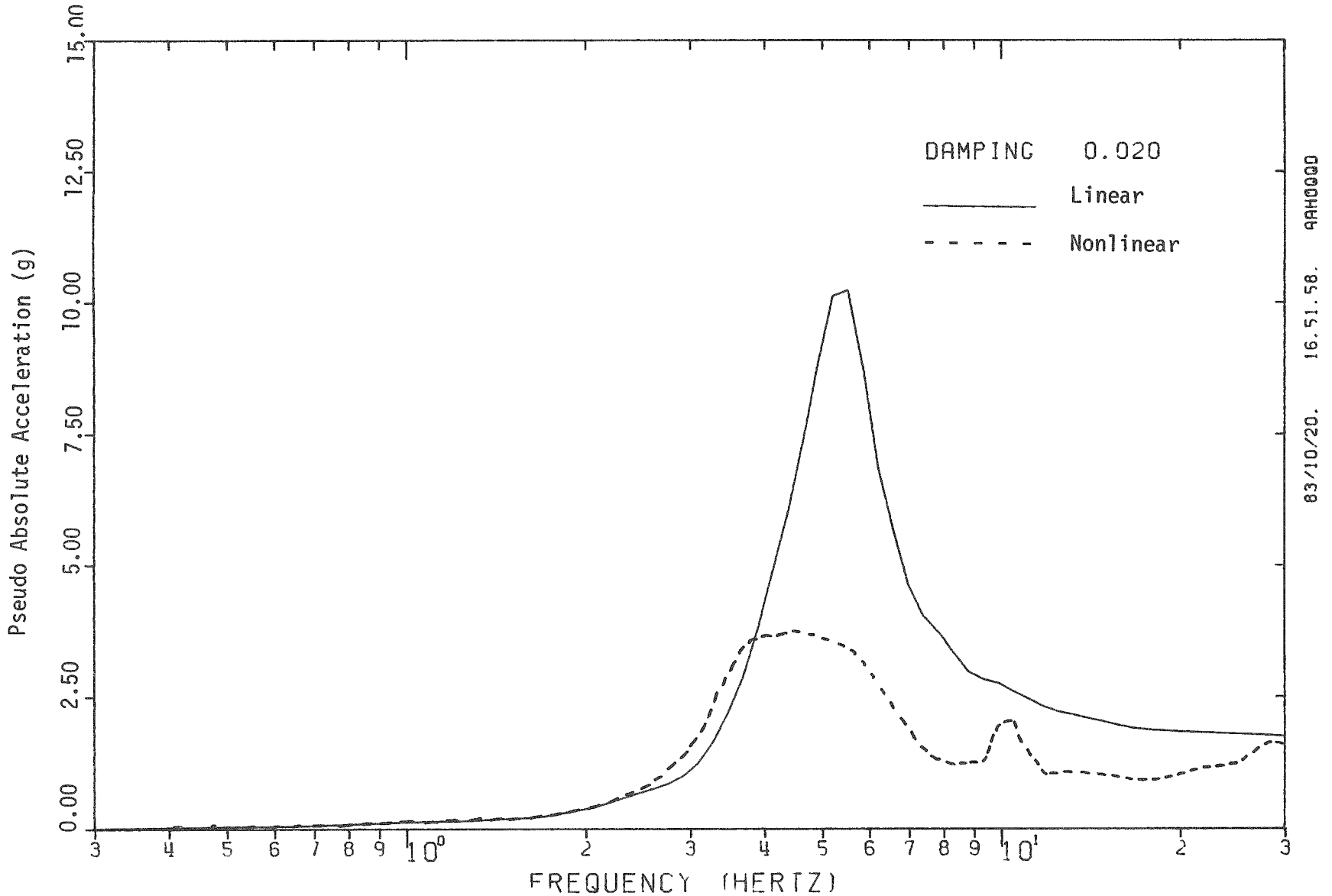

FIGURE 3-12. COMPARISON OF ELASTIC AND INELASTIC IN-STRUCTURE RESPONSE SPECTRA AT NODE 14 IN INTERNAL STRUCTURE FOR MELENDY RANCH EARTHQUAKE (0.5g), FIXED BASE MODEL

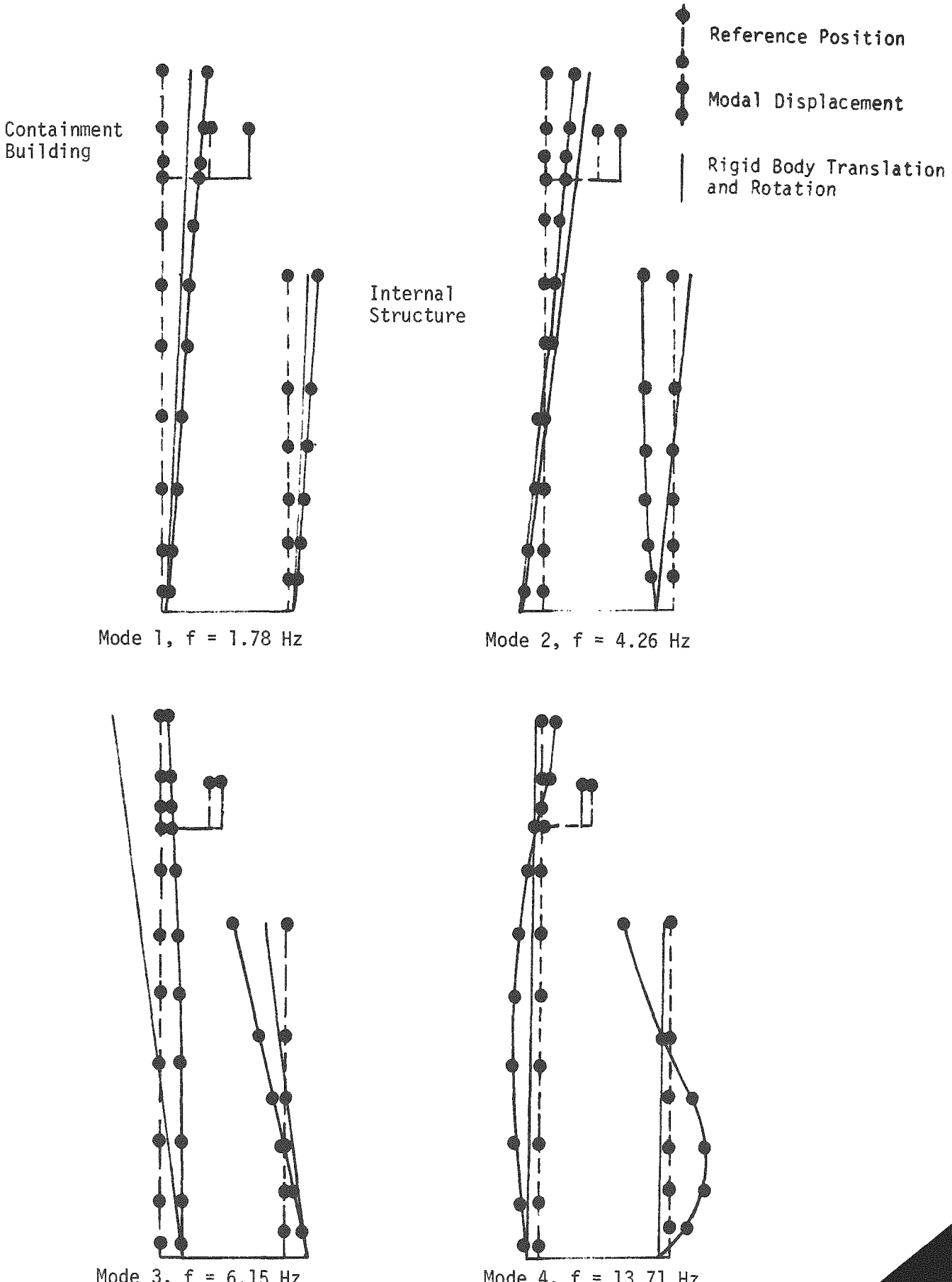

FIGURE 2-14. MODE SHAPES AND FREQUENCIES, INTERMEDIATE SOIL PROFILE

4. SOIL-STRUCTURE INTERACTION ANALYSES

4.1 FACTORS INFLUENCING SOIL-STRUCTURE INTERACTION RESULTS

Consideration of soil-structure interaction in evaluating PWR seismic response leads to substantially different loads and story drift ductilities as compared to fixed base results. Section 4.2.4 presents a comparison of PWR linear and nonlinear response for the fixed base, stiff, and intermediate soil profiles to quantify these differences. However, many of the factors contributing to these differences are important to understanding linear and nonlinear soil-structure interaction results and will be introduced here.

Two of the most important effects of soil-structure interaction are the frequency of the soil-structure system and dynamic feedback from structure into the surrounding soil. Consideration of soil stiffness reduces the overall system frequency below the fixed base structure frequency. For long duration ground motions with broad frequency content, this frequency shift does not significantly change the loads experienced by the structure since the response spectrum is constant in this region. However, for narrow banded response spectra such as Parkfield or Melendy Ranch, structural response can dramatically increase or decrease depending on whether the system frequency is in resonance with a spectral peak.

Inertial dynamic feedback from the structure into the surrounding soil tends to radiate energy away from the structure decreasing response. This effect typically becomes more important as the site conditions beneath the structure soften. In some instances however, such as when there is a large impedance mismatch between two soil layers, energy may become entrapped between the structure and a deeper layer resulting in less energy radiated away from the foundation.

Other factors which tend to generally reduce structural response include kinematic interaction between the foundation and surrounding soil causing wave scattering of the impinging ground motion. Embedment effects tend to reduce the ground motion experienced by the structures since the input motion typically reduces with depth. Nonlinear response of the structure due to basemat uplift also reduces response somewhat. However, References 2 and 3 demonstrated that for the PWR dynamic model used in this study, results determined considering nonlinear basemat uplift were within 15 percent or less of linear shears, moments, and in-structure response spectra. It was concluded in References 2 and 3 a linear seismic analysis of the PWR structure was adequate for structural design even if significant uplift of the foundation is anticipated. Therefore, basemat uplift is not considered to be a significant factor influencing PWR response and is not considered in this study.

4.2 LINEAR SEISMIC RESPONSE

Tables 4-1 and 4-2 present seismic shear loads determined from elastic time history analyses at the base of the internal structure and containment structure, respectively, for both the intermediate and stiff soil profiles. Figures 4-1 through 4-8 present the corresponding peak displacement diagrams for the PWR structure. Peak moments at the base of the internal structure and containment building are presented in Table 4-3.

Comparisons of seismic shear loads and peak displacements for the intermediate soil profile indicate that maximum linear response is obtained under Parkfield excitation. Seismic shears determined for Parkfield at the base of the internal structure are 36 percent larger than those obtained from the Artificial record and over 120 percent larger than those determined from either El Centro #5 or Melendy Ranch. Similar trends are noted in the peak displacements presented in Figures 4-1 through 4-4 and in containment shear loads presented in Table 4-2. Examination of the Parkfield response spectrum presented in Figure 2-7 indicates these results are reasonable since, at the fundamental soil-structure frequency of 1.78 Hz, the structure is tuned to the peak of the elastic spectrum.

Similar results are noted for the stiff soil profile. For this case, peak internal structure seismic shear loads determined for Parkfield are 14 percent, 65 percent, and 211 percent larger than the loads determined from the Artificial, El Centro #5, and Melendy Ranch base excitations, respectively. Peak displacements and shears at the base of the containment structure exhibit these same general trends. Comparison of the elastic spectra presented in Figure 2-7 at the structure fundamental frequency of 2.62 Hz indicate that based on only first mode response, similar behavior would be expected for both Parkfield and Artificial ground motion. Significantly lower response would be expected for both Melendy Ranch and El Centro #5 because of reduced spectral amplification of these time histories in this frequency range.

Peak overturning moments at the base of the containment structure are presented in Table 4-3. In all cases, the seismic response moments are lower than the cracking moment required to overcome structure dead-weight and prestress forces such that elastic response of the containment occurs. Comparisons of seismic response moments to the yield moments for all internal structure elements were also conducted and demonstrated linear moment response of the internal structure occurs in all cases.

A comparison of internal structure seismic shear loads for the bottom two shear walls between Elevation 0' and Elevation 25'-4" to the yield shear for both the intermediate and stiff soil profiles are presented in Table 4-1. For the intermediate soil case, very limited inelastic shear yielding behavior is expected for the Artificial earthquake. Significantly more inelastic behavior is expected for Parkfield based on the high elastic shear loads. No nonlinear response will occur for either El Centro #5 or Melendy Ranch since elastic shear loads are below yield in both cases.

Significantly more nonlinear behavior is expected for the stiff soil profile. Based on a comparison of elastic seismic shear loads, the largest inelastic response is expected for Parkfield followed by the Artificial and El Centro #5 earthquakes. Nonlinear shear response will not occur for Melendy Ranch since elastic seismic shears are below yield.

The peak elastic overturning moments at the base of the internal structure is compared to the bond slip moment, M_{bond}, in Table 4-3. These results indicate minor bond slip nonlinearity is expected for the Artificial and Parkfield ground motions for the intermediate soil profile. For the stiff soil profile, bond slip inelasticity is expected for Artificial, El Centro #5, and Parkfield excitations. No significant bond slip will occur for the remaining cases because of the low moment response of the internal structure.

4.3 COMPARISON OF LINEAR AND NONLINEAR SOIL-STRUCTURE INTERACTION RESULTS

Maximum nonlinear displacements throughout the PWR structure as determined from nonlinear time history analyses are presented in Figures 4-1 through 4-8. Comparisons of maximum linear and nonlinear shears at the base of the internal structure and containment structure are presented in Tables 4-1 and 4-2, respectively. Maximum shear story drift ductilities are presented in Table 4-4. Selected in-structure response spectra for the PWR building are presented in Figures 4-9 and 4-10.

For the intermediate soil profile, maximum nonlinear response occurs under Parkfield excitation. At the top of the internal structure, nonlinear displacements are about 10 percent larger than elastic results. Inelastic shears at the base of the internal structure exceed elastic loads by 5 percent. Maximum shear story drift ductilities of 6.3 and 5.3 were determined in the lower and upper yielding shear walls for Parkfield. At these ductility levels, the PWR structure is expected to be at the onset of significant strength degradation of the shear walls leading to rapidly increasing displacement ductilities for longer strong motion durations.

Under Artificial excitation, little nonlinear response of the PWR structure occurs as evidenced by the low story drift ductility of 1.2 determined for this record. Inelastic and elastic shears and displacements are virtually identical for this case. No observable damage in PWR internal structure would be expected for these low required ductilities. Nonlinear time history analyses were not conducted for either El Centro #5 or Melendy Ranch ground motions since the structure remained elastic.

For the stiff soil profile, significantly more nonlinear response of the PWR structure is seen as evidenced by the story drift ductilities tabulated in Table 4-4. Under Artificial excitation, maximum story drift ductilities of 9.2 and 7.8 were observed in the lower and upper yielding shear walls, respectively. Inelastic shears at the base of the containment structure are slightly reduced below elastic results while at the base of the internals nonlinear shears exceed the corresponding elastic results by about 10 percent.

Similar results are noted for Parkfield. Story drift ductilities ranged from 12.9 in the bottom shear wall to 11.4 in the upper shear wall. Inelastic displacements at the top of the internal structure exceed elastic results by 42 percent. At the base of the containment structure, inelastic shear loads are 8 percent lower than elastic results while at the base of the internals inelastic shears exceed elastic shears by about 10 percent. Unacceptable performance of the PWR structure would be expected for both Parkfield and Artificial ground motions based on the large required story drift ductilities.

Nonlinear displacements and shears in the PWR structure remained essentially unchanged from elastic results for El Centro #5 excitation. Only minor inelastic yielding occurred in bottom structural shear walls as evidenced by the peak story drift ductility of 1.7 determined for this case. Nonlinear time history analyses were not conducted for Melendy Ranch since elastically calculated shear loads were less than shear wall yield capacities.

Minor increases in internal structure inelastic shears as compared to elastic results were observed for Parkfield excitation for the intermediate soil profile and for both Artificial and Parkfield excitation for the stiff soil profile. These three cases all experienced significant inelasticity with calculated story drift ductilities of 6 or greater at the base of the internal structure. The increased response for these high ductility cases is due to the structure softening and moving closer to the frequency of the overall soil-structure system. Additional seismic response of the system results from dynamic amplification due to system resonance. Minor decreases in inelastic seismic shears are noted for all cases where story drift ductilities are low and increased amplification does not occur since sufficient softening of the internal structure has not occurred.

The lack of beneficial reduction in load at other locations due to structural inelasticity may also be noted in the in-structure response spectra determined for the PWR reactor building for the soil-structure interaction cases evaluated. Previous results for the fixed base analyses demonstrated inelastic results generally suppressed the large elastic spectral peak. Typical results presented in Figures 4-9 and 4-10 for the stiff soil profile, Parkfield excitation, do not show this effect.

For the stiff profile, at the fundamental structure frequency of 2.62 Hz, the peak spectral response at node 4 on the containment structure is reduced by about 25 percent as a result of internal structure shear wall yielding. Inelastic and elastic in-structure response spectra are virtually identical at all other frequencies. At node 14 in the internals, inelastic spectral response increases slightly as the structure frequency lowers and response is shifted towards resonance with the fundamental soil-structure frequency. Thus, for the soil-structure interaction cases studied, it appears little beneficial suppression of elastic in-structure response spectrum peaks occurs as a result of shear wall yielding.

In summary, results for Parkfield demonstrated collapse of the internal structure is probable when the PWR studied is situated on the stiff soil profile. Significant strength degradation short of collapse is expected for Parkfield because of the short duration of this record when the structure is sited on the intermediate profile. The very large required story drift ductilities determined for these cases are due to the soil-structure fundamental frequency being aligned with the peak of the Parkfield spectrum. The higher observed ductilities of 12.9 and 11.4 for the stiff soil profile are a consequence of the soil-structure fundamental frequency of 2.62 Hz being aligned at the high frequency end of the Parkfield spectrum peak presented in Figure 2-7. As the structure softens, the fundamental soil-structure frequency lowers but remains aligned with the spectrum peak during this frequency shift. This would not be the case for the intermediate soil profile since the fundamental soil-structure frequency would tend to shift off the peak as the structure went nonlinear. In addition, the second mode frequency of 4.84 Hz also is reduced and begins to shift internal structure response upward onto more highly amplified regions of the Parkfield spectrum resulting in large ductilities for this case.

For the long duration Artificial time history, large story drift ductilities were determined for the stiff soil profile. Essentially elastic response was calculated for the intermediate soil profile. A comparison of the linear internal structure base shears indicates that results for the stiff soil profile were about 54 percent higher than for the intermediate soil profile. However, a comparison of elastic spectral accelerations from the free-field response spectrum presented in Figure 2-7 at the corresponding fundamental frequencies of 2.62 and 1.78 Hz for the stiff and intermediate soil profiles indicates the Artificial time history response spectrum is relatively constant in this region. Thus, it is surmised that the substantially lower loads predicted for the intermediate soil profile are due to beneficial aspects of soil-structure interaction such as wave-scattering due to kinematic interaction, structure embedment, and soil radiation damping from structure inertial interaction.

These factors become very important for soft sites and protect the PWR structure from higher than designed for ground motion with little inelasticity occurring in the structure.

Results for the El Centro #5 earthquake showed good performance of the PWR structure was expected for both the intermediate and stiff soil cases. The low required story drift ductilities determined for these cases are primarily due to the beneficial aspects of soil-structure interaction discussed in Section 4.1.

No nonlinear response of the PWR structure was determined for Melendy Ranch. For both soil cases evaluated, the most significant factor reducing response appears to be that the low fundamental soil-structure frequency had shifted structure response to a deamplified acceleration region of the Melendy Ranch spectrum.

4.4 SUMMARY OF FIXED BASE AND SOIL-STRUCTURE INTERACTION ANALYSES OF PWR STRUCTURE

The previous section compared linear and nonlinear soil-structure interaction results for the PWR reactor building. This section summarizes fixed base and soil-structure interaction results in order to demonstrate the reductions in fixed base seismic response loads which may occur when the beneficial aspects of soil-structure interaction are properly considered.

Comparisons of linear and nonlinear seismic shear loads at the base of the internal structure for the fixed base, stiff soil profile, and intermediate soil profile are presented in Table 4-5. Comparisons of linear seismic response results indicate that, with the exception of Parkfield, large beneficial reductions occur in the seismic shear loads when soil-structure interaction effects are considered. For example, shear loads determined for the stiff soil profile are 61 percent, 51 percent, and 20 percent of the shear loads determined for the fixed base case for the Artificial, El Centro #5, and Melendy Ranch earthquakes,

respectively. Elastic results for the intermediate soil profile demonstrate even larger reductions in anticipated shear loads.

For long duration earthquakes such as the Artificial and El Centro #5, these reductions are almost entirely due soil-structure interaction effects such as earthquake wave scattering, structure embedment, and soil radiation damping, since the fundamental structure frequency is located in an approximately constant acceleration region of input spectrum. For Melendy Ranch, these reductions are a combined effect which account for inertial and kinematic interaction of the structure and surrounding soil and shifting of the fundamental frequency away from the spectral peak. In the case of Parkfield, consideration of soil-structure interaction increased loads as a result of shifting the system fundamental frequency onto highly amplified regions of the spectra as demonstrated for the stiff soil profile where seismic response loads were 43 percent larger than fixed base results.

The nonlinear seismic shear loads presented in Table 4-5 show the same general trends. For the stiff soil profile, seismic shears are 88 percent, 73 percent, 180 percent and 44 percent of the loads determined for the fixed base case for the Artificial, El Centro #5, Parkfield and Melendy Ranch ground motions, respectively. With the exception of Parkfield, these loads represent reductions in anticipated response ranging from 12 percent to 56 percent of fixed base results.

These comparisons indicate proper consideration of soil-structure interaction effects will generally reduce anticipated PWR seismic response. Reductions in seismic response loads due to earthquake wave scattering, structure embedment, and soil radiation damping are of the same relative magnitude as are reductions due to localized structure nonlinearities determined from fixed base analyses. In some cases, such as for El Centro #5, Melendy Ranch, and the intermediate soil profile for Artificial ground motion, the beneficial aspects of soil-structure interaction reduce seismic loads and required story drift ductilities such

that little damage is expected in the PWR structure even though the input ground motion is approximately 2.5 times the original design ground motion of 0.2g. Table 4-6 presents a comparison of required story drift ductilities for the bottom internal structure shear wall illustrating this point.

The beneficial reduction in required story drift ductilities is illustrated most dramatically for the El Centro #5 and Melendy Ranch earthquakes. For fixed based excitation, a story drift ductility of 5.6 and 4.7 was determined for El Centro #5 and Melendy Ranch, respectively. Consideration of soil-structure interaction effects reduced the required ductility to 1.7 and elastic, respectively. For the intermediate soil case, the structure remained elastic in both earthquakes. No nonlinear response occurred for Melendy Ranch primarily due to beneficial shifting of the system frequency away from the peak spectral input for the soil-structure interaction cases studied.

Similar but less dramatic results were noted for the Artificial ground motion. For fixed base excitation, a story drift ductility of 11.9 in the bottom shear wall was determined. Inelastic loads and ductilities remained virtually the same for the stiff soil case. However, for the intermediate soil case, essentially elastic response of the structure was calculated with a maximum story drift ductility of only 1.2.

In the case of Parkfield excitation, the required story drift ductilities increased from 2.0 determined for the fixed base analysis to 12.9 for the stiff soil case. The ductility then decreased to 6.3 for the intermediate soil profile. The corresponding inelastic base shears increased from the 2.09×10^7 lb determined for fixed base to 3.76×10^7 lb for the stiff soil profile and then dropped off slightly to 2.63×10^7 for the intermediate soil profile. These increased ductilities and shear loads resulted from shifting the fundamental system frequency to the peak amplified region of the Parkfield spectra as discussed in the previous section.

Another interesting trend is presented in Table 4-7. In this table, ratios of the nonlinear to linear seismic internal structure base shears are presented for each of the three foundation conditions evaluated. For the fixed base case, consideration of structural nonlinearities reduced PWR response anywhere from 93 to 46 percent of linear response. However, in the soil-structure interaction cases, consideration of structural nonlinearities did not always results in additional reductions in PWR response. In two cases minor reductions of 4 to 5 percent accurred, minor increases of 6 to 18 percent were noted in three cases, and there was no variation in the remaining three cases since the structure remained elastic. Therefore, to calculate conservative structural response when significant structural nonlinearity is expected and soil-structure interaction effects are important, proper consideration of the nonlinear behavior should be included in the analysis since seismic response loads may slightly increase due to increased response of the system.

In summary, for long duration, broad-band frequency content ground motions studied here, seismic response for the PWR structure is generally decreased due to a number of interrelated factors including: wave scattering due to kinematic interaction, reduction in ground motion input due to embedment, and radiation of energy away from the structure due to inertial feedback. For short duration, narrow frequency content ground motions, changes in the fundamental system frequency due to consideration of the soil stiffness can result in large increases or decreases in seismic response and overshadow the generally beneficial decreases due to the factors presented above. Improved performance of the PWR structure as evidenced by decreasing story drift ductilities generally occurs as site conditions soften except when system response is shifted from a valley to a peak of a short duration ground motion. Thus, in order to evaluate the damage capability of the ground motion, an adequate engineering characterization must retain the frequency content of the record.

The large beneficial decreases in the nonlinear in-structure response spectra noted in the fixed base analyses do not occur in the soil-structure interaction cases. For these cases, nonlinear and linear response spectra were very similar since they are primarily effected by the overall system frequency and not by local structure nonlinearities. Thus, for the soil-structure interaction cases studied, it appears little beneficial suppression of elastic in-structure response spectrum peaks occurs as a result of shear wall yielding.

TABLE 4-1

SEISMIC SHEARS AT BASE OF INTERNAL STRUCTURE

Soil Profile	Shear Wall Location	Response	Seismic Response Shear (lb.)			
			Artificial	El Centro #5	Parkfield	Melendy Ranch
Intermediate	Elevation 0' to Elev. 13' - 5"	Linear	1.83×10^7	1.11×10^7	2.49×10^7	1.13×10^7
		Nonlinear	1.76×10^7	Elastic	2.63×10^7	Elastic
	Elevation 13'-5" to Elevation 25'-4"	Linear	1.70×10^7	1.03×10^7	2.33×10^7	1.06×10^7
		Nonlinear	1.64×10^7	Elastic	2.46×10^7	Elastic
Stiff	Elevation 0' to Elev. 13'-5"	Linear	2.81×10^7	1.94×10^7	3.20×10^7	1.03×10^7
		Nonlinear	3.09×10^7	1.85×10^7	3.76×10^7	Elastic
	Elevation 13'-5" to Elevation 25'-4"	Linear	2.65×10^7	1.82×10^7	2.98×10^7	9.61×10^6
		Nonlinear	2.90×10^7	1.72×10^7	3.51×10^7	Elastic

- Shear walls for which nonlinear response is expected since elastic loads exceed the yield shear of 1.73×10^7 lbs.

TABLE 4-2

SEISMIC SHEARS AT BASE OF CONTAINMENT STRUCTURE

Soil Profile	Containment Structure Element	Response	Seismic Response Shear (lb.)			
			Artificial	El Centro #5	Parkfield	Melendy Ranch
Intermediate	11	Linear	2.79×10^7	1.70×10^7	4.10×10^7	6.56×10^6
		Nonlinear	2.78×10^7	1.70×10^7	4.08×10^7	6.56×10^6
Stiff	11	Linear	4.68×10^7	2.79×10^7	4.85×10^7	1.01×10^7
		Nonlinear	4.44×10^7	2.82×10^7	4.44×10^7	1.01×10^7

TABLE 4-3

SOIL-STRUCTURE INTERACTION PEAK ELASTIC MOMENTS

a) Peak Overturning Moments at Base of Containment Structure

Soil Profile	Seismic Response Moment (in-lb)				Cracking Moment[1] (in-lb)
	Artificial	El Centro #5	Parkfield	Melendy Ranch	
Inter-mediate	5.10×10^{10}	3.37×10^{10}	7.01×10^{10}	1.26×10^{10}	9.38×10^{10}
Stiff	8.14×10^{10}	4.72×10^{10}	8.04×10^{10}	1.82×10^{10}	9.38×10^{10}

1) From Reference 2

b) Peak Overturning Moments at Base of Internal Structure

Soil Profile	Seismic Response Moment (in-lb)				M_{bond}[2] (in-lb)	M_{Yield} (in-lb)
	Artificial	El Centro #5	Parkfield	Melendy Ranch		
Inter-mediate	1.24×10^{10}	7.84×10^{9}	1.83×10^{10}	7.54×10^{9}	7.70×10^{9}	6.29×10^{10}
Stiff	2.15×10^{10}	1.42×10^{10}	2.30×10^{10}	7.76×10^{9}	7.70×10^{9}	6.29×10^{10}

2) See Figure 2-6

TABLE 4-4

PWR INTERNAL STRUCTURE STORY DRIFT DUCTILITIES

Soil Profile	Shear Wall Location	Story Drift Ductilities			
		Artificial	El Centro #5	Parkfield	Melendy Ranch
Intermediate	El 0' to El 13'-5"	1.2	Elastic	6.3	Elastic
	El 13'-5" to El 25'-4"	1.0	Elastic	5.3	Elastic
Stiff	El 0' to El 13'-5"	9.2	1.7	12.9	Elastic
	El 13'-5" to El 25'-4"	7.8	1.0	11.4	Elastic

TABLE 4-5

COMPARISON OF LINEAR AND NONLINEAR SEISMIC SHEARS AT BASE OF INTERNAL STRUCTURE

Earthquake	Linear Seismic Shears (lb)			Nonlinear Seismic Shears (lb)		
	Fixed Base	Stiff Soil Profile	Intermediate Soil Profile	Fixed Base	Stiff Soil Profile	Intermediate Soil Profile
Artificial	4.62×10^7 (2.67)	2.81×10^7 (1.62)	1.83×10^7 (1.06)	3.53×10^7	3.09×10^7	1.76×10^7
El Centro #5	3.79×10^7 (2.19)	1.94×10^7 (1.12)	1.11×10^7 (0.64)	2.52×10^7	1.85×10^7	Elastic
Parkfield	2.24×10^7 (1.29)	3.20×10^7 (1.85)	2.49×10^7 (1.44)	2.09×10^7	3.76×10^7	2.63×10^7
Melendy Ranch	5.13×10^7 (2.97)	1.03×10^7 (0.60)	1.13×10^7 (0.65)	2.35×10^7	Elastic	Elastic

( ) presents Demand/Capacity Ratio (i.e., ratio of elastically computed shear loads for 0.5g ground motion to member yield strength)

TABLE 4-6

STORY DRIFT DUCTILITIES IN INTERNAL STRUCTURE
SHEAR WALL LOCATED BETWEEN ELEVATION 0' AND ELEVATION 13'-5"

Earthquake	Story Drift Ductilities		
	Fixed Base	Stiff Soil Profile	Intermediate Soil Profile
Artificial	11.9	9.2	1.2
El Centro #5	5.6	1.7	Elastic
Parkfield	3.2	12.9	6.3
Melendy Ranch	4.7	Elastic	Elastic

TABLE 4-7

RATIO OF NONLINEAR TO LINEAR SEISMIC SHEARS AT BASE OF INTERNAL STRUCTURE

Earthquake	Analysis	Internal Structure Base Shears		
		Fixed Base	Stiff Soil	Intermediate Soil
Artifical	Linear	4.62×10^7 lb	2.81×10^7 lb	1.83×10^7 lb
	Nonlinear	3.53×10^7 lb	3.09×10^7 lb	1.76×10^7 lb
	Nonlinear/Linear	0.76	1.10	0.96
El Centro #5	Linear	3.79×10^7 lb	1.94×10^7 lb	1.11×10^7 lb
	Nonlinear	2.52×10^7 lb	1.85×10^7 lb	Elastic
	Nonlinear/Linear	0.66	0.95	1.00
Parkfield	Linear	2.24×10^7 lb	3.20×10^7 lb	2.49×10^7 lb
	Nonlinear	2.09×10^7 lb	3.76×10^7 lb	2.63×10^7 lb
	Nonlinear/Linear	0.93	1.18	1.06
Melendy Ranch	Linear	5.13×10^7 lb	1.03×10^7 lb	1.13×10^7 lb
	Nonlinear	2.35×10^7 lb	Elastic	Elastic
	Nonlinear/Linear	0.46	1.00	1.00

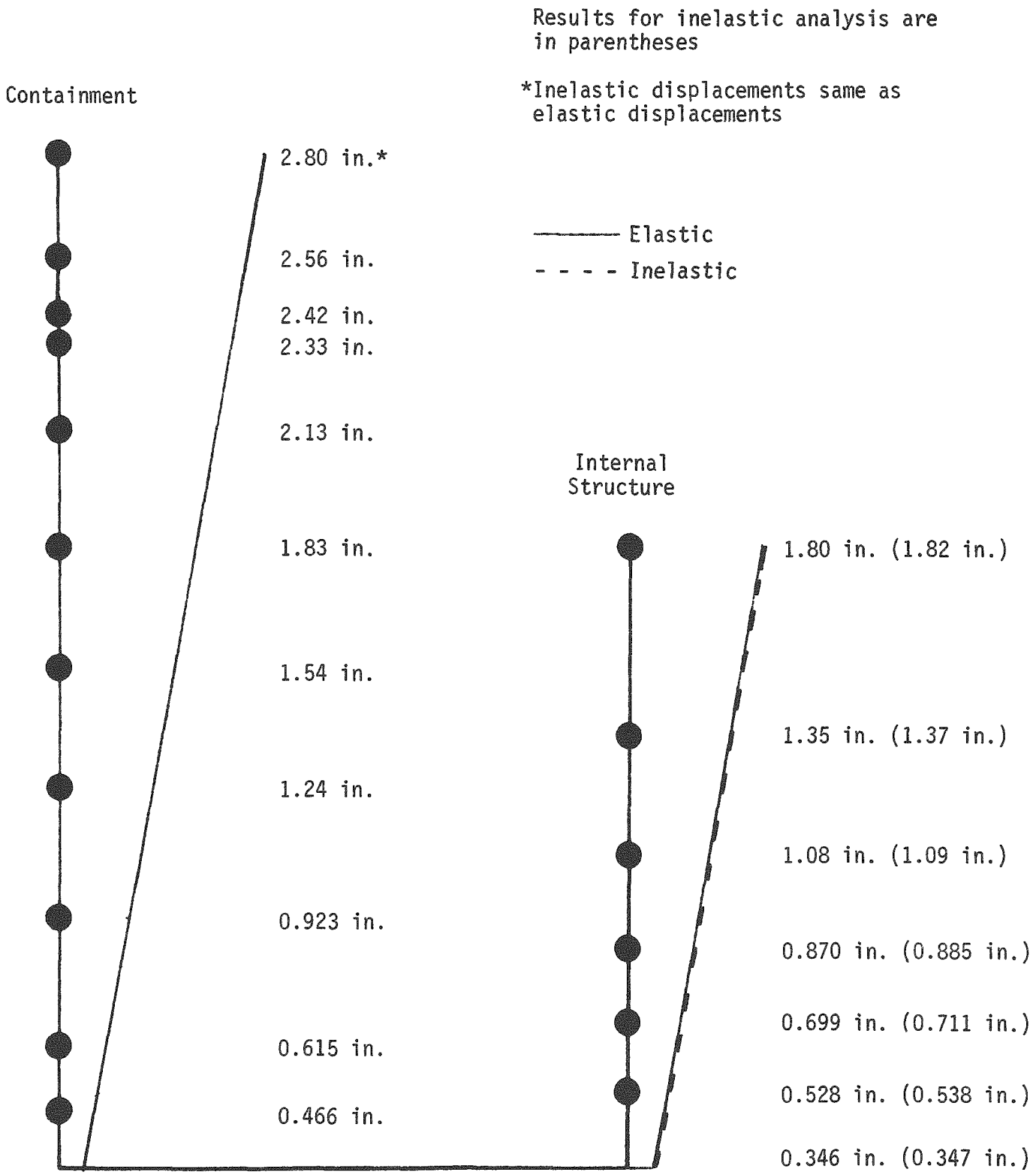

FIGURE 4-1. COMPARISON OF MAXIMUM ELASTIC AND INELASTIC DISPLACEMENTS FOR ARTIFICIAL EARTHQUAKE, INTERMEDIATE SOIL PROFILE

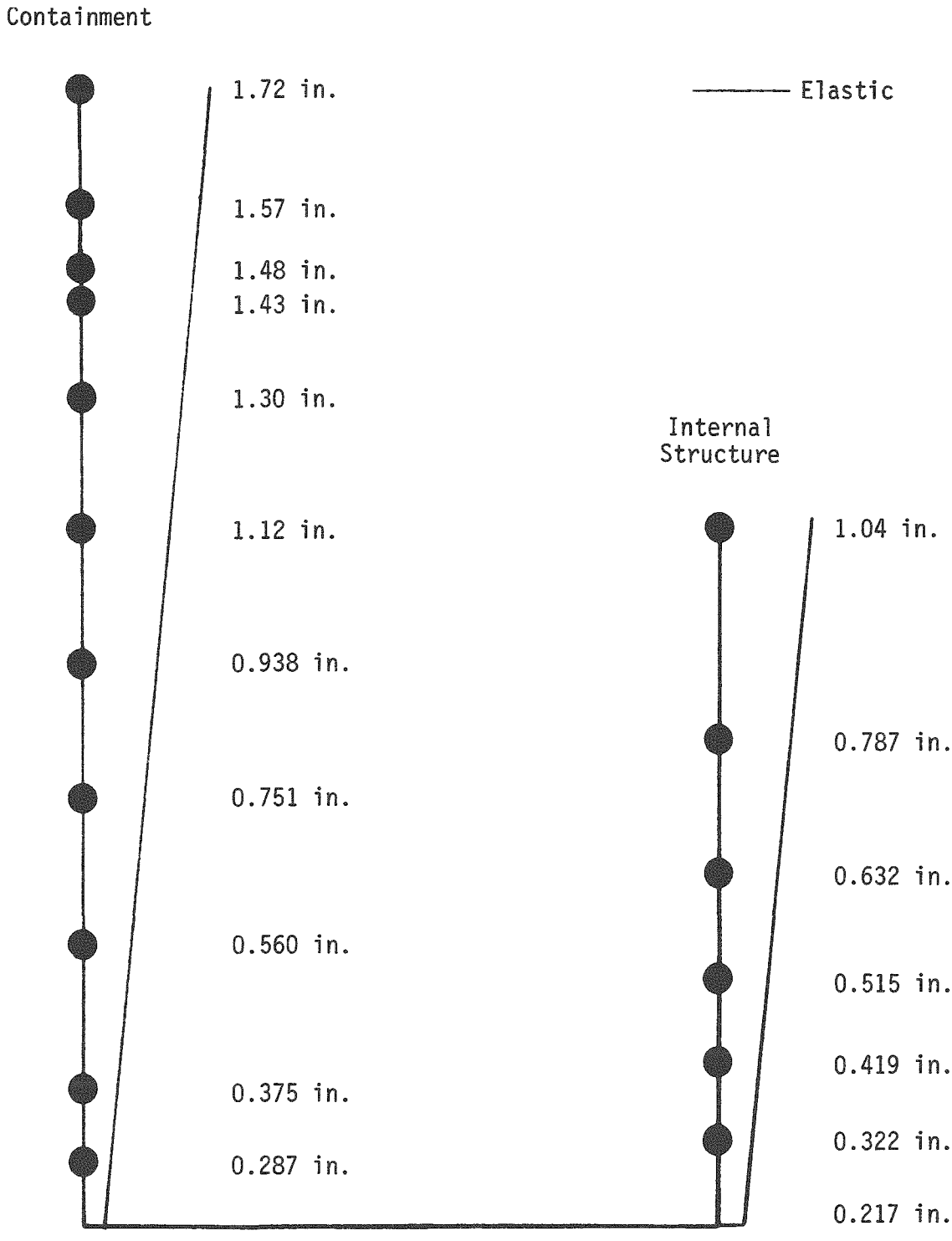

FIGURE 4-2. MAXIMUM ELASTIC DISPLACEMENTS FOR EL CENTRO #5 EARTHQUAKE, INTERMEDIATE SOIL PROFILE

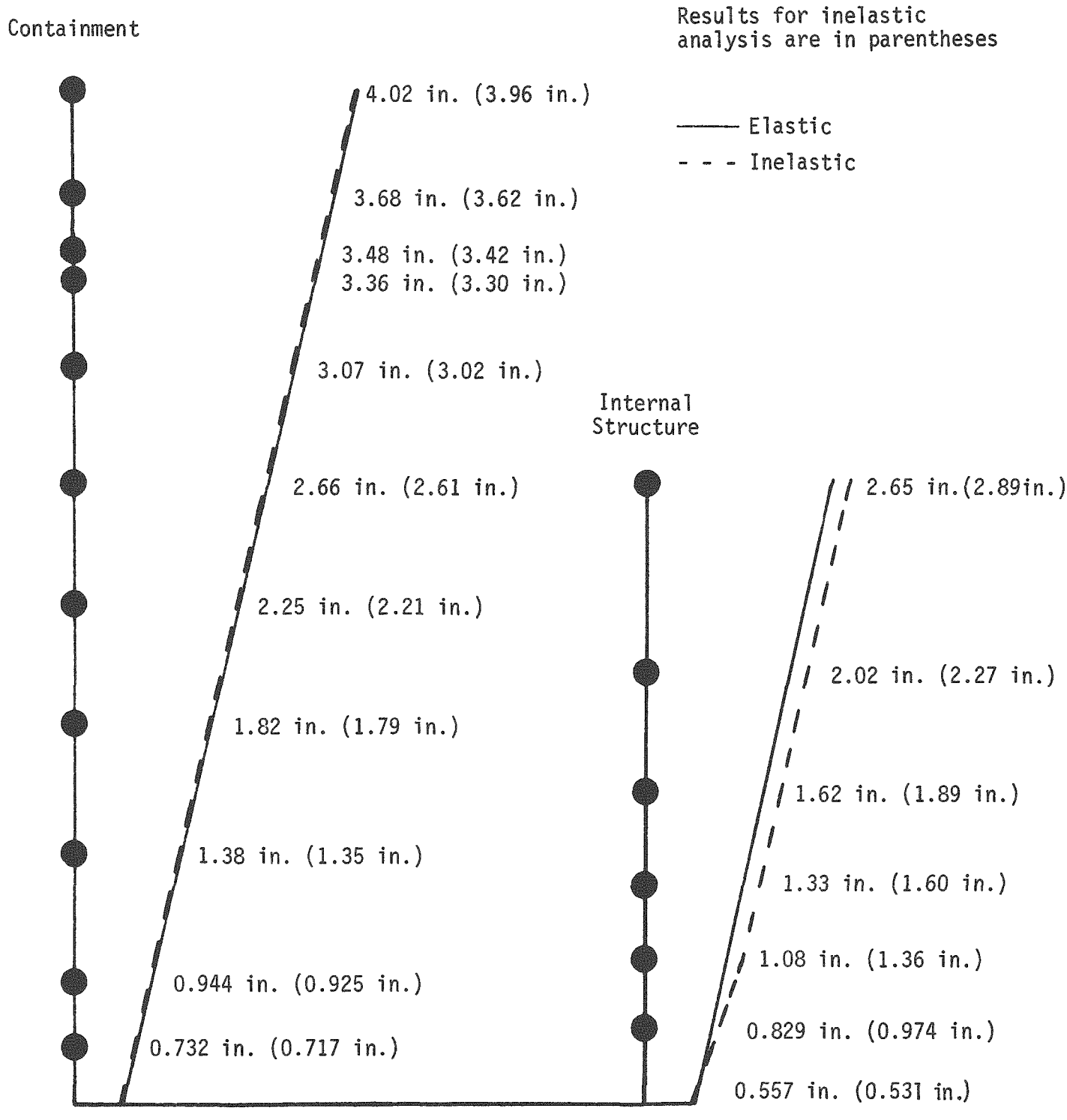

FIGURE 4-3. COMPARISON OF MAXIMUM ELASTIC AND INELASTIC DISPLACEMENTS FOR PARKFIELD EARTHQUAKE, INTERMEDIATE SOIL PROFILE

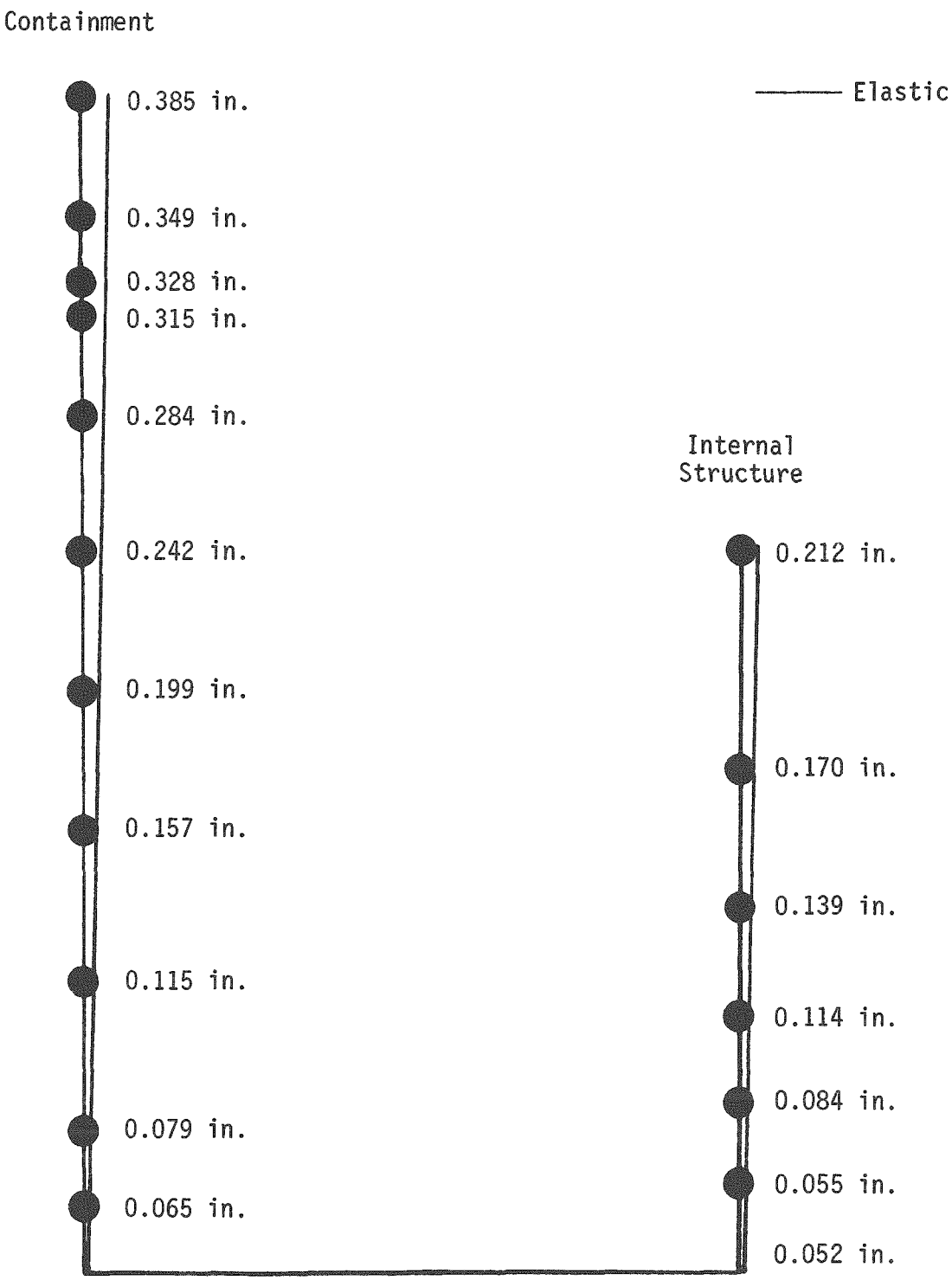

FIGURE 4-4. MAXIMUM ELASTIC DISPLACEMENTS FOR MELENDY RANCH EARTHQUAKE, INTERMEDIATE SOIL PROFILE

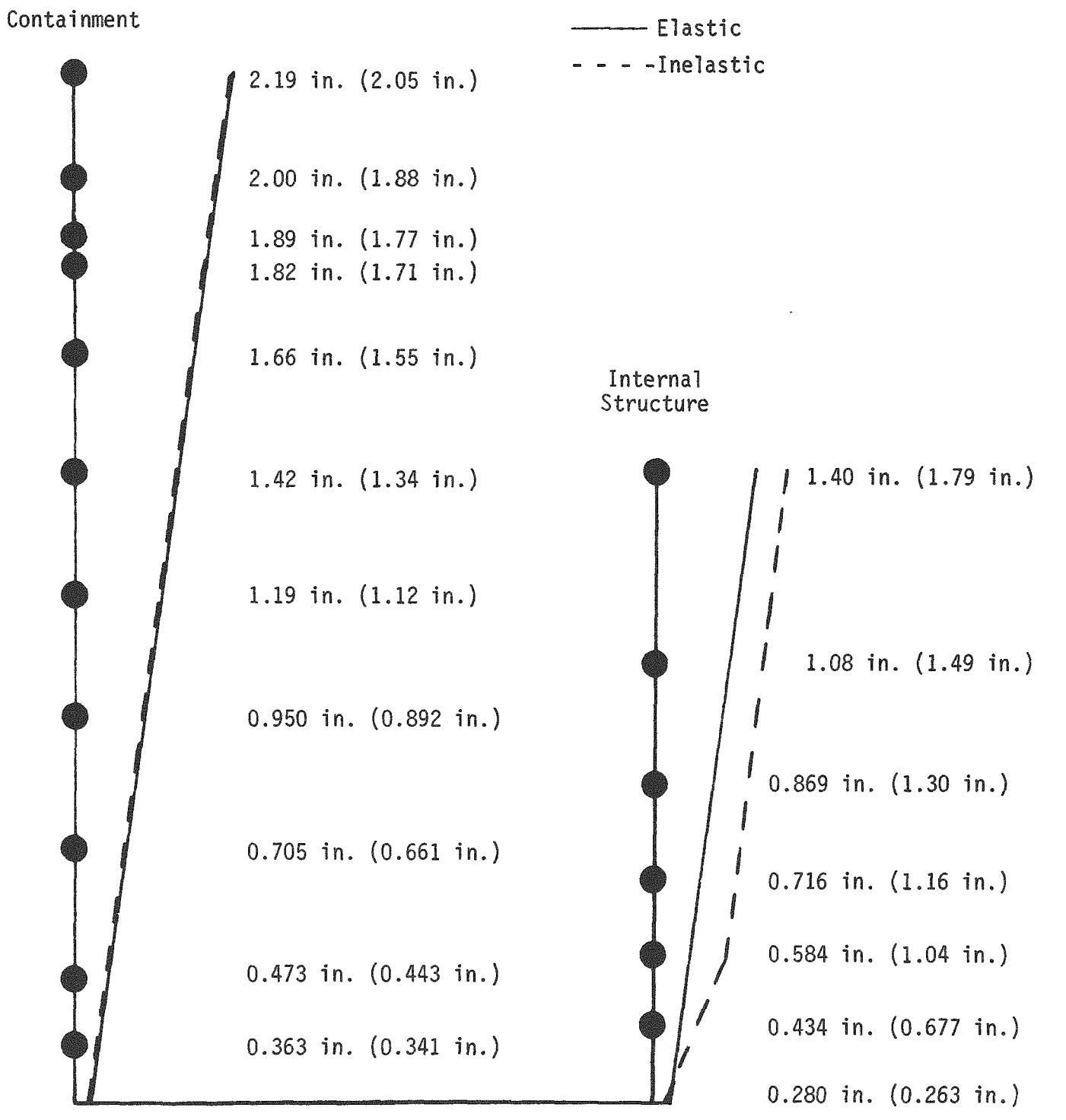

FIGURE 4-5. COMPARISON OF MAXIMUM ELASTIC AND INELASTIC DISPLACEMENTS FOR ARTIFICIAL EARTHQUAKE, STIFF SOIL PROFILE

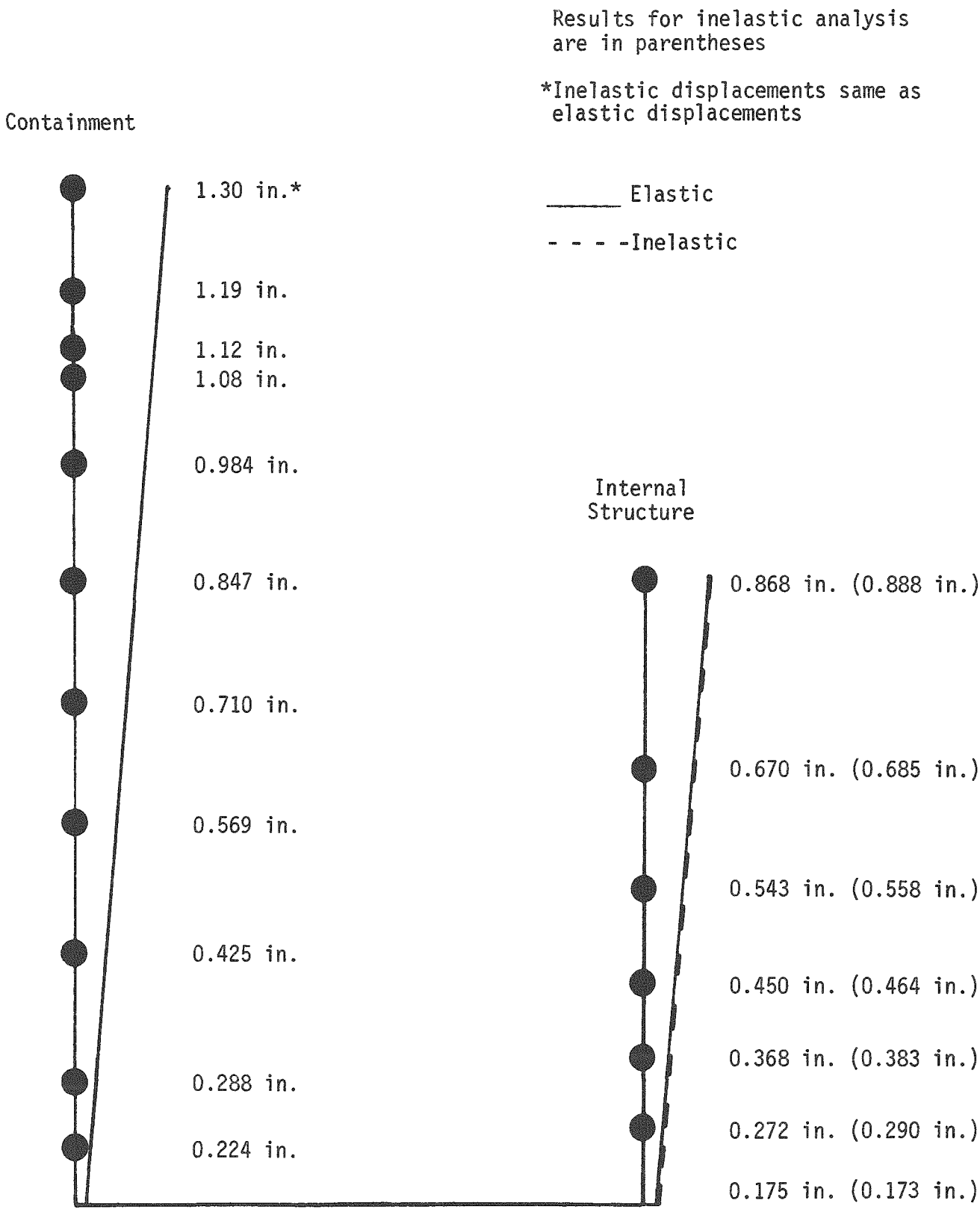

FIGURE 4-6. COMPARISON OF MAXIMUM ELASTIC AND INELASTIC DISPLACEMENTS FOR EL CENTRO #5 EARTHQUAKE, STIFF SOIL PROFILE

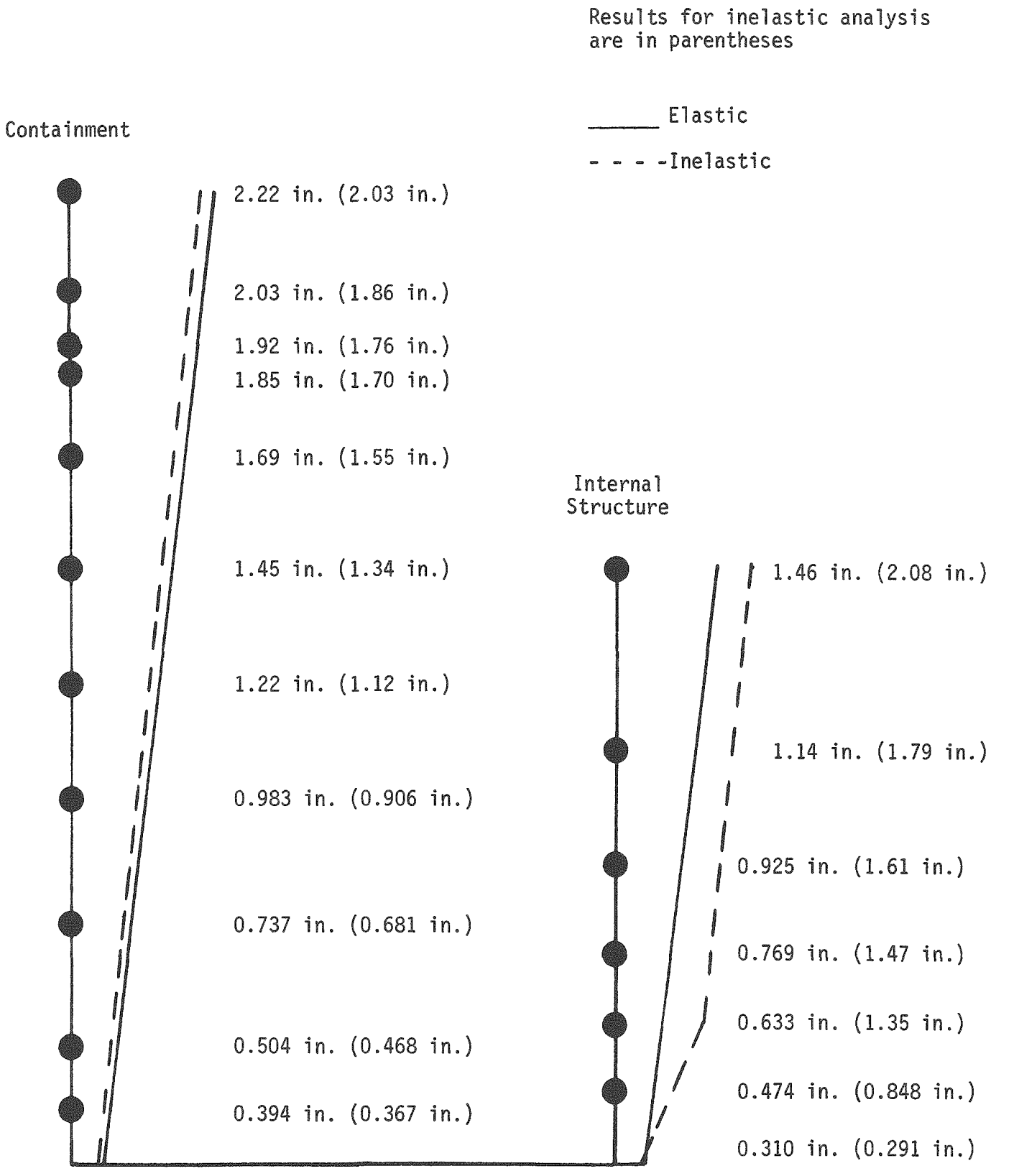

FIGURE 4-7. COMPARISON OF MAXIMUM ELASTIC AND INELASTIC DISPLACEMENTS FOR PARKFIELD EARTHQUAKE, STIFF SOIL PROFILE

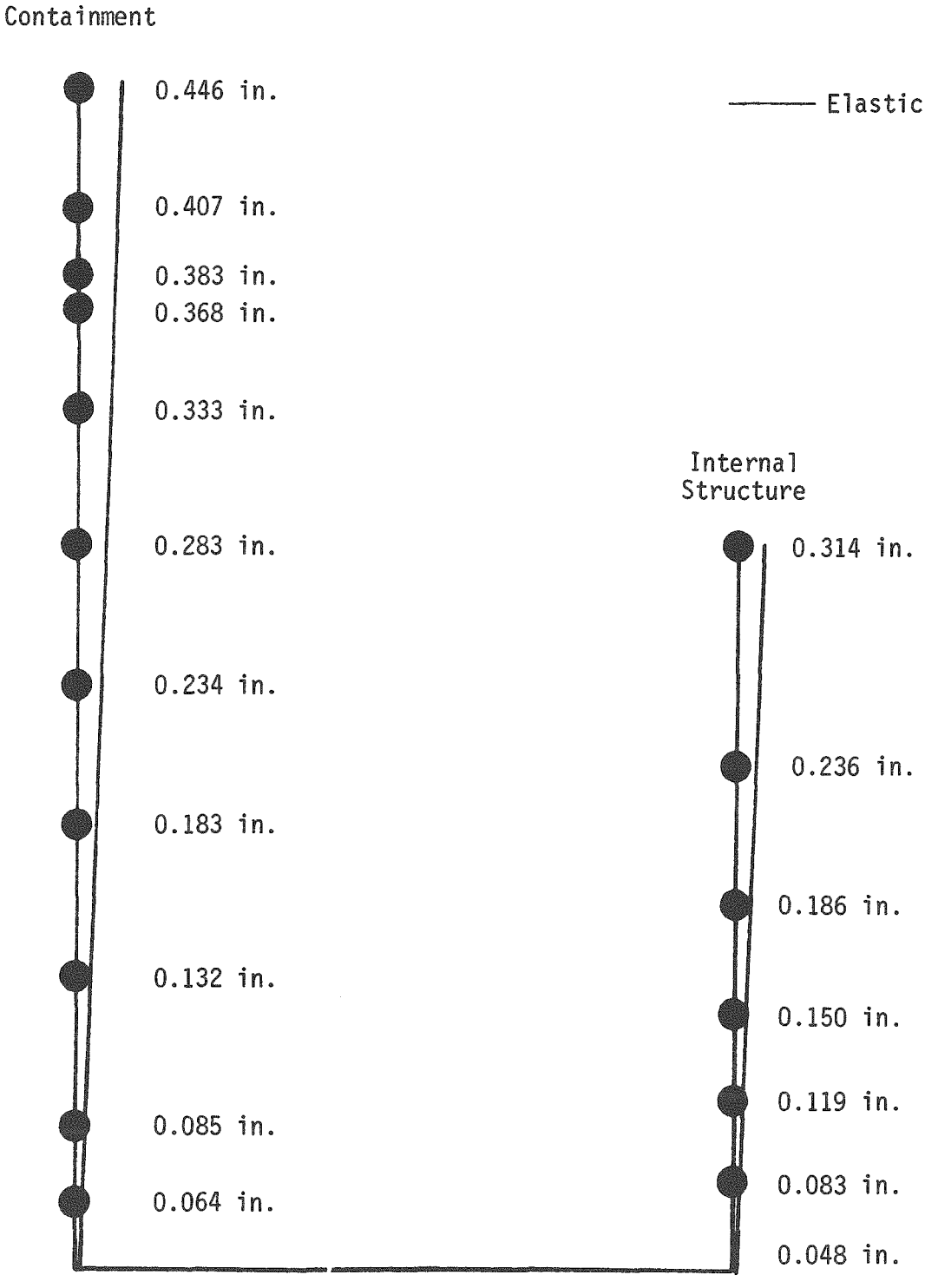

FIGURE 4-8. MAXIMUM ELASTIC DISPLACEMENTS FOR MELENDY RANCH EARTHQUAKE, STIFF SOIL PROFILE

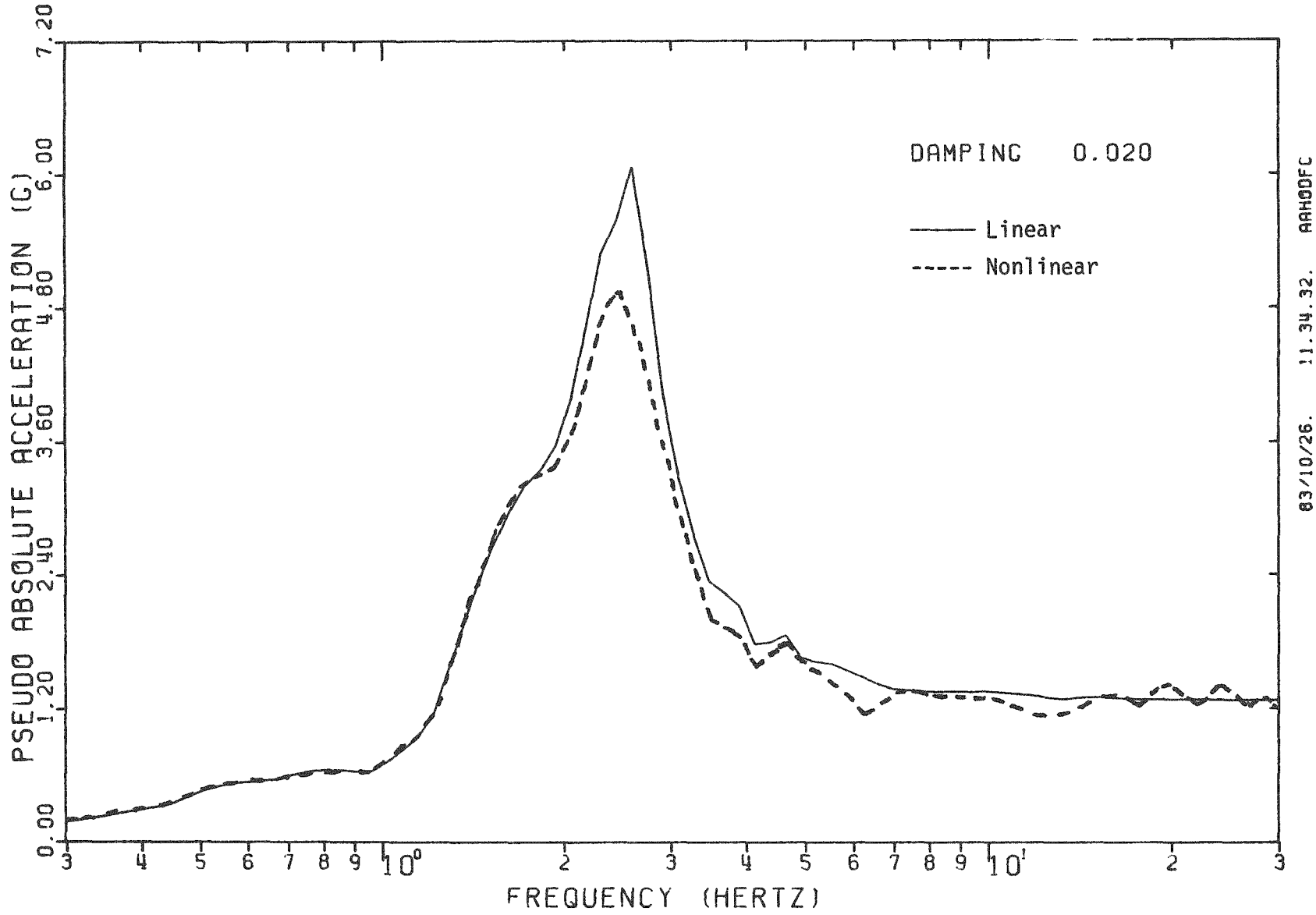

FIGURE 4-9. COMPARISON OF LINEAR AND NONLINEAR IN-STRUCTURE RESPONSE SPECTRA AT NODE 4 IN CONTAINMENT STRUCTURE FOR PARKFIELD EARTHQUAKE, STIFF SOIL PROFILE

5. USE OF TASK I METHODOLOGY TO ESTIMATE STORY DRIFT DUCTILITIES

This chapter presents procedures whereby the techniques developed in Task I (Reference 1) for estimating inelastic response from pseudo-elastic analysis for single-story shear walls may be applied to multi-story structural systems. These procedures will first be demonstrated for the fixed-base cases (Chapter 3) and then will also be applied to the soil-structure interaction cases (Chapter 4). The procedures will be explained in terms of a step-by-step process.

5.1 ESTIMATE STORY DRIFT DUCTILITIES FROM SINGLE ELASTIC ANALYSIS

5.1.1 Step No. 1

Determine from elastic analysis the Demand/Capacity Ratio (i.e., ratio of elastic computed load to yield strength) for each element which might go nonlinear. For the fixed-base cases, these Demand/Capacity Ratios for shear are presented in Table 3.2b. For any story where the Demand/Capacity Ratio exceeds unity, this ratio represents the input scale factor F_{μ_s} corresponding to that story level (i.e., the factor by which the input must be scaled to bring the computed response to elastic yield levels). Thus for story s:

$$F_{\mu_s} = \left(\frac{\text{Demand}}{\text{Capacity}}\right)_s = \frac{V_s}{V_Y} \qquad (5\text{-}1)$$

where V_s is the elastic computed shear at story s and V_Y is the yield shear at story s.

5.1.2 Step No. 2

Based upon elastic modal analyses, determine those modes which predominantly contribute to those response quantities which have Demand/Capacity Ratios greater than unity. For instance, the fixed-base PWR model internal structure shears are primarily caused by the 5.22 Hz internal structure mode.

For each important modal frequency, determine the relationship between F_μ and μ using either the point estimate approach (Equation 1-2) or the spectral averaging approach of the Task I methodology (Reference 1). Figures 5-1 through 5-4 presents plots of F_μ versus μ values ranging from $\mu = 1.5$ up to $\mu = 15$ for the Artificial, El Centro #5, Parkfield, and Melendy Ranch records. These plots were developed using the point estimate approach of Task I together with a modal frequency of 5.22 Hz and a modal damping of 6%.

It should be noted that the point estimate approach is an approximate approach for estimating F_μ versus μ and that actual nonlinear time history results reported in the Task I report for SDOF systems differ somewhat from these point estimate approach results. Several actual nonlinear time history results from the Task I report are also plotted on these figures for comparison. Therefore, one should not use the exact point estimate computed values of F_μ for a given μ, but rather should pass a smooth "best-fit" line through these point estimate computed values. Next, confidence bounds should be estimated about this "best-fit" line in recognition of uncertainty of this approach. Based upon Task I (Reference 1), it is estimated that the 90% Confidence Bounds (5% to 95% Non-Exceedance Probability) on F_μ can be approximated by the following error bounds.

μ	Error Bounds on F_μ
2	$\pm$ 15%
4	$\pm$ 20%
6	$\pm$ 25%
8	$\pm$ 30%
10	$\pm$ 35%

Using this procedure, approximate 90% Confidence Bounds on F_μ for a given μ can be determined. Figures 5-1 through 5-4 present plots of such bounds for the four earthquakes studied. Note that these plots are not a direct estimate of the ductility in the PWR shear walls and should not be compared to the nonlinear time history results since these plots are developed based on SDOF structures and implicitily assume uniform yielding for all stories which is not the case for this structure. Estimation of story drift ductilities from these results for the PWR structure is discussed below.

If more than one mode is important for the response quantity of interest, then the "best-fit" line for F_μ versus μ should be based upon a weighted-averaging of the F_μ versus μ values obtained for each modal frequency of interest. This weighted-averaging technique should be based on percentage of mass participating in each mode or a similar weighting method which approximately accounts for the importance of the various modes. Confidence Bounds about this "best-fit" line should be broadened somewhat to account for uncertainties associated with this weighted averaging procedure.

5.1.3 Step No. 3

Based upon $F\mu_s$ values from Step No. 1 (Equation 5-1) and the F_μ versus μ Confidence Bound values of Step No. 2 (Figures 5-1 through 5-4), estimate an effective ductility, μ_e, range for each element that has $F\mu_s$ values greater than unity. Table 5-1 presents effective ductility estimates, μ_e, for the lower two internal structure shear elements for each of the four earthquake records.

The μ_e values obtained in this way do not represent either the overall system ductility, μ, or the story drift ductility, μ_s. Instead:

$$\mu \leq \mu_e \leq \mu_s \qquad (5\text{-}2)$$

The ductility, μ_e, was estimated assuming that all elements in the structure have the same Demand/Capacity Ratio of F_{μ_s} because plots of F_μ versus μ for single-story structures were used to estimate μ_e. As a result, μ_e conservatively overestimates the system ductility, μ, and unconservatively underestimates the story drift shear ductility, μ_s, for structures that have highly nonuniform Demand/Capacity ratios.

Thus, the μ_e values shown in Table 5-1 represent lower bound estimates of the story drift shear ductilities, μ_s, which might be obtained from nonlinear analysis. An estimate of μ_s can be obtained from:

$$\mu_s \approx M_e(\mu_e - 1) + 1 \qquad (5\text{-}3)$$

The estimate of M_e is highly judgmental and depends upon the nonuniformity of Demand/Capacity ratios. With a uniform Demand/Capacity ratio, M_e = 1.0. With fixed-base structures with highly nonuniform Demand Capacity ratios and "weak-links" near the base, M_e would begin to approach 2.0. In the case of strong soil-structure interaction effects where the fundamental mode is predominantly a soils mode whose frequency would not be strongly influenced by local structure nonlinearities, M_e is also close to 2.0. Using this rather general guidance, one might estimate for the PWR structure being considered:

$$\text{(Fixed-Base \& SSI)} \qquad M_e \approx 1.8 \text{ to } 2.0 \qquad (5\text{-}4)$$

Table 5-1 also presents estimates of μ_s obtained using Equations 5-3 and 5-4. Note that these estimated μ_s values based upon elastic analyses agree reasonably well with the actual nonlinear computed values for μ_s.

5.1.4 Discussion of Method

The primary advantage of this method to estimate μ_s is that it only requires a single linear elastic analysis of the structure to determine Demand/Capacity ratios, F_{μ_s}, for each of the elements which are expected to go nonlinear. Ductility estimates, μ_e and μ_s, are then obtained using plots of F_μ versus μ for the earthquake record being

considered. These plots are quickly developed using the point estimate technique of Task I (Reference 1) and are independent of the structure being evaluated.

The primary disadvantages of this method are:

1. A judgmental estimate of M_e must be made.
2. In some cases, the uncertainty bands on μ_e and μ_s may be very wide.

The width of the uncertainty bands depends primarly on the slope of the F_μ versus μ curves (Figures 5-1 through 5-4). For Melendy Ranch, this slope is very steep (a small change in μ corresponds to a large change in F_μ) and the resultant uncertainty band on μ_s is narrow. For El Centro #5, the slope is also steep but less so than for Melendy Ranch. Thus, the uncertainty bands on μ_s are somewhat wider. The slope is less steep for the Artificial record and the uncertainty bands are still wider, particularly at large ductility ratios.

For Melendy Ranch, El Centro #5, and the Artificial record, the uncertainty bands on μ_s are sufficiently narrow to enable engineering design decisions to be made using this approximate procedure based upon a single elastic analysis. However, because of the very shallow slope of the Parkfield F_μ versus μ plot (Figure 5-3), this method does not produce a meaningful estimate of the uncertainty range for μ_s for this structure for the Parkfield records. The method predicts that μ_s lies between 2.4 and greater than 30 for this structure subjected to Parkfield. Such a broad uncertainty range makes the prediction meaningless in this case.

5.2 ESTIMATE STORY DRIFT DUCTILITIES FROM MULTIPLE PSEUDO-ELASTIC ANALYSES

The estimating procedure of Section 5.1 suffers from the necessity of estimating μ_s from μ_e using a judgmentally determined M_e value. This deficiency can be eliminated using multiple pseudo-elastic analyses as described in this section.

5.2.1 Step #1

For each nonlinear element, estimate the story drift ductility, μ_s. These estimates can be made by guess or by using the procedures of Section 5.1.

Next, use the point estimate procedure of Task I (Reference 1) to estimate an effective stiffness, k'_e, and effective damping, β'_e, for each nonlinear element based upon the elastic stiffness, k, elastic damping, β, and estimated story drift ductility, μ_s, for that element. Note that Task I enables the frequency ratio (f'_e/f) and damping ratio (β'_e/β) to be estimated. Thus:

$$k'_e = (f'_e/f)^2 \, k \tag{5-5}$$

$$\beta'_e = (\beta'_e/\beta) \, \beta \tag{5-6}$$

Plots of $(k'_e/k)_s$ and $(\beta'_e)_s$ versus story drift ductility, μ_s, obtained using Task I methodology for various numbers (N) of strong nonlinear response cycles are presented in Figures 5-5 and 5-6. The N=1 line is appropriate for Melendy Ranch, N=2 is appropriate for Parkfield, and El Centro #5, and N=3 is appropriate for the Artificial record.

5.2.2 Step #2

Perform an elastic response analysis of the pseudo-elastic structure model based on the pseudo-elastic effective stiffnesses, $(k'_e)_s$, and damping, $(\beta'_e)_s$, for each nonlinear element as determined in Step #1. The element load obtained from this pseudo-elastic response is $(V'_e)_s$ for story s. These pseudo-elastic loads are then compared to the predicted element load, $(V'')_s$, in story s which is calculated based on the estimated story drift ductility, μ_s.

The actual member nonlinear shear behavior used in DRAIN time history analyses is presented is Figure 5-7. Initially the member has a stiffness k up to the shear yield load, V_Y. Beyond this point, additional load is carried by the member at a reduced stiffness of 0.1k up to the maximum displacement, δ_{max}. Model equivalence between the actual nonlinear time history results and the pseudo-elastic model is based on maintaining the correct member ductility, μ_s. Thus, in order to reach a displacement δ_{max} consistent with actual nonlinear time history analysis results, a member stiffness k'_e is used which results in a predicted load of $(V'')_s$ for story s. Using the relationships presented in Figure 5-7, it can be shown that:

$$(V'')_s = V_{Y_s} (k'_e/k)_s \mu_s \qquad (5\text{-}7)$$

The ratio $(E_R)_s$ given by:

$$(E_R)_s = \left(\frac{V'_e}{V''}\right)_s \qquad (5\text{-}8)$$

represents the model error for element s. This error should be estimated from Equation 5-8 for each model link.

5.2.3 Step #3

Repeat Steps #1 and #2 until a plot of $(E_R)_s$ versus μ_s is developed for the region in the vicinity of $(E_R)_s = 1.0$. Figure 5-8 presents such an error plot for the bottom element (link 20) of the fixed-base model for the four earthquake records studied.

Note that this pseudo-elastic structure model procedure is an approximate procedure. Therefore, one must determine uncertainty bands for the computed μ_s values. A single μ_s value corresponding to $(E_R)_s$ =

1.0 is insufficient because in some cases very substantial changes in μ_s can be made with little change in $(E_R)_s$. To account for uncertainties, μ_s values associated with the error range:

$$0.8 \leq (E_R)_s \leq 1.2 \qquad (5\text{-}9)$$

are considered to be possible values. Therefore, Figure 5-8 can be used to obtain the improved μ_s estimates presented in Table 5-1.

5.2.4 Discussion of Method

The primary advantages of this method over the single elastic analysis method of Section 5.1 are:

1. No judgmental estimate of M_e must be made. The story drift ductilities, μ_s, are directly obtained.

2. The uncertainty bands on μ_s are narrower than those for the method of Section 5.1.

The uncertainty range for μ_s is quite narrow for the Melendy Ranch, El Centro #5, and Artificial records. Although the uncertainty range for Parkfield has been substantially narrowed from that for the Section 5.1 method, the range is still large. Either procedure will be highly approximate for computing μ_s when the slope of the F_μ versus μ plot is shallow.

The primary disadvantage of this method is that multiple pseudo-elastic analyses must be performed. Once a set of μ_s values are found for which the $(E_R)_s$ values are close to 1.0, several additional analyses will still be needed to construct the plot of $(E_R)_s$ versus μ_s so that the uncertainty range on μ_s can be estimated. The method does converge rapidly. Even so, about 5 or 6 pseudo-elastic analyses were required for each earthquake record using the Section 5.1 results as a starting point. If the Section 5.1 method had not been previously performed, more analyses would have been required.

5.3 APPLICATION TO SOIL-STRUCTURE INTERACTION CASES

The method of Section 5.1 for predicting story drift ductilities may also be applied to the soil-structure interaction (SSI) cases for both the intermediate and stiff soil profile for the Artificial, El Centro #5, and Parkfield records. Results for the stiff soil case are presented as an example. First, the Demand/Capacity Ratios of all yielding elements are calculated based on the elastic shear loads presented in Table 4-1 for the stiff soil case. These ratios are presented in Table 4-5 for the bottom shear wall (element 20).

Next, the point estimate technique given by Equation 1-2 is used with the two important internal structure modes to develop confidence bound estimates of F_μ versus μ. These modes correspond to a 2.62 Hz soil rocking mode and the 4.84 Hz internal structure translational mode. These estimates are shown in Figures 5-9 through 5-11 for the three earthquake records. A weighted "best-fit" line is passed through these estimates. The 4.84 Hz results are weighted approximately 70 percent while the 2.62 Hz results are weighted about 30 percent in determining this "best-fit" estimate.

Wider confidence bounds are required for the soil-structure interaction estimates than were used in the fixed base case. This is primarily due to uncertainties in how structural nonlinearities effect overall system response. In Table 4-6 it was shown that a nonlinear structure on soil could result in somewhat larger or smaller loads in the structure. For this soil case, large changes in the localized member ductility have little effect on fundamental mode response at 2.62 Hz since this mode is primarily a linear soil rocking mode. Thus, when estimating the "best-fit" line, the 4.84 Hz internal structure translational mode F_μ versus μ results were more heavily weighted. However, confidence bounds should generally envelope the F_μ versus μ estimates for both important internal structure modes in order to account for the possibility response may be more heavily influenced by the fundamental soil-structure mode than accounted for by "best-fit" estimates.

Estimates of μ_e and μ_s determined using the techniques presented in Section 5.1 are presented in Table 5-2. Also shown in this table are improved estimates of μ_s using the Section 5.2 method. These results were determined using E_R versus ductility plots presented in Figure 5-12 for the three ground motions studied. Note that the actual nonlinear results lie with these uncertainty bonds. Estimates for both the Artificial and Parkfield ground motions indicate significant structural damage would probably occur. Results for the El Centro #5 record demonstrate good behavior of the structure would be expected based on the low story drift ductility estimates.

5.4 CONCLUSIONS

Two techniques are presented for estimating story drift ductilities of multi-story structures based upon elastic analyses and the methodology developed in Task I (Reference 1) for single-story structures. The first technique (Section 5.1) uses the elastic computed Demand/Capacity Ratios and plots of F_μ versus μ for the earthquake record developed from the Task I methodology. The second technique (Section 5.2) uses a series of elastic analyses of the structure with pseudo-elastic member elements whose stiffnesses have been reduced and damping increased to account for story drift ductilities. These reduced stiffnesses and increased damping values are obtained using the Task I methodology.

Either method can approximately predict the actual nonlinear analysis results for story drift ductilities (see Tables 5-1 and 5-2). Thus, by using pseudo-elastic approximate analysis techniques, the Task I methodology for estimating ductilities may also be applied to multi-story structures. For this reason, the engineering characterictics of the ground motion given in Task I are also applicable to multi-story structures.

It is recognized that for multi-degree-of-freedom stuctures, particularly ones with highly nonuniform Demand/Capacity Ratios such as the PWR structure studied in this report, the predicted ductilities

developed based on Task I methodology have significant uncertainty bands associated with them. More parametric evaluations of different structures having significant multi-mode response excited by a wider variety of earthquakes and with more uniform ductility demand throughout the structure would help quantify the actual uncertaintly associated with these analysis techniques.

One of the advantages of these elastic and pseudo-elastic methods for estimating story drift ductilities is that time history analyses are not necessary. It is only necessary to have an estimate of the elastic response spectrum and strong motion duration of the record. A second advantage is that the methods provide considerable insight into the causes of differing levels of nonlinear response from differing earthquake records. Thirdly, the methods are amenable to efficient performance of wide variation parametric studies on nonlinear response.

On the other hand, if one has a time history record and plans to perform a very limited number of deterministic nonlinear analyses, it would be more cost effective to perform the nonlinear time history analyses rather than using these estimating procedures with a linear analysis. Use of these estimating procedures requires more effort (particularly the Section 5.2 method) than does a single nonlinear time history analysis. Also, if nonlinear response spectra or nonlinear seismic response loads are required, deterministic nonlinear time history analyses must be conducted to obtain these quantities.

TABLE 5-1

ESTIMATED STORY DRIFT DUCTILITIES FROM ELASTIC ANALYSIS - FIXED BASE CASES

Earthquake Record	Structure Model Link	Story Drift Ductility Estimates			
		Lower Bound on μ_s, μ_e	Estimated μ_s $\mu_s \simeq M_e(\mu_e-1)+1$ $M_e = 1.8$ to 2.0	Improved μ_s (Section 5.2)	Actual Nonlinear Result, μ_s
Artificial	20	5.7 - 14.2	9.5 - 27	9.4 - 15.5	11.9
	18	5.5 - 13.5	9.1 - 26	9.0 - 14.5	10.8
El Centro #5	20	2.9 - 5.9	4.4 - 10.8	5.0 - 7.8	5.6
	18	2.7 - 5.5	3.9 - 10.0	4.5 - 7.0	5.1
Parkfield	20	1.8 - >15.0	2.4 - >30	1.3 - 6.8	3.2
	18	1.3 - >15.0	1.5 - >30	1.1 - 5.4	2.0
Melendy Ranch	20	2.1 - 3.0	3.0 - 5.0	3.2 - 4.8	4.7
	18	2.1 - 2.9	3.0 - 4.8	3.1 - 4.6	4.5

TABLE 5-2

ESTIMATED STORY DRIFT DUCTILITIES FROM
ELASTIC ANALYSIS - STIFF SOIL CASE

Earthquake Record	Structure Model Link	Story Drift Ductility Estimates			
		Lower Bound on μ_s, μ_e	Estimated μ_s $\mu_s \approx M_e(\mu_e-1)+1$ $M_e = 1.8$ to 2.0	Improved μ_s (Section 5.2)	Actual Nonlinear Result, μ_s
Artificial	20	2.2 - 7.5	3.2 - 14.0	3.5 - 11.0	9.2
	18	2.0 - 6.5	2.8 - 11.0	3.0 - 9.8	7.8
El Centro #5	20	1.2 - 1.5	1.4 - 2.0	1.2 - 1.8	1.7
	18	1.0	1.0	1.0 - 1.5	1.0
Parkfield	20	3.2 - >15	5.0 - >30	5.4 - 14.3	12.9
	18	3.0 - >15	4.6 - >30	4.8 - 13.0	11.4

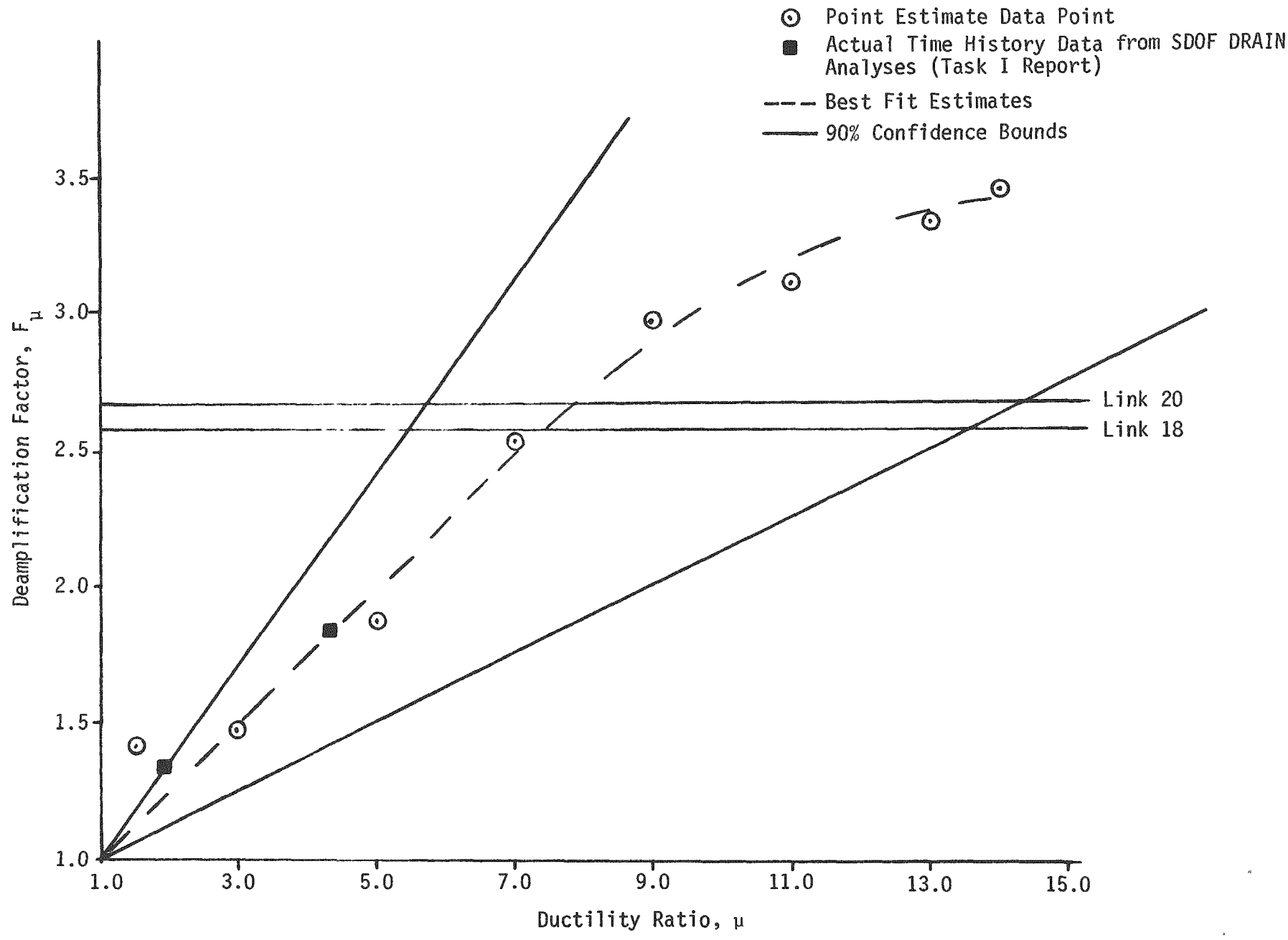

FIGURE 5-1. ESTIMATED F_μ VERSUS μ FOR FIXED BASE CASE - ARTIFICIAL RECORD

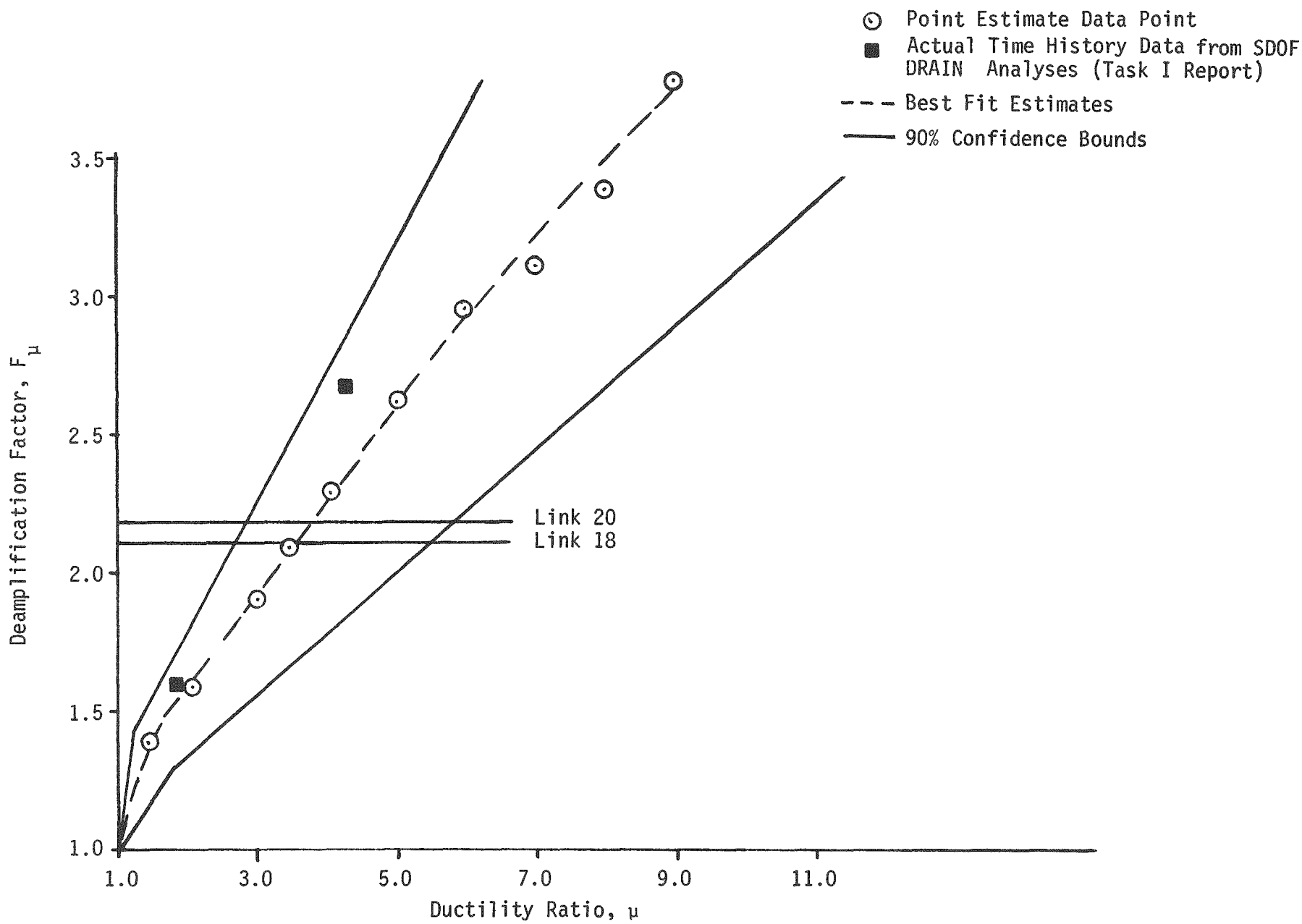

FIGURE 5-2. ESTIMATED F_μ VERSUS μ FOR FIXED BASE CASE - EL CENTRO #5 RECORD

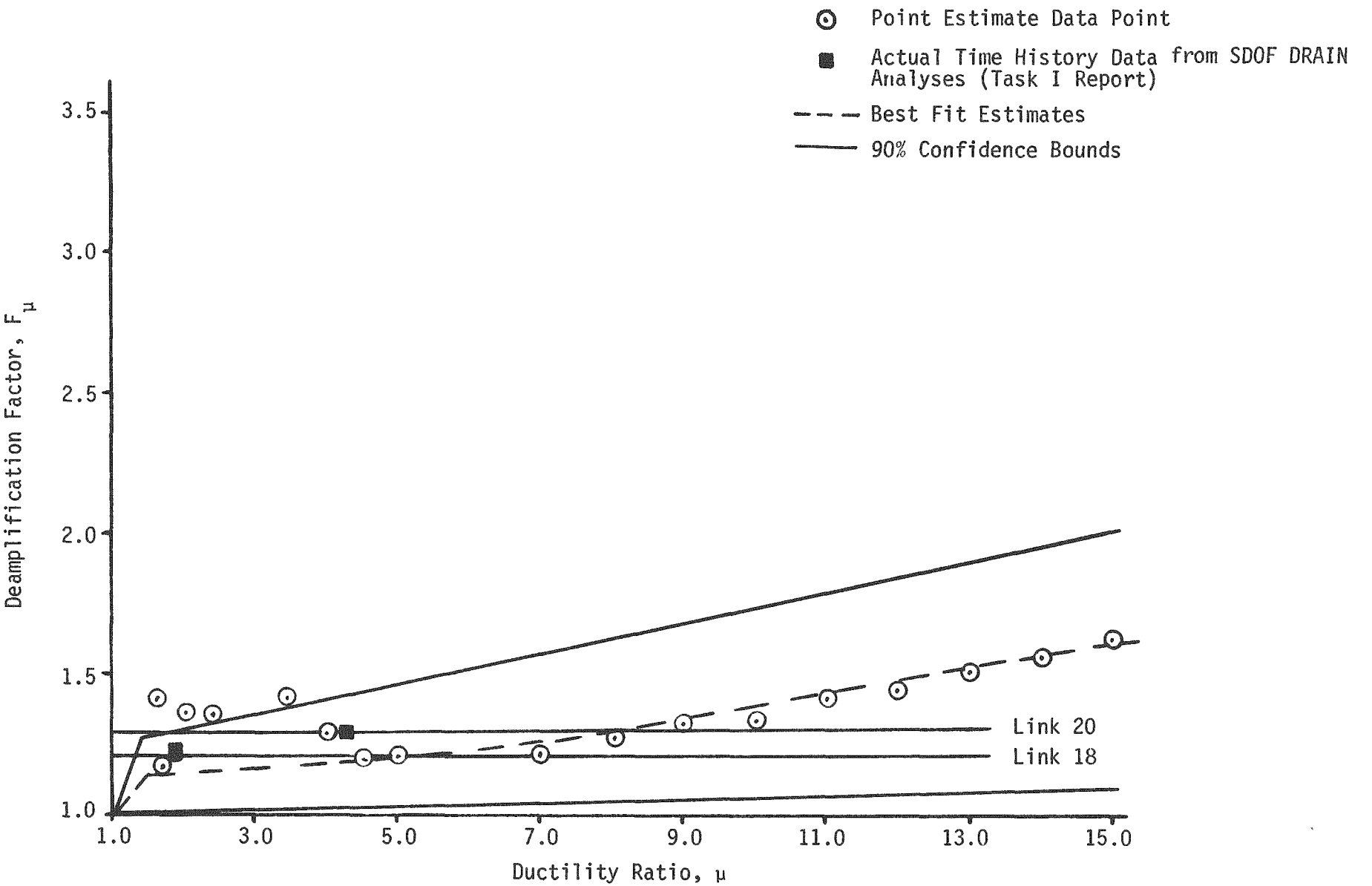

FIGURE 5-3. ESTIMATED F_μ VERSUS μ FOR FIXED BASE CASE - PARKFIELD RECORD

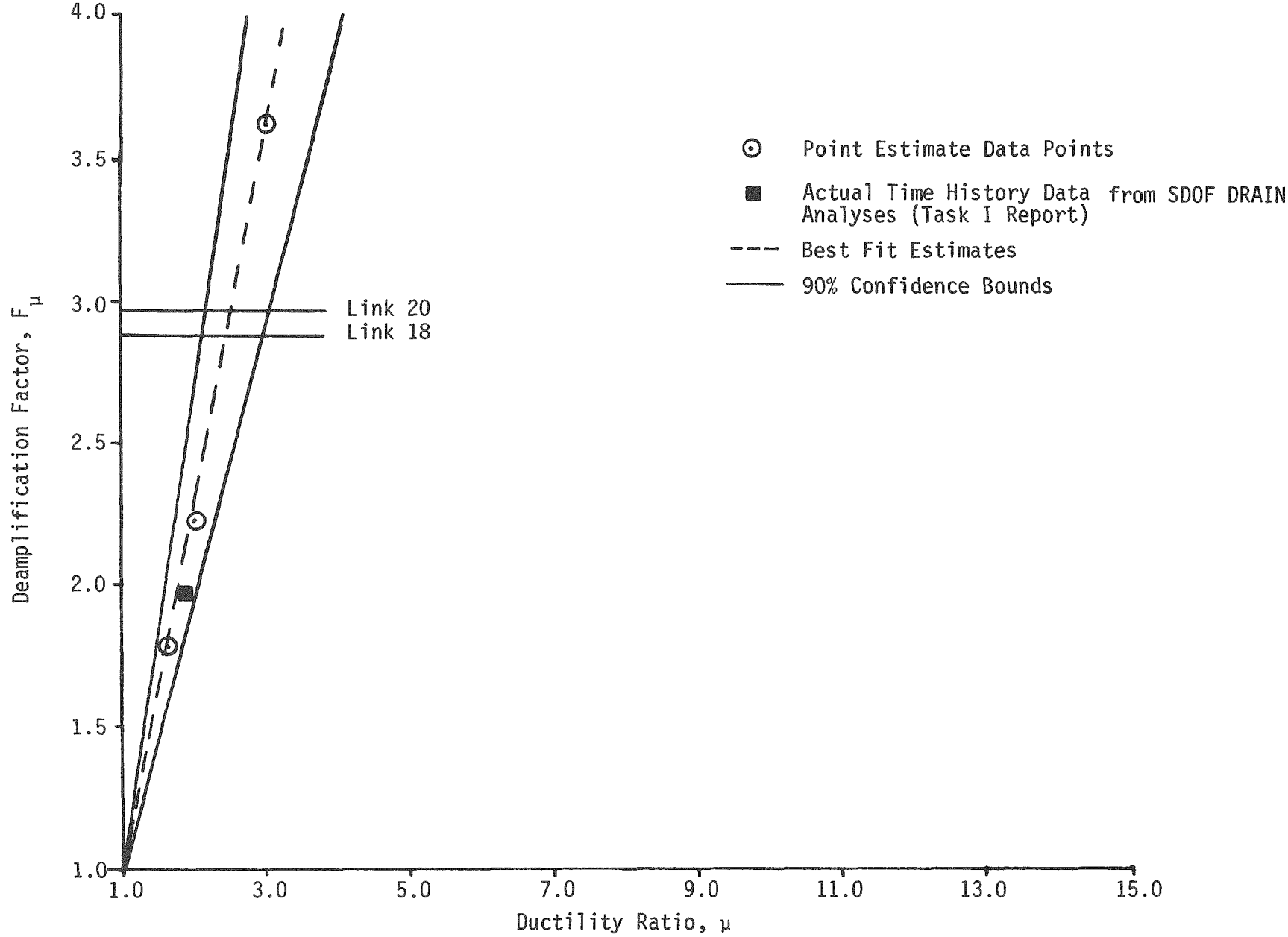

FIGURE 5-4. ESTIMATED F_μ VERSUS μ FOR FIXED BASE CASE - MELENDY RANCH RECORD

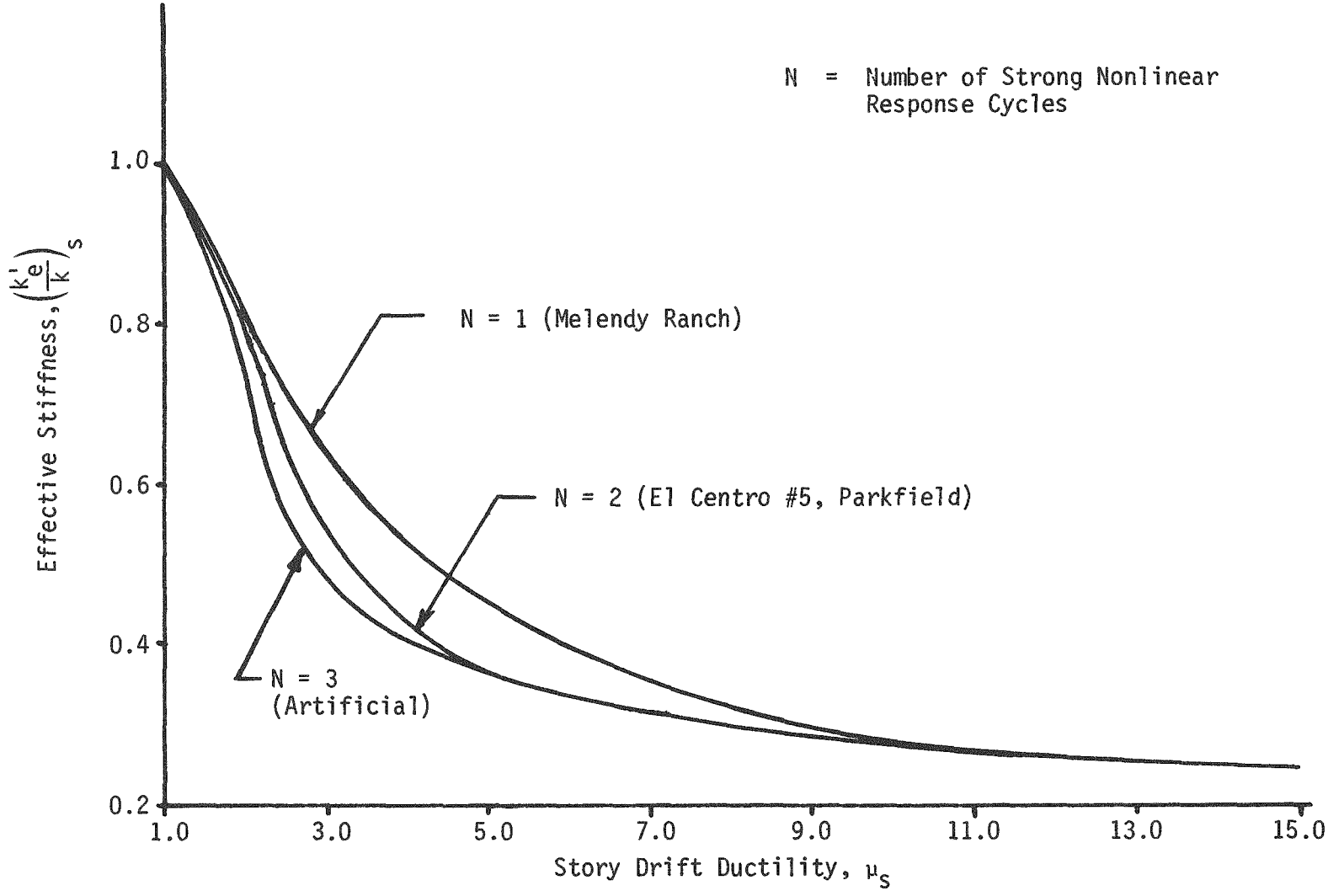

FIGURE 5-5. EFFECTIVE STIFFNESS VERSUS STORY DRIFT DUCTILITY

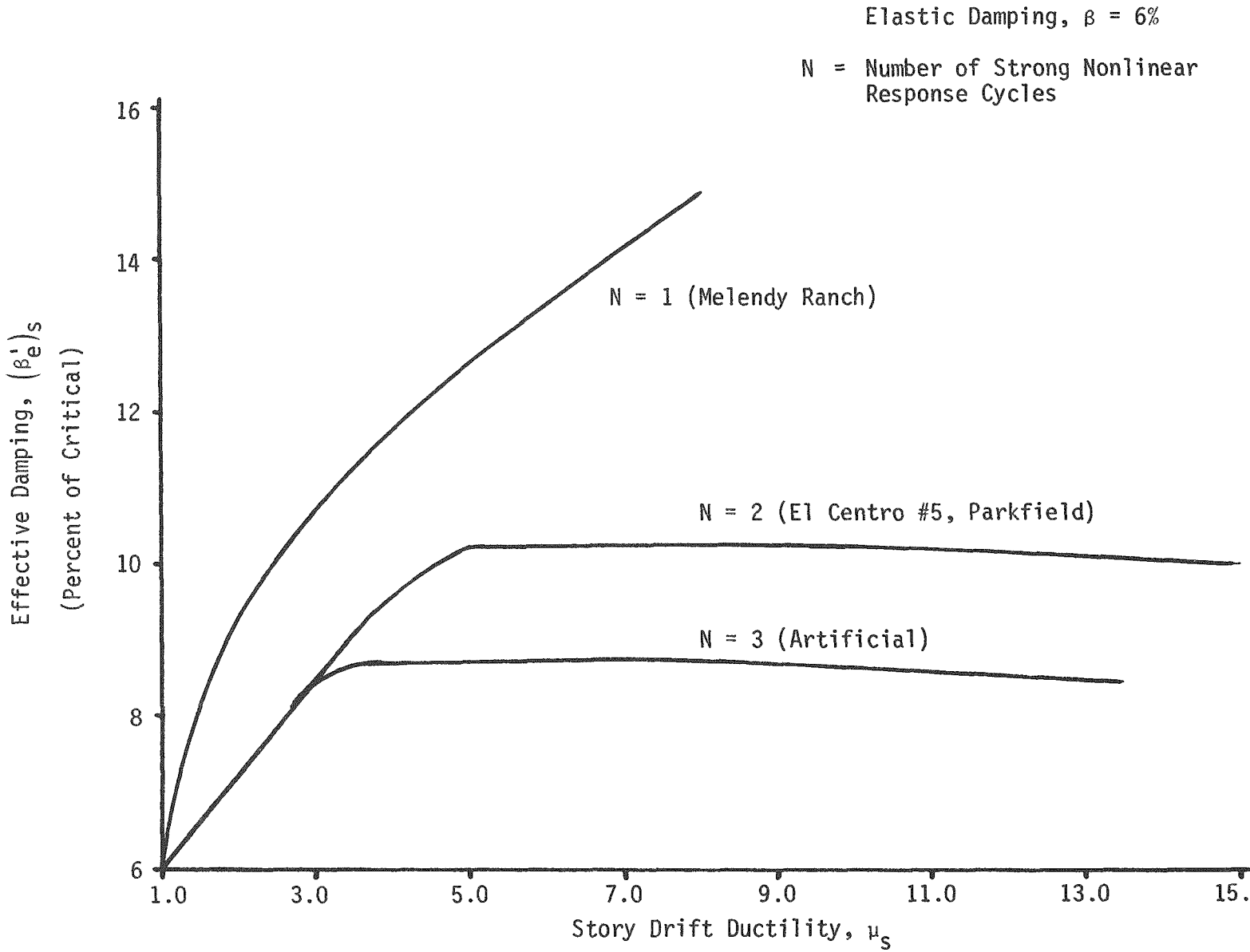

FIGURE 5-6. EFFECTIVE DAMPING VERSUS STORY DRIFT DUCTILITY

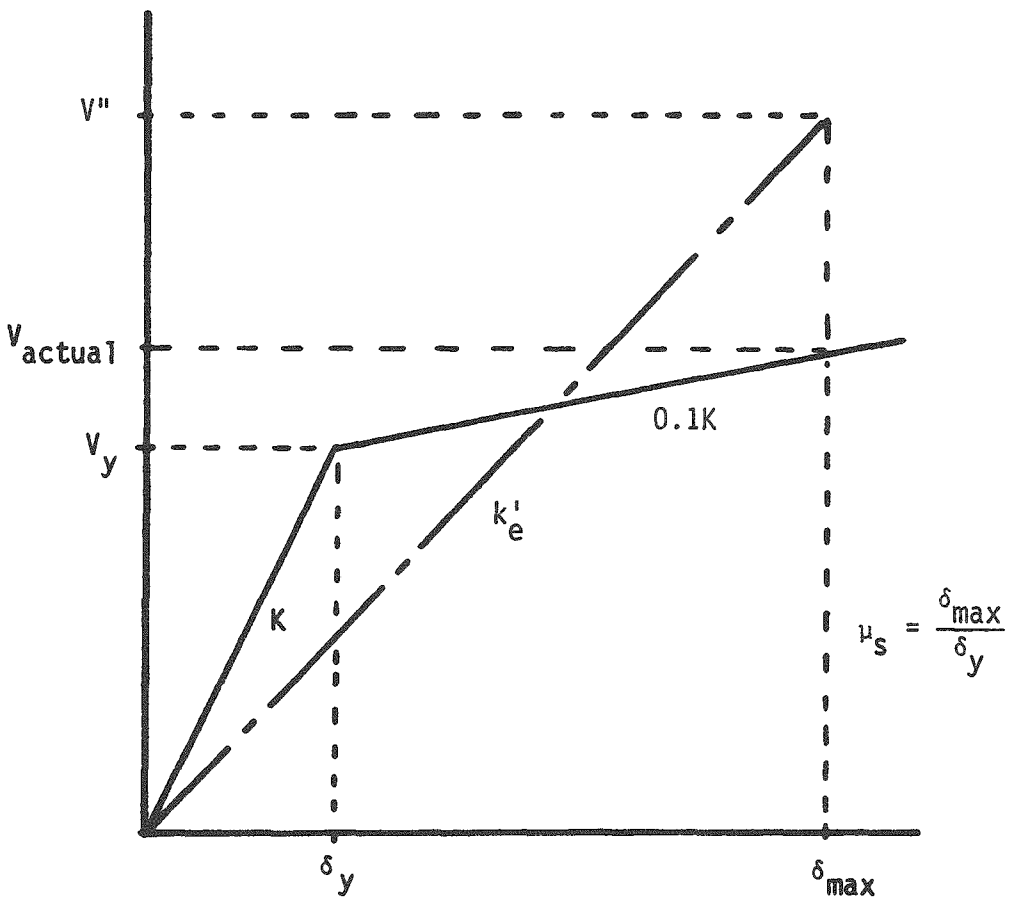

FIGURE 5-7. RELATIONSHIP OF EQUIVALENT LINEAR STIFFNESS, k'_e AND EQUIVALENT SHEAR, V", IN MEMBER TO ACTUAL NONLINEAR SHEAR BEHAVIOR

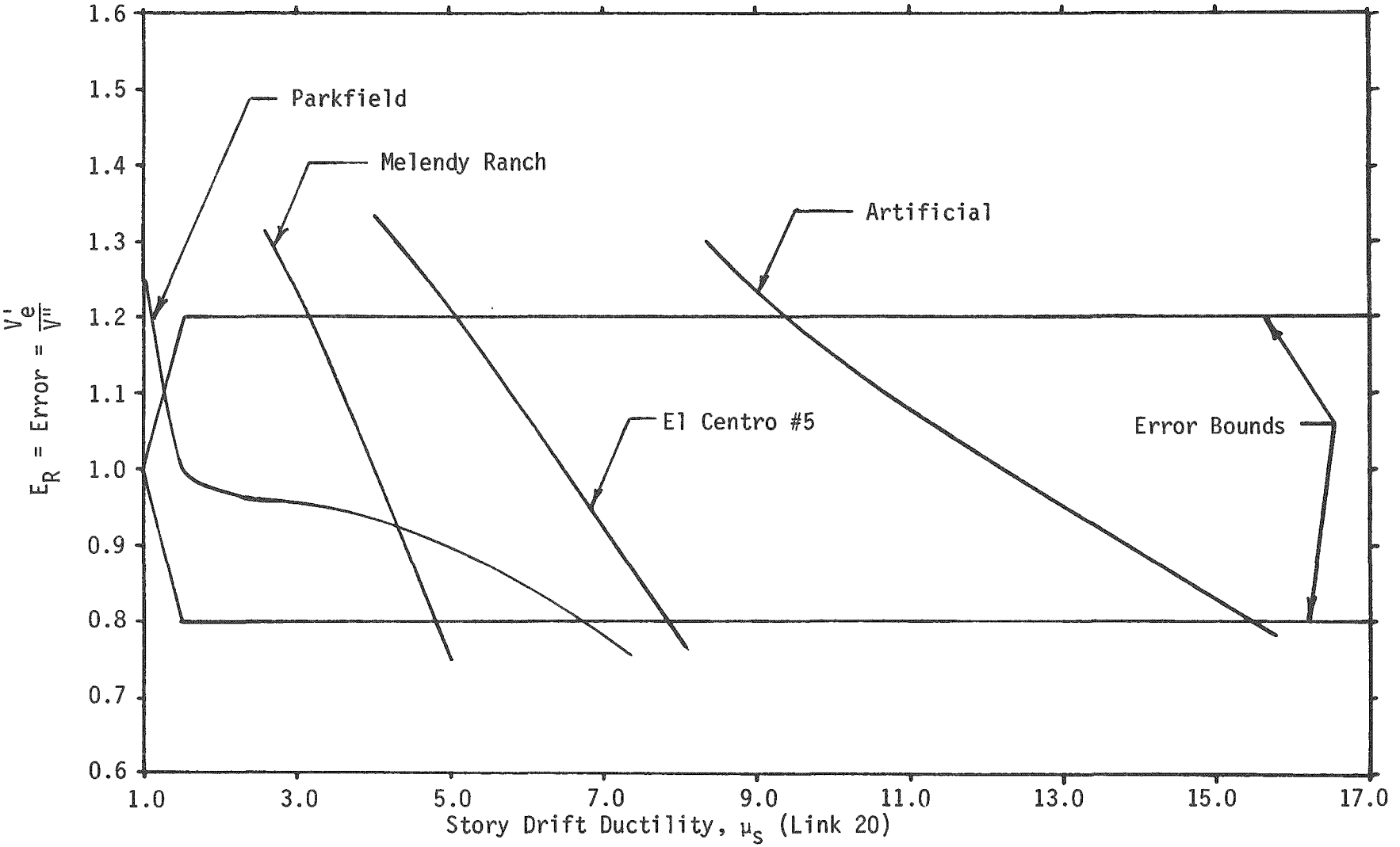

FIGURE 5-8. MODEL ERROR VERSUS STORY DRIFT DUCTILITY FOR ELEMENT 20, FIXED BASE ANALYSES

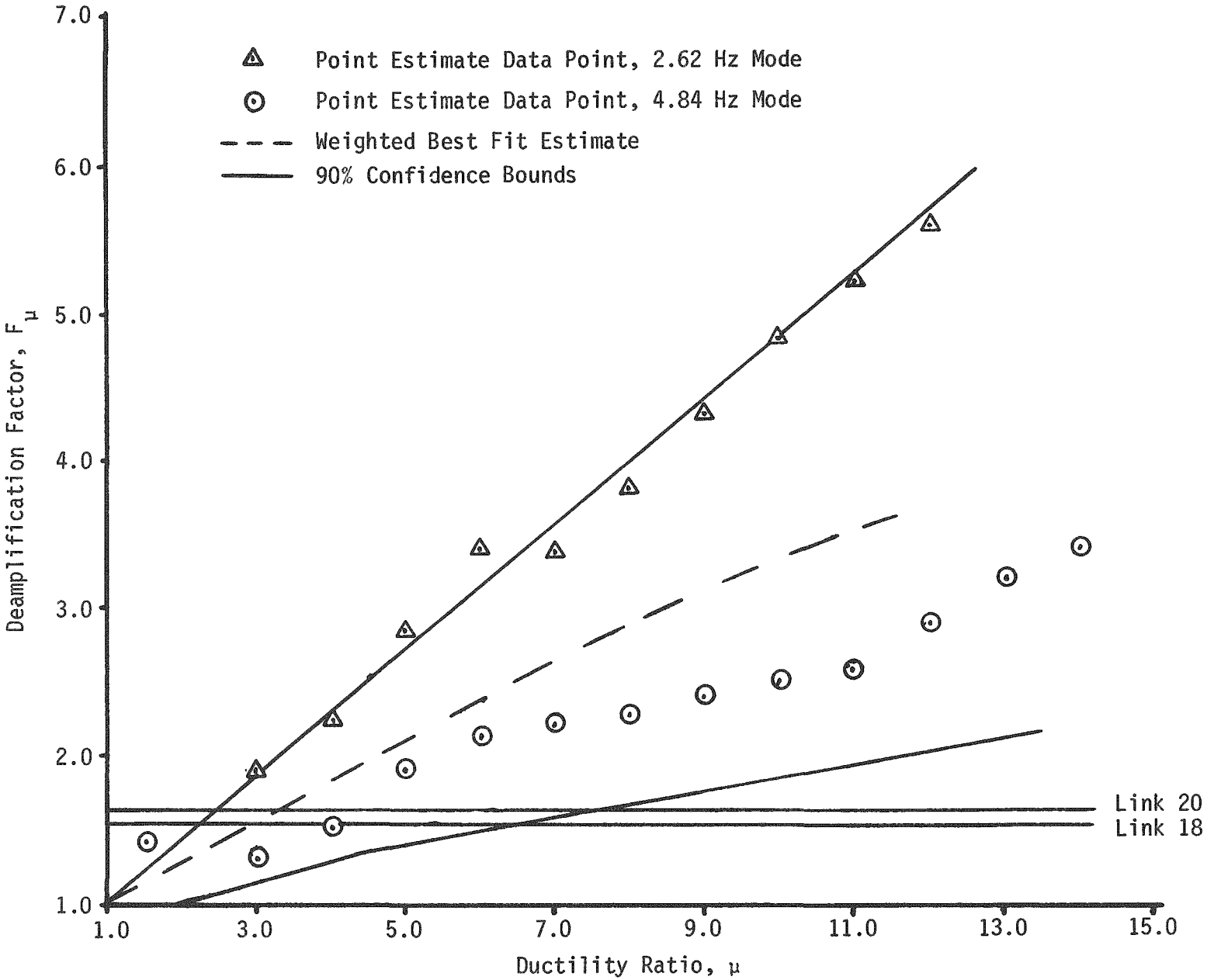

FIGURE 5-9. ESTIMATED F_μ VERSUS μ FOR STIFF SOIL CASE - ARTIFICIAL RECORD

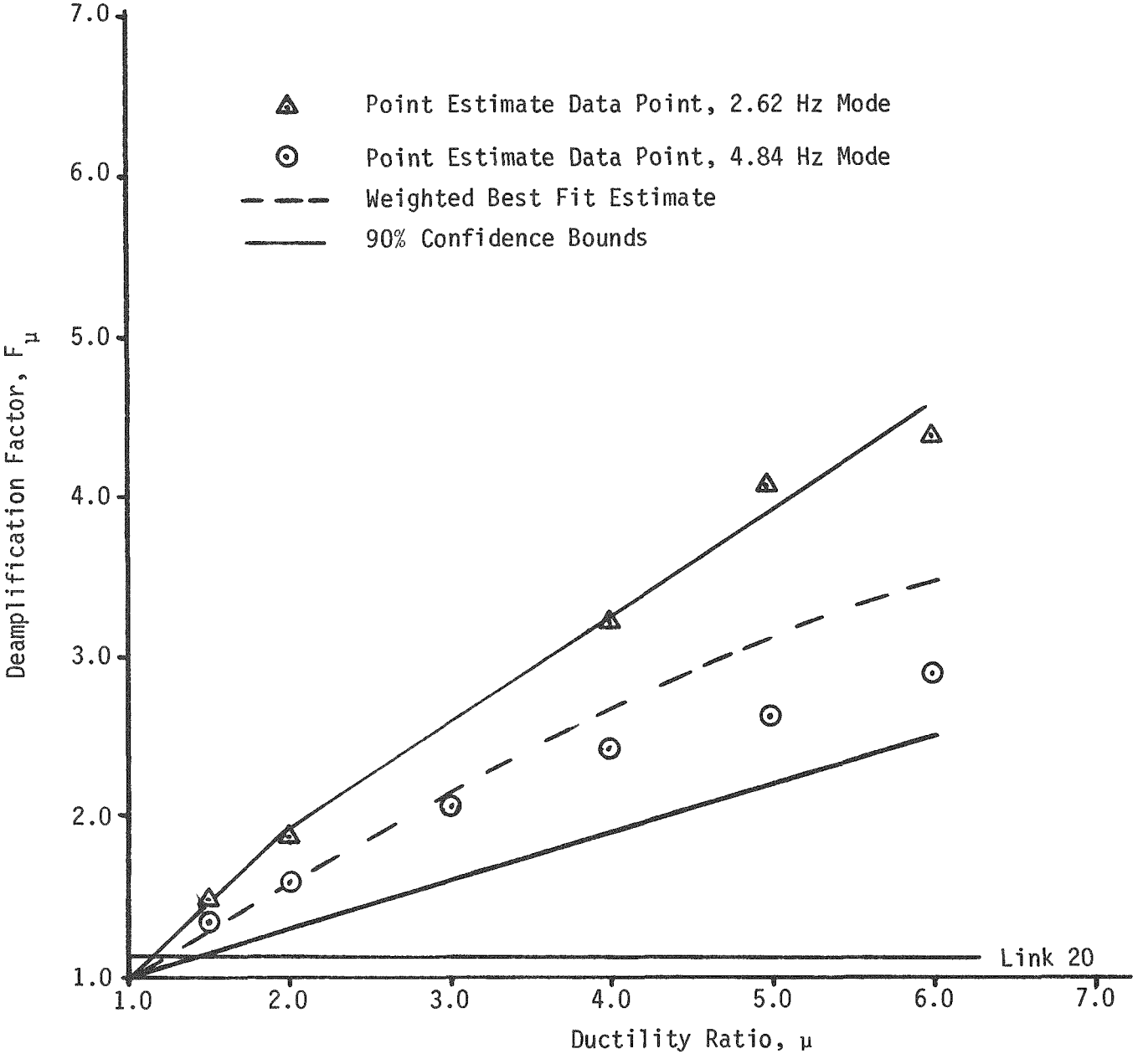

FIGURE 5-10. ESTIMATED F_μ VERSUS μ FOR STIFF SOIL CASE - EL CENTRO #5 RECORD

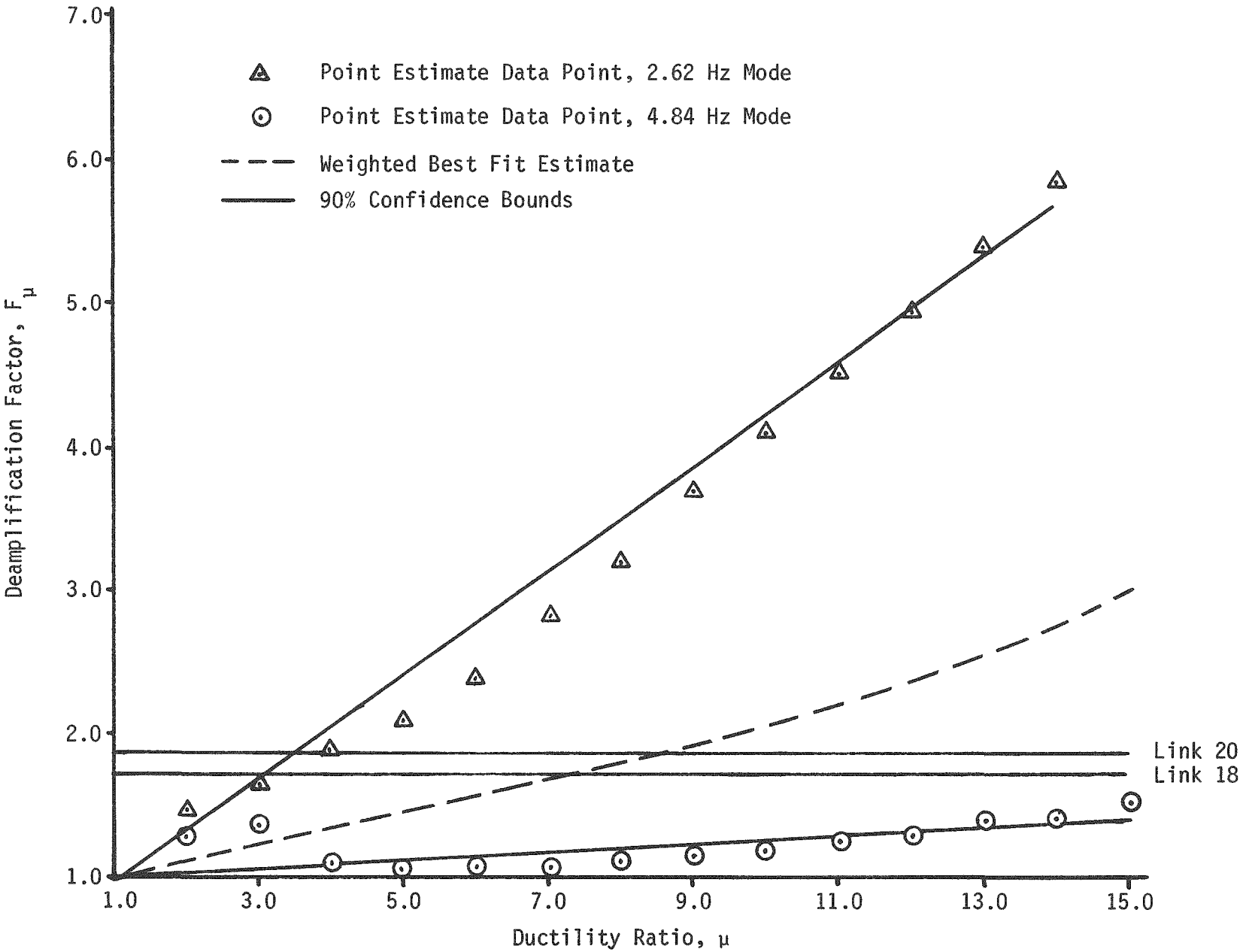

FIGURE 5-11. ESTIMATED F_μ VERSUS μ FOR STIFF SOIL CASE - PARKFIELD RECORD

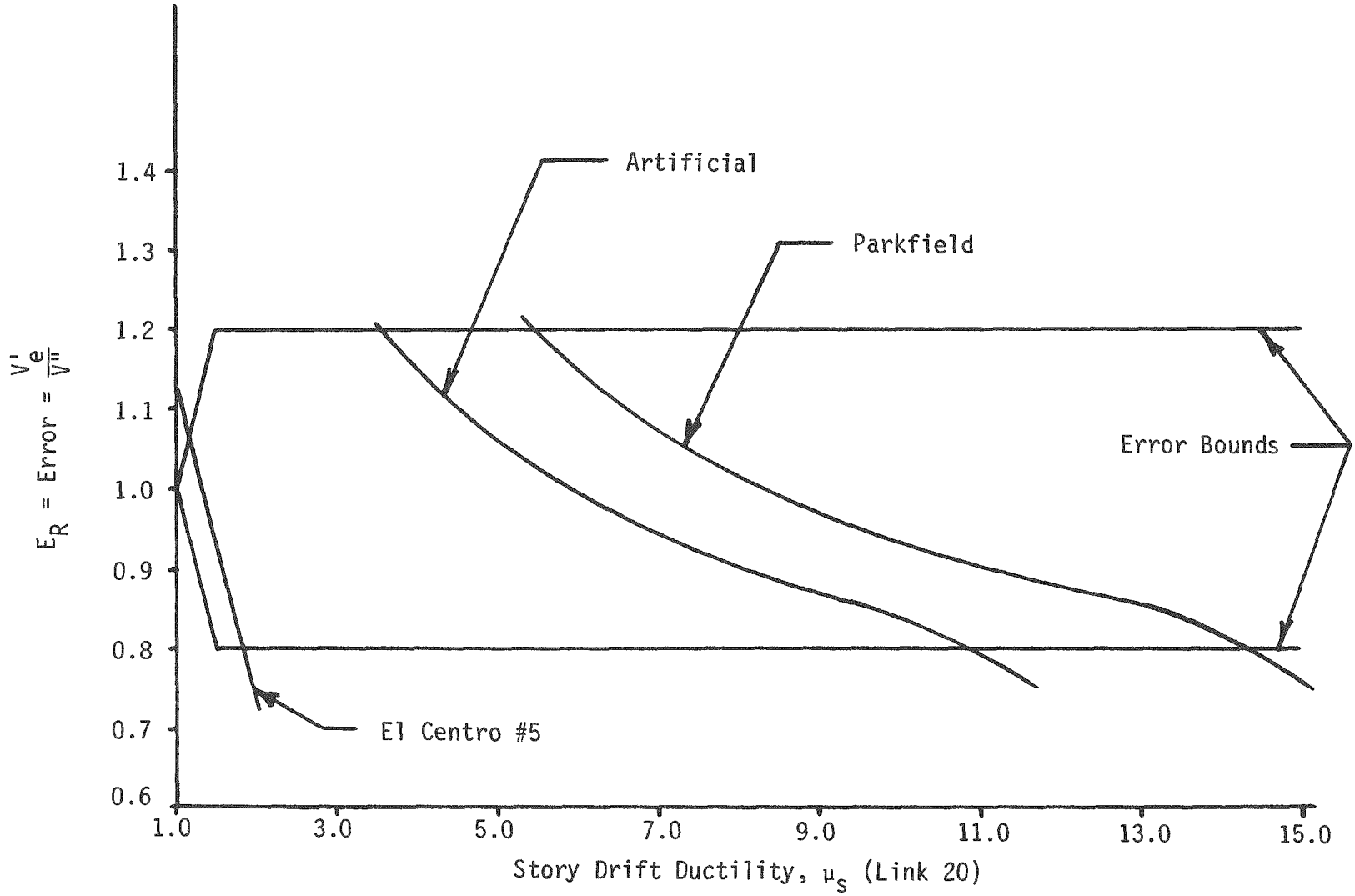

FIGURE 5-12. MODEL ERROR VERSUS STORY DRIFT DUCTILITY FOR ELEMENT 20, STIFF SOIL CASE

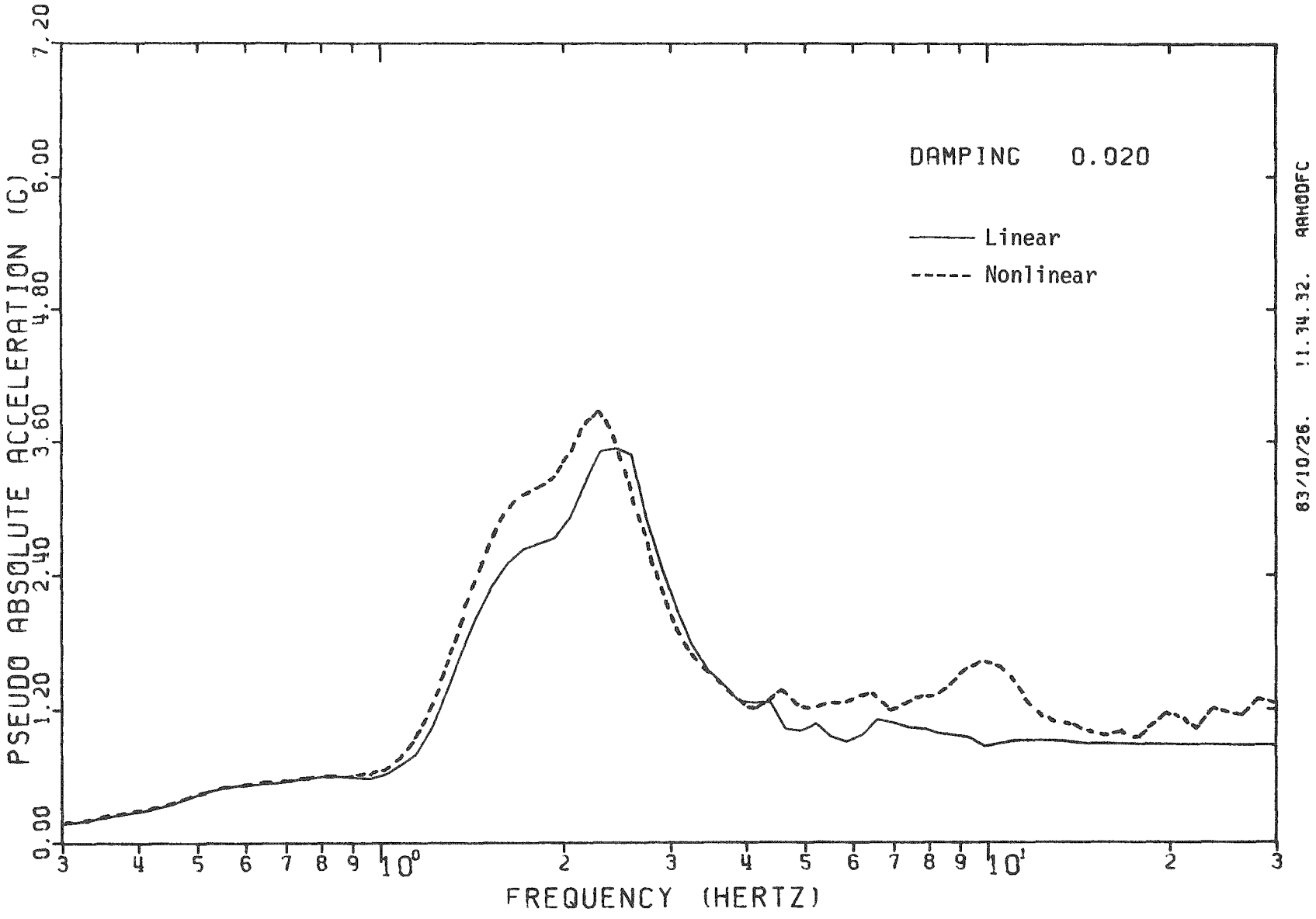

FIGURE 4-10. COMPARISON OF LINEAR AND NONLINEAR IN-STRUCTURE RESPONSE SPECTRA AT NODE 14 IN INTERNAL STRUCTURE FOR PARKFIELD EARTHQUAKE, STIFF SOIL PROFILE

6. CONCLUSIONS

The PWR reactor building considered in this study is shown in Figure 2-3. This structure consists of both an internal structure and a containment. The containment has very high seismic capacity so that only the shear wall internal structure is susceptible to inelastic response and damage under the earthquakes considered in this study. Four earthquakes scaled to 0.5g free-field ground acceleration were considered in this study. These were a long duration 0.5g Artificial time history matching the R. G. 1.60 spectrum, El Centro #5, Parkfield, and Melendy Ranch. Figure 2-7 presents 7% damped spectra for each of these records scaled to one g.

The PWR was considered to be sited on a fixed-base site, as well as embedded 40 feet in a stiff soil site (Figure 2-11) and an intermediate soil site (Figure 2-9). When sited on a fixed-base site the fundamental frequency of the containment is 4.5 Hz and that of the internal structure is 5.2 Hz. When embedded in the stiff soil and intermediate soil sites, the PWR has a predominantly rocking soil mode frequency of 2.6 and 1.8 Hz, respectively, and a predominantly internal structure mode frequency of 4.8 and 4.3 Hz, respectively.

This study compares linear and nonlinear response of the internal structure for the four 0.5g earthquakes and three sites mentioned. For the soil sites, modification of structural response due to soil-structure interaction frequency shifting, embedment effects and kinematic interaction (deamplification of ground motion with depth and wave scattering effects) were all included.

The PWR internal structure being studied was designed to remain elastic for a 0.2g broadbanded response spectrum similar to the Reg. Guide 1.60 spectrum when sited on a stiff soil site ignoring embedment, wave

scattering and kinematic interaction effects. Therefore, for this design earthquake level, no inelastic shear deformations would be expected. When scaled to 0.2g, for fixed-base conditions, the artificial time history and the Melendy Ranch record would result in base shears in the internal structure which are 7% and 19%, respectively, greater than the yield shear while the other two earthquakes scaled to 0.2g would result in base shears less than the yield shear.

The internal structure being studied has highly nonuniform ratios of Shear Demand to Shear Capacity (i.e., elastic computed shear loads versus yield shear strength up the height of the structure). These Demand to Capacity Ratios are presented in Table 3-4 for elastic response of the fixed base structure for the four records being studied scaled to 0.5g. Note that the Demand to Capacity ratios are much higher in the lowest portion of the internal structure than at higher elevations. Thus, the lower region of the internal structure represents a "weak-link" and prevents a relatively uniform distribution of inelastic energy absorption throughout the height of the structure. Instead, all of the inelastic energy absorption must occur in a local region at the base of the internal structure. This "weak-link" aspect to the structure being studied has a very substantial influence on the amount of damage which might result from each of the ground motion records scaled to any ground acceleration level. This structure with a "weak-link" near its base will undergo substantially greater story drift ductilities than would a structure with relatively uniform Demand to Capacity ratios up its height. Any damage characterization of ground motion effects must take into account potential "weak-links" because of nonuniform Demand to Capacity ratios.

The Demand to Capacity ratio for any given story levels, s, represents the input scale factor, F_{μ_s}, corresponding to that story level

(i.e., the factor by which the input must be scaled to bring the computed response to elastic yield levels). Thus:

$$F_{\mu_s} = \left(\frac{\text{Demand}}{\text{Capacity}}\right) = \frac{V_s}{V_{Y_s}} \qquad (6\text{-}1)$$

where V_s is the elastic computed shear at story s and V_{Y_s} is the yield shear at story s. If F_{μ_s} is nearly constant up the height of the structure, the conclusions of Task I (Reference 1) relating F_μ to the system ductility μ would be applicable also to a multi-degree-of-freedom structure. For such structures, the damage characterizations of the ground motion described in Reference 1 are sufficient. However, when F_{μ_s} is highly non-uniform up the height of the structure, conclusions on the damage capability of various ground motions based upon Reference 1 are likely to be overly optimistic. Thus, it was decided to study a structure with localized "weak-links" in Task II.

The PWR internal structure being studied is representative of many nuclear plant structures in that these structures seldom have nearly uniform Demand to Capacity Ratios up their height. However, the structure being studied has a more non-uniform ratio than most nuclear plant structures. Thus, the detrimental influence of highly non-uniform Demand to Capacity ratios are overemphasized in this study. Performance of most structures subjected to ground motions substantially greater than the design ground motion would generally be expected to lie between that predicted in this study for a highly non-uniform Demand to Capacity Ratio structure and that predicted by the methods of Task I for a uniform Demand to Capacity Ratio structure.

It should be noted that all conclusions are for ground motion records scaled to 0.5g which is 2.5 times the design ground motion level at which yield responses of the local "weak-links" are expected. Thus, when scaled to 0.5g each of the earthquake records used represent very severe ground motion relative to the design ground motion level corresponding to yield stress levels.

6.1 DAMAGE CHARACTERIZATION FOR STRUCTURES BASED UPON NONLINEAR RESPONSE FOR 0.5G EARTHQUAKE LEVEL

Structural damage levels for the 0.5g ground motion are best described by the shear story drift ductilities, μ_s, listed in Table 4-6. With ground acceleration levels 2.5 times the level for which this structure was designed to remain elastic, the maximum story drift ductility levels are highly variable ranging from elastic to a ductility of nearly 13 for the differing earthquake motions and site characteristics. For shear wall structures, story drift ductilities in the range of 3 to 4 would be expected to represent relatively moderate damage levels with negligible safety consequences. Story drift ductilities in the 4 to 6 range would be expected to represent the onset of serious structural strength degradation leading to possible collapse after multiple nonlinear response cycles. Certainly, shear story drift ductilities in excess of 8 would likely correspond to collapse under multiple nonlinear response cycles. Thus, the reported results range from rather benign behavior to total collapse despite the constant 2.5 factor increase of ground acceleration over design. Clearly, ground acceleration is not an adequate description of damage even for stiff structures.

For three of the cases, the structure remained elastic. In two more cases, the maximum story drift ductility was less than 2. These low ductilities occurred in nearly half the cases studied despite the fact that the ground motion was increased over design by a factor of 2.5. All of these cases which showed low ductility levels were embedded soil cases. Clearly, the potential reduction in response due to embedment effects is very important for any damage characterization of ground motion.

Four cases lead to maximum story drift shear ductilities between 3 and 7. These cases would not represent collapse but would surely represent observable structural damage. Lastly, three cases lead to maximum story drift shear ductilities between 9 and 13. These cases represent collapse. Clearly, one must understand the causes of these very high

story drift ductilities for this structure in these three cases. One would not generally expect such severe damage for a ground motion only 2.5 times the yield design level.

Each of the following factors have an important influence on the story drift ductilities reported:

1. Non-uniformity of Demand/Capacity Ratio up height of structure. The fact that "weak-links" are local to the base of the internal structure greatly increases the story drift ductilities over those which would have been obtained with more uniform Demand/Capacity Ratios.

2. Elastic spectral acceleration at important natural frequencies of structure. Artificial, El Centro #5, and Melendy Ranch exhibit 7% damped spectral amplification factors between 2 and 3 for the internal structure fixed-base natural frequency of 5.2 Hz. Similarly, the Artificial and Parkfield records show 7% damped spectral amplification factors between 2 and 3 at the soil site rocking frequencies of 2.6 and 1.8 Hz. All of the cases with ductilities greater than 4 correspond to cases with spectral amplifications greater than 2.

3. Breadth of frequency content for frequencies lower than the elastic natural frequencies of the soil-structure system. Figure 2-7 illustrates that the Melendy Ranch spectral acceleration drops off very rapidly at frequencies below 4.5 Hz. This dropoff explains why the Melendy Ranch story drift ductility is much lower for the fixed-base case than one would otherwise expect based upon the very high 5.2 Hz elastic spectral acceleration for Melendy Ranch. Oppositely, the Parkfield record shows high spectral accelerations from 1.3 to 3 Hz and generally increasing spectral accelerations as frequency is reduced within the frequency range of interest (2.6 to 5.2 Hz for the fixed-base case, 1.9 to 4.8 Hz for the stiff soil case, and 1.3 to 4.3 Hz for the intermediate soil case). For this reason, Parkfield shows greater story drift ductilities than one would otherwise expect based upon the spectral accelerations at the elastic natural frequencies. The average spectral acceleration within a frequency range from about 50% to 100% of the elastic frequencies of interest have greater influence on the ductilities reported in Table 4-6 than do the elastic frequency spectral accelerations.

4. Strong Motion duration. As noted in Reference 1, duration has some influence on ductility level reached for degrading stiffness structures. This effect is less significant than the other factors considered. However, the number of strong nonlinear response cycles (which is closely correlated to duration) also influences the amount of damage that would occur for a given story drift ductility. Melendy Ranch which produces only one strong nonlinear response cycle and Parkfield will produce less damage at a story drift ductility of 5 than would El Centro #5 or the Artificial record at this same ductility.

5. Embedment, spacial variation of ground motion, and wave scattering effects. For soil sites, these effects significantly reduce the story drift ductilities below those which would be predicted if these effects are ignored. These reductions are greater for the intermediate soil profile than for the stiff soil profile. Ignoring these reductions is likely to result in severe overprediction of damage.

6. Frequency shifts due to soil-structure interaction (SSI). For longer duration broad frequency content records (Artificial and El Centro #5) frequency shifts due to SSI have very little influence on the story drift ductilities. However, for narrow frequency content records (Parkfield, and Melendy Ranch) these SSI frequency shifts to lower frequencies than the fixed-base modal frequencies have a substantial influence on the story drift ductilities. Such SSI frequency shifts help explain the reduction in story drift ductilities for Melendy Ranch for the soil sites. Similarly, these frequency shifts are the predominant cause of the story drift ductility increases for Parkfield for the soil sites. In fact, the increase in spectral acceleration due to SSI frequency shift is significantly more important for Parkfield than are the response reductions due to embedment, spacial variation, and wave scattering effects.

All of these factors should be considered in any damage characterization of the ground motion.

6.2 DAMAGE CHARACTERISTICS FOR STRUCTURES BASED UPON LINEAR RESPONSE FOR 0.5G EARTHQUAKE LEVEL

The basic question is whether elastic response analyses can be used to estimate the damage level for structures. In other words, can the seismic margin against a certain level of damage be approximately estimated based upon elastic analysis.

One possible method which might be used to estimate damage would be to determine the maximum Story Demand/Capacity Ratio based upon elastic computed response. Such ratios are presented in Table 4-5 for the three site conditions and four earthquake records scaled to 0.5g. Figure 6-1 plots the maximum Story Drift Shear Ductility Ratios of Table 4-6 versus these maximum Demand/Capacity Ratios from Table 4-5. There is a wide scatter between the elastic computed maximum Demand/Capacity Ratio, F_{μ_s}, and the Maximum Story Drift Ductility, μ_s. Thus, the elastic computed F_{μ_s} can only provide a rough approximation of μ_s.

If one were to mistakenly assume that these F_{μ_s} ratios in Figure 6-1 all came from (1) moderate to long duration ($T_D' > 3$ second) records with broad frequency content, (2) SSI effects were unimportant, and (3) that the Demand/Capacity ratio was relatively uniform up the height of the structure, then for stiff structures it would be common to assume that the ratio of system ductility, μ, to F_{μ_s} could be approximated by:

$$F_{\mu_s} \approx \sqrt{2\mu - 1} \qquad (6\text{-}2)$$

One could improve Equation 6-2 by recognizing that the Demand/Capacity Ratio is not uniform so that the maximum story drift inelastic deformation is some multiplier of the system inelastic deformation (i.e.,

$$(\mu_s - 1) \approx M(\mu - 1) \qquad (6\text{-}3)$$

Thus, Equation 6-2 becomes:

$$F_{\mu_s} \approx \sqrt{\frac{2(\mu_s-1)}{M} + 1} \qquad (6\text{-}4)$$

Theoretically, with a uniform Demand/Capacity ratio, M=1. However, in practice, this is difficult to achieve and some non-uniformity in ductility demand in the structure almost always occurs. In this study, this effect has been exaggerated since the PWR being studied has a highly non-uniform Demand/Capacity ratio. Based primarily on the broad frequency content and longer duration records (Artificial and El Centro #5), one might estimate for this PWR internal structure:

(Fixed Base Cases) $M = 3.33$ (6-5a)

(SSI Cases) $M = 10$ (6-5b)

Thus:

(Fixed Base Cases) $F_{\mu_s} \approx \sqrt{0.6(\mu_s-1) + 1}$ (6-6a)

(SSI Cases) $F_{\mu_s} \approx \sqrt{0.2(\mu_s-1) + 1}$ (6-6b)

These curves were developed based on a limited number of cases for a particular structure. While they are not meant to be a design tool, they do indicate some interesting trends as discussed below.

For the cases studied, these curves imply the story drift ductility, μ_s, experienced by the structure for a given Demand/Capacity Ratio, F_{μ_s}, is higher for the soil-structure interaction cases as compared to the fixed base results. The primary effect of nonlinear structural behavior is to lower the effective structure frequency and

raise the effective damping due to hysteretic energy dissipation. For fixed base analyses, this phenomena resulted in substantially reduced loads and in-structure response spectra. However, when soil-structure interaction effects are also included, large changes in the the structure stiffness resulted in only negligible changes in the overall system frequency and seismic response loads. In addition, increased structural damping due to hysteretic behavior is of only minor benefit in reducing seismic response loads since structural damping is small compared to soil radiation damping and has negligible effect on the fundamental soil-structure response mode.

Another factor which may contribute to this phenomena for embedded structures, is that when the shape of foundation level input motion response spectra are compared to response spectra developed from ground surface free-field input motion, the foundation level spectra tend to be reduced in amplitude in the higher frequency range. As the embedded structure goes nonlinear and its effective frequency lowers, the seismic excitation is increased somewhat as compared to a stucture located at the ground surface due to this shape effect. This effect again tends to result in increased ductilities in the structure to achieve the same level of load reduction demonstrated in the fixed base analyses. These three reasons are the primary factors accounting for the trends demonstrated in Figure 6-1.

Typical design practice is to account for the frequency shifting due to SSI effects. However, the reduction in structural response which generally occurs due to embedment effects and kinematic interaction (spatial variation of ground motion and wave scattering effects) is often ignored or conservatively underestimated. Such practice will usually lead to a factor of conservatism, F_{SSI}. As an example, let one assume that the factor is $F_{SSI} = 1.6$ for a typical situation. Now, in addition to this F_{SSI} factor of conservatism, there is the additional factor of conservatism, F_{μ_s}, to go from yield stress levels to

the onset of significant strength degradation for the structure. If one assumes that an acceptable story drift ductility is $\mu_s = 5$, then Equation 6-6 would predict:

(Fixed Base Cases) $F_{\mu_s} = 1.8$

(SSI Cases) $F_{\mu_s} = 1.3$

It would be unconservative to combine an F_{μ_s} factor based upon fixed-base nonlinear structural analyses with an F_{SSI} factor based on elastic SSI analyses. If one were to do this combination, one would incorrectly estimate the overall safety margin, F, to be:

$$F = F_{\mu_s} \times F_{SSI} = 1.8(1.6) = 2.9$$

For such a margin estimate, it would be necessary to use the lower F_{μ_s} values associated with the SSI cases to combine with the separately obtained SSI factor. Thus:

$$F = 1.3\ (1.6) = 2.1$$

<u>In other words, one must be cautious when combining margins shown in this study with other sources of margin defined by other studies in order not to double-count the overall seismic margin.</u>

A final point is that conclusions about damage of stiff structures based upon elastic computed responses are likely to be reasonable for the longer duration ($T_D' > 3$ seconds) and broader frequency content records so long as one considers the uniformity or non-uniformity of the Demand/Capacity ratio throughout the structure when arriving at such conclusions through the use of equations similar to Equation 6-4 rather than Equation 6-2. However, conclusions about damage based upon elastic response are likely to be misleading for short duration ($T_D' < 3$ seconds) narrow frequency content records. This later point is most

clearly illustated by the fixed-base Melendy Ranch case. This case had the largest Demand/Capacity Ratio of F_{μ_s} = 2.97. Yet, the maximum Story Drift Shear Ductility, μ_s, for this case was only 4.7 whereas the use of Equation 6-6a would have predicted a Story Drift Ductility of 14. One must also consider whether spectral accelerations are increasing or decreasing as the natural frequency is reduced due to nonlinear behavior. In the fixed-base Melendy Ranch case, elastic spectral accelerations are substantially reducing as the frequency is reduced below the elastic frequency of 5.2 Hz. The opposite situation is true for the fixed-base Parkfield case. Here spectral accelerations are substantially increased as the elastic frequency is reduced below 5.2 Hz. The elastic Demand/Capacity ratio is only 1.29 from which Equation 6-6a would predict μ_s = 2.1 versus the nonlinear analysis computed value of 3.2.

6.3 IMPROVED ESTIMATES OF STORY DRIFT DUCTILITIES BASED UPON PSEUDO-ELASTIC ANALYSES USING TASK I METHODOLOGY

Section 6.1 defined the important factors influencing story drift ductilities. Section 6.2 presented some very approximate relationships between elastic computed Demand/Capacity ratios and story drift ductilities appropriate for the PWR structure used in this study. However, one must be cautious about extrapolating relationships to other structures. Thus, an improved method for extrapolating elastic computed Demand/Capacity Ratios to Story Drift Ductilities is desirable. Chapter 5 demonstrates how the methodology developed in Task I (Reference 1) for performing pseudo-elastic analysis of one-story shear wall structures can be extended to multi-story shear wall structures.

Two techniques are presented for estimating story drift ductilities of multi-story structures based upon elastic analyses and the methodology developed in Task I (Reference 1) for single-story structures. The first technique (Section 5.1) uses the elastic computed Demand/Capacity Ratios and plots of F_μ versus μ for the earthquake record developed from the Task I methodology. The second technique (Section 5.2) uses a series of elastic analyses of the structure with pseudo-elastic

member elements whose stiffnesses have been reduced and damping increased to account for story drift ductilities. These reduced stiffnesses and increased damping values are obtained using the Task I methodology.

It is shown that either method can approximately predict the actual nonlinear analysis results for story drift ductilities (see Tables 5-1 and 5-2). Thus, by using pseudo-elastic approximate analysis techniques, the Task I methodology for estimating ductilities may also be applied to multi-story structures. For this reason, the engineering characterization of the ground motion given in Task I are also applicable to multi-story structures. It should be recognized that for multi-degree-of-freedom structures, particularly ones with highly nonuniform Demand/Capacity Ratios such as the PWR structure studied in this report, the predicted ductilities developed based on Task I methodology may have significant uncertainty bands associated with them. More parametric evaluations of different structures having significant multi-mode response excited by a wider variety of earthquakes and with more uniform ductility demand throughout the structure would help quantify the actual uncertainty associated with these analysis techniques.

One of the advantages of these elastic and pseudo-elastic methods for estimating story drift ductilities is that time history analyses are not necessary. It is only necessary to have an estimate of the elastic response spectrum and strong motion duration of the record. A second advantage is that the methods provide considerable insight into the causes of differing levels of nonlinear response from differing earthquake records. Thirdly, the methods are amenable to efficient performance of wide variation parametric studies on nonlinear response.

On the other hand, if one has a time history record and plans to perform a very limited number of deterministic nonlinear analyses, it would be more cost effective to perform the nonlinear time history analyses rather than using these estimating procedures with a linear

analysis. Use of these estimating procedures requires more effort (particularly the Section 5.2 method) than does a single nonlinear time history analysis.

6.4 DAMAGE CHARACTERIZATION FOR EQUIPMENT MOUNTED HIGH WITHIN STRUCTURES

The seismic response of equipment is generally evaluated using low damped elastic computed floor spectra. For fixed-base cases, when an important modal frequency of the structure corresponds to the strong frequency content of the earthquake, floor spectra for floors high on the structure show very high spectral amplifications. Figures 3-9 through 3-12 provide 2% damped elastic computed floor spectra for Node 14 high on the interior structure. The 5.2 Hz internal structure is in resonance with the strong frequency content of the 0.5g Artificial, El Centro #5, and Melendy Ranch records. On the other hand, the 5.2 Hz internal structure is not in resonance with the strong frequency content of the Parkfield record. The ratios of peak 2% damped floor spectral acceleration to floor zero period acceleration, $(S_a/ZPA)_{max}$, for these four fixed-base cases are:

Record	Linear $(S_a/ZPA)_{max}$
Artificial	9.8
El Centro #5	8.2
Parkfield	5.9
Melendy Ranch	6.9

Note that the longer duration, broad frequency content records show greater floor spectral amplification than do the short duration records.

When properly anchored, even off-the-shelf equipment (i.e., equipment with no special seismic design provisions) is generally capable of withstanding at least 3g spectral acceleration but is unlikely to be capable of withstanding 10g spectral accelerations. Thus, for an item of

equipment with a natural frequency of 5.2 Hz mounted near the top of the interior structure, one would conclude based upon an elastic computed floor spectrum shown in Figures 3-9 through 3-12 that this equipment was likely to be severely damage by the 0.5g Artificial, El Centro #5, and Melendy Ranch records. Such a conclusion is likely to be highly inaccurate.

Based upon the nonlinear computed floor spectrum, the high resonant floor spectral accelerations at 5.2 Hz only occur when the structure behaves nearly elastic. In fact, for the cases of strong nonlinear response of the structure, no extremely high $(S_a/ZPA)_{max}$ ratios occur at any frequency. For the four fixed-base cases:

Record	Nonlinear $(S_a/ZPA)_{max}$
Artificial	5.3
El Centro #5	4.1
Parkfield	4.0
Melendy Ranch	4.1

Based upon these nonlinear computed floor spectra, it would be unlikely that well-anchored equipment would fail under any of these 0.5g earthquakes, irrespective of the equipment fundamental frequency.

Elastic computed floor spectra place too much emphasis on resonant amplification through the structure. When subjected to earthquakes substantially greater than the design earthquake, real structures are not likely to behave elastically if the structure natural frequency is in resonance with the strong frequency content of the ground motion. Thus, real structures are not likely to show the high resonant amplifications which are obtained for low damped elastic computed floor spectra.

The problem with elastic computed low damped floor spectra is not as great for the SSI cases. The introduction of large radiation damping through wave scattering effects reduces the elastic computed $(S_a/ZPA)_{max}$ ratio. For instance, Figure 4-10 shows this ratio to be only about 4.0 for Parkfield on the stiff soil profile even though the structure frequency is in resonance with the strong frequency content of the Parkfield record. When the linear computed floor spectra do not show high resonance amplification, it appears that linear and nonlinear computed floor spectra will be similar even in the case of large story drift ductilities. In this case, linear computed floor spectra may be appropriate for equipment evaluation.

It appears that elastic computed $(S_a/ZPA)_{max}$ ratios greater than the 4 to 6 range are unrealistic for the following reasons. First, much longer strong motion durations are required to build up to the same level of response predicted by a fixed-base analysis because of increased energy dissipated by the structure through inertial and kinematic interaction. More importantly, when high response is expected due to a sufficiently long ground motion duration and low soil radiation damping, nonlinear yielding of critical members tend to protect equipment located high in the structure resulting in reduced seismic loads.

Although beyond the scope of this study, further study is necessary to better define the engineering characterization of ground motion effects on structure mounted equipment. Clearly, elastic computed floor spectra are excessively conservative in some cases.

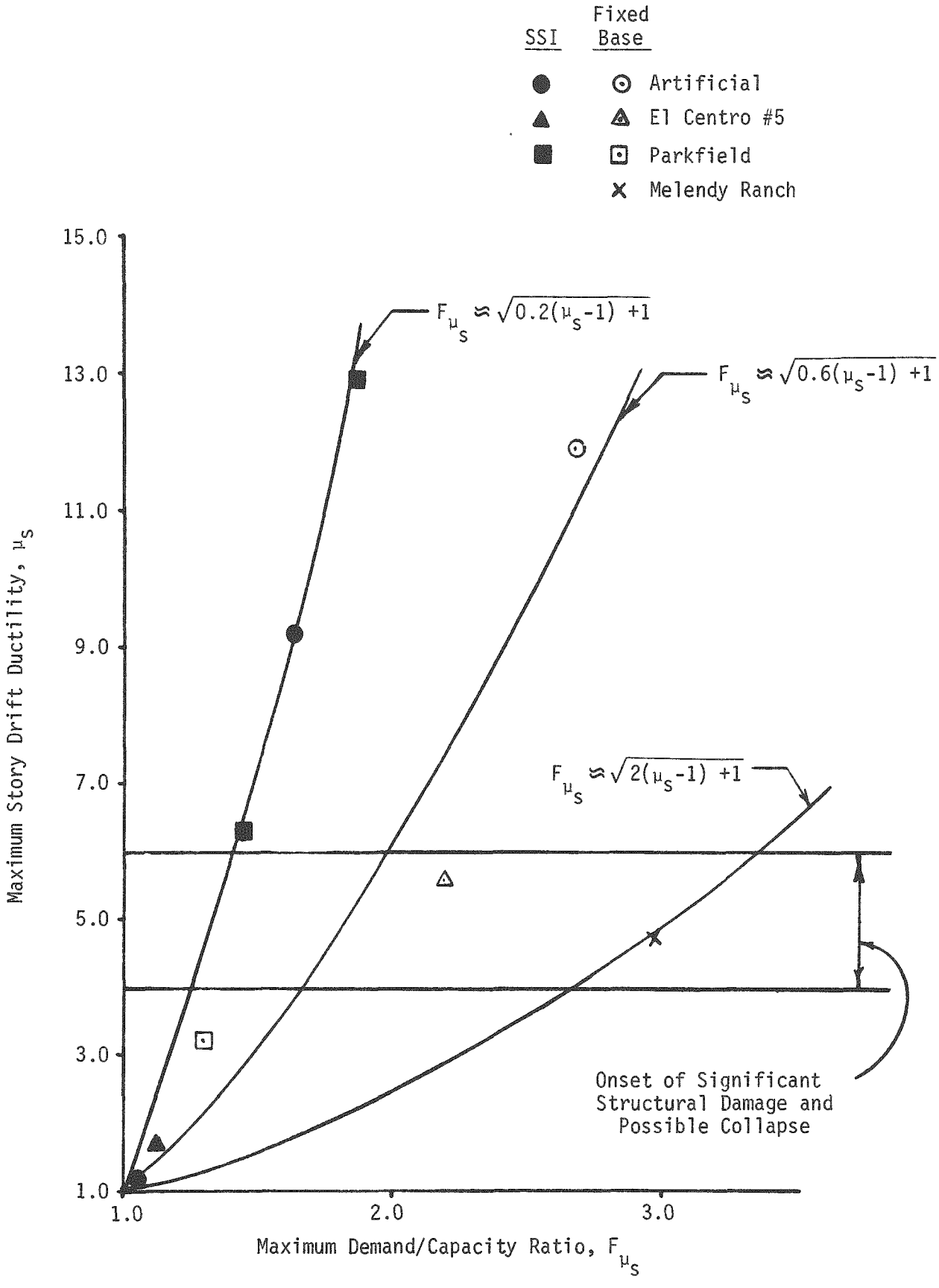

FIGURE 6-1. MAXIMUM STORY DRIFT DUCTILITY VERSUS MAXIMUM DEMAND/ CAPACITY RATIO

REFERENCES

1. Kennedy, R. P., Short, S. A. Kipp, T. R., Banon, H., Tokarz, F. J. and K. L. Merz. "Engineering Characterization of Ground Motion - Task I: Effects of Characteristics of Free-Field Motion on Structural Response", Structural Mechanics Associates, SMA 12702.01, NUREG/CR-3805, Vol. 1, May 1984.

2. Newmark, N. M., Kennedy, R. P., and S. A. Short, "Final Report Evaluation of a Typical PWR Reactor Building Subjected to a High Acceleration, Short Duration Earthquake", Nathan M. Newmark Consulting Engineering Services and Engineering Decision Analysis Company, Inc., August, 1979.

3. Kennedy, R. P., Short, S. A., and N. M. Newmark, "The Response of a Nuclear Power Plant to Near-Field Moderate Magnitude Earthquakes", Transactions of the 6th International Conference on Structural Mechanics in Reactor Technology, Paris, France, August, 1981, Volume K(a), paper 8/1.

4. Powell, G. H., "DRAIN-2D Users Guide", University of California, Berkeley, California, August, 1975.

APPENDIX A

DEVELOPMENT OF SOIL IMPEDANCES FOR SOIL-STRUCTURE INTERACTION ANALYSES OF PWR REACTOR BUILDING

APPENDIX A

A.1 DESCRIPTION OF PROBLEM

Soil-structure interaction analyses of the PWR reactor building were conducted by SMA for the intermediate and stiff soil profiles previously presented in Figures 2-9 and 2-11 and discussed in Section 2.4.2. Soil impedances representing frequency dependent stiffness and damping characteristics of these profiles were supplied to SMA by Woodward-Clyde Consultants. In addition, Woodward-Clyde provided foundation input motions incorporating kinematic interaction for the four ground motions discussed in Section 2.3. The frequency dependent soil impedances and basemat ground motion supplied to SMA for the soil-structure interaction analyses were developed by Dr. J. E. Luco of the University of California at San Diego and Dr. H. L. Wong of the University of Southern California using computer program CLASSI (Reference A-1).

In general, soil impedances representing the stiffness and damping of the underlying soil are frequency dependent. However, computer program DRAIN (Reference A-2) which was used by SMA in Task II to conduct linear and nonlinear time history analyses of the PWR structure, requires the soil be modeled by a unique, single frequency soil spring and dashpot. Therefore, a step by step procedure was developed to determine soil springs and dashpots consistent with the frequency dependent soil impedances. The remainder of this Appendix presents this procedure along with the soil springs and dashpots used in DRAIN analyses to represent the intermediate and stiff soil profiles.

A.2 INTERPRETATION OF FREQUENCY DEPENDENT SOIL IMPEDANCES

In general, soil impedances may be specified by:

$$\begin{Bmatrix} F \\ M \end{Bmatrix} = \begin{bmatrix} K_{xx} & K_{x\phi} \\ K_{\phi x} & K_{\phi\phi} \end{bmatrix} \begin{Bmatrix} u \\ \phi \end{Bmatrix} \qquad \text{(A-1)}$$

where the impedance functions K_{xx}, $K_{x\phi}$, and $K_{\phi\phi}$ are frequency dependent complex functions and for this study are defined with respect to the bottom of the PWR foundation mat (node 30 in Figure 2-3).

The expanded complex stiffness terms in Equation A-1 are:

$$\left.\begin{aligned} K_{xx} &= GL\,(k_{xx} + ia_o\,c_{xx}) \\ K_{x\phi} &= K_{\phi x} = GL^2\,(k_{x\phi} + i\,a_o c_{x\phi}) \\ K_{\phi\phi} &= GL^3\,(k_{\phi\phi} + i\,a_o c_{\phi\phi}) \end{aligned}\right\} \qquad \text{(A-2)}$$

where $a_o = \frac{\omega L}{V_S}$, $i = \sqrt{-1}$, ω = circular frequency of excitation, L = characteristic dimension of the foundation, and V_S = shear wave velocity of the soil medium.

The stiffness and damping coefficients in Equation A-1 include a coupling term, $K_{x\phi}$, between horizontal translation and rocking. This equation may be rewritten in terms of an uncoupled stiffness coefficient, K_S, and uncoupled rocking coefficient, K_M, expressed by:

$$\begin{Bmatrix} F' \\ M' \end{Bmatrix} = \begin{bmatrix} K_S & o \\ o & K_M \end{bmatrix} \begin{Bmatrix} u' \\ \phi' \end{Bmatrix} \qquad \text{(A-3)}$$

where u' and ϕ' are the transformed coordinates at the center of rotation of the foundation basemat and are located at a distance H above the bottom of the foundation basemat. The parameter H is defined by:

$$H = -\frac{K_{x\phi}}{K_{xx}} \tag{A-4}$$

Expanding equation A-3:

$$K_S = K_{xx} = GL\ (k_{xx} + i\ a_o c_{xx})$$

$$K_M = K_{\phi\phi} - \frac{K_{x\phi}\ K_{\phi x}}{K_{xx}} = GL^3\ (k_M + i\ a_o c_M) \tag{A-5}$$

Figures A-1 and A-2 present the frequency dependent translational real and imaginary coefficients, k_{xx} and c_{xx} for both soil profiles. Similarly, Figures A-3 and A-4 present the uncoupled rocking real and imaginary coefficients k_M and c_M. Figures A-5 and A-6 present the variation of height of center of foundation stiffness, H, with frequency as determined from Equation A-4. In this study, $G=5.64 \times 10^7$ psf, L = 63.3 ft, and V_S = 3600 fps.

Interpretation of complex soil impedances in terms of soil springs and viscous dashpots may be demonstrated for the stiffness term K_{xx}. Substituting:

$$u = \frac{\dot{u}}{\omega}$$

into Equations A-3 and A-5:

$$F' = GL\ k_{xx}\ u + i\left(\frac{a_o c_{xx} GL}{\omega}\right)\dot{u}$$

and noting $a_o = \frac{\omega L}{V_S}$

$$F' = GL\ k_{xx}\ u + i\ \frac{\omega L}{V_S}\ \frac{c_{xx}\ GL}{\omega}\ \dot{u}$$

This equation may be interpreted as:

$$\left.\begin{aligned} K_x' &= GL\ k_{xx} \\ C_x' &= \frac{GL^2\ c_{xx}}{V_S} \end{aligned}\right\} \qquad \text{(A-6)}$$

where K_x' and C_x' are the soil spring and velocity dependent dashpot compatible with DRAIN.

Similarly, for rocking:

$$\left.\begin{aligned} K_M' &= GL^3\ k_M \\ C_M' &= \frac{GL^4\ c_M}{V_S} \end{aligned}\right\} \qquad \text{(A-7)}$$

A Rayleigh damping definition was used to model structure damping in the time history analyses. Because a Rayleigh definition smears the system damping over the entire structure including the soil springs and dashpots, the rocking and translational dashpots must be artificially reduced to avoid double-counting of structural damping.

This may be approximately accomplished by assuming all soil-structure interaction occurs at the fundamental soil-structure frequency, ω. Defining:

$$C_{cr} = 2\sqrt{K'_X M} \tag{A-8}$$

$$\omega = \sqrt{\frac{K'_X}{M}} \tag{A-9}$$

where M is the mass of the structure and combining A-8 and A-9, the critical damping ratio, C_{cr}, is:

$$C_{cr} = 2 \frac{K'_X}{\omega} \tag{A-10}$$

Assuming λ_i is the desired fraction of critical damping to be removed from the dashpot, the actual dashpot used in DRAIN analyses is given by:

$$C''_X = C'_X - 2 \frac{K'_X}{\omega} \lambda_i \tag{A-11}$$

$$C''_M = C'_M - 2 \frac{K'_M}{\omega} \lambda_i \tag{A-12}$$

A.3 METHODOLOGY TO DEVELOP SOIL SPRINGS AND DASHPOTS FOR DRAIN ANALYSES

Using the equations developed in the previous section, a procedure for estimating the soil springs and dashpots for use in DRAIN was developed. A flowchart of this procedure follows. For each soil case:

1. Using an estimate of the fundamental soil-structure frequency, f, estimate the desired average stiffness or damping coefficient from Figures A-1 through A-4 within a range of 0.8f to 1.25f. The purpose of using an average coefficient is to minimize the effects of local peaks and valleys on the desired impedance.

2. Use equations A-6 and A-7 to estimate the translational and rocking stiffnesses using the coefficients determined in step 1 above.

3. Use Equations A-11 and A-12 in conjunction with the stiffness determined in step 2 to determine estimated translational and rocking soil dashpots.

4. Noting that the coupled soil impedances in Equation A-1 are defined with respect to the bottom of the PWR foundation, use Figures A-5 or A-6 to determine the location of the uncoupled soil springs and dashpots considered the change in height, H, at soil-structure frequency, f, which occurs when the impedance functions are uncoupled. This adjustment must also be applied to input time histories by using a rigid body transformation of the rotational and translational basemat ground motion.

5. Use results from step 4 to conduct a modal analysis of the PWR structure. Check that the actual soil-structure frequency, f', equals the estimated frequency, f, from step 1. Iterate on steps 1 through 5 until desired convergence is achieved.

6. To further validate results, compare elastic shears, moments, and peak spectral response in the PWR structure determined from a linear time history analysis using computer program DRAIN, to corresponding linear analysis results determined from CLASSI.

Table A-1 presents the soil springs and dashpots determined using the above procedure for both the intermediate and stiff soil profiles. These soil springs and dashpots were determined assuming a fundamental frequency, f, of 1.8 Hz and 2.6 Hz for the intermediate and stiff soil profiles, respectively.

Comparisons of elastic moments and shears for these soil impedances determined using DRAIN with those calculated by CLASSI are presented in Table A-2. Note the excellent agreement with a maximum difference between results of 8.4 percent in one case and all other comparisons generally within 5 percent or less. Similar comparisons of elastic in-structure response spectra demonstrated very good agreement with differences in peak spectral response of 10 percent or less for all cases.

TABLE A-1

DRAIN SOIL SPRINGS AND DASHPOTS

Soil Profile	Response	Soil Spring	Dashpot	Height Correction[1] H	
				Stiffness	Damping
Intermediate	Translation	1.46×10^{8} lb/in	8.51×10^{6} $\frac{\text{lb-sec}}{\text{in}}$	154 in	0 in
	Rocking	6.97×10^{13} $\frac{\text{lb-in}}{\text{rad}}$	8.42×10^{11} $\frac{\text{lb-sec-in}}{\text{rad}}$		
Stiff	Translation	3.65×10^{8} lb/in	1.13×10^{7} $\frac{\text{lb-sec}}{\text{in}}$	75 in	15 in
	Rocking	2.12×10^{14} $\frac{\text{in-lb}}{\text{rad}}$	1.82×10^{10} $\frac{\text{lb-sec-in}}{\text{rad}}$		

1. Height correction, H, is distance above bottom of basemat, node 30, in Figures 2-3 and 2-4.

TABLE A-2

COMPARISON OF PEAK ELASTIC SHEARS AND OVERTURNING MOMENTS AT BASE OF PWR CONTAINMENT STRUCTURE AND INTERNAL STRUCTURE, INTERMEDIATE SOIL PROFILE

Earthquake	Location	Peak Shear (lb)		% Difference $(\frac{\text{DRAIN}}{\text{CLASSI}})$	Peak Moment (in-lb)		% Difference $(\frac{\text{DRAIN}}{\text{CLASSI}})$
		CLASSI	DRAIN		CLASSI	DRAIN	
Artificial	Containment	2.71×10^{7}	2.79×10^{7}	3.0	4.91×10^{10}	5.10×10^{10}	3.9
	Internals	1.80×10^{7}	1.83×10^{7}	1.7	1.20×10^{10}	1.24×10^{10}	3.3
El Centro #5	Containment	1.71×10^{8}	1.70×10^{7}	-0.6	3.22×10^{10}	3.37×10^{10}	4.7
	Internals	1.20×10^{8}	1.11×10^{7}	-7.5	8.20×10^{9}	7.84×10^{9}	-4.4
Parkfield	Containment	3.95×10^{8}	4.10×10^{7}	3.8	6.72×10^{10}	7.01×10^{10}	4.3
	Internals	2.44×10^{8}	2.48×10^{7}	1.6	1.81×10^{10}	1.83×10^{10}	1.1
Melendy Ranch	Containment	6.56×10^{8}	6.56×10^{6}	0	1.26×10^{10}	1.26×10^{10}	0
	Internals	1.16×10^{8}	1.13×10^{7}	2.6	7.99×10^{9}	7.54×10^{9}	-5.6

TABLE A-3

COMPARISON OF PEAK ELASTIC SHEARS AND OVERTURNING MOMENTS AT BASE OF PWR CONTAINMENT STRUCTURE AND INTERNAL STRUCTURE, STIFF SOIL PROFILE

Earthquake	Location	Peak Shear (lb)		% Difference $(\frac{DRAIN}{CLASSI})$	Peak Moment (in-lb)		% Difference $(\frac{DRAIN}{CLASSI})$
		CLASSI	DRAIN		CLASSI	DRAIN	
Artificial	Containment	4.51×10^{7}	4.68×10^{7}	3.8	7.78×10^{10}	8.14×10^{10}	4.6
	Internals	2.71×10^{8}	2.81×10^{7}	3.7	2.06×10^{10}	2.16×10^{10}	4.9
El Centro #5	Containment	2.70×10^{8}	2.79×10^{7}	3.3	4.56×10^{10}	4.72×10^{10}	3.5
	Internals	1.87×10^{8}	1.94×10^{7}	3.7	1.37×10^{10}	1.42×10^{10}	3.9
Parkfield	Containment	4.67×10^{7}	4.84×10^{7}	3.6	7.73×10^{10}	8.04×10^{10}	4.0
	Internals	3.14×10^{7}	3.20×10^{7}	1.9	2.25×10^{10}	2.30×10^{10}	2.2
Melendy Ranch	Containment	1.01×10^{7}	1.01×10^{7}	0	1.83×10^{10}	1.82×10^{10}	-0.5
	Internals	9.50×10^{6}	1.03×10^{7}	8.4	7.67×10^{9}	7.76×10^{9}	1.2

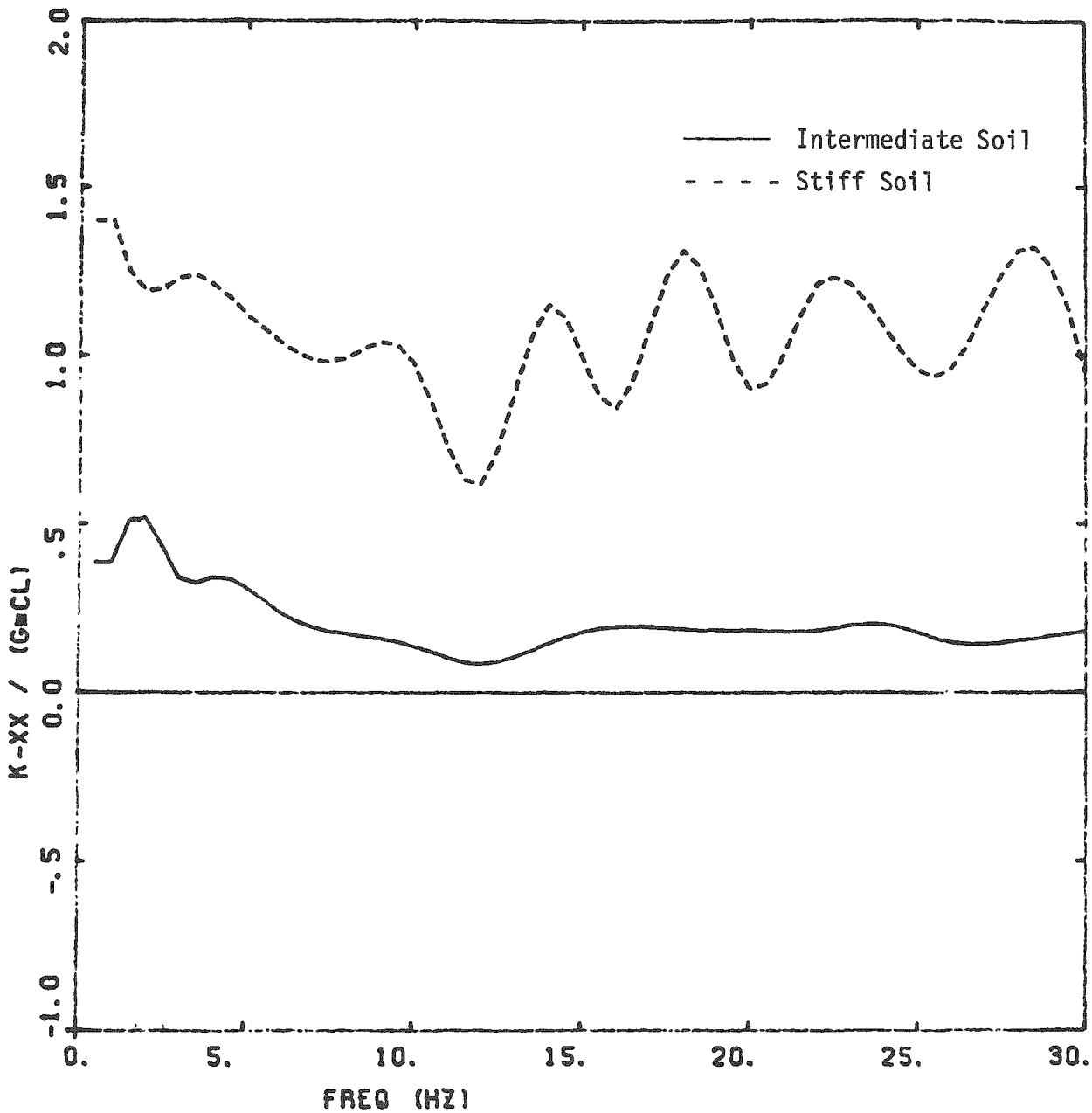

FIGURE A-1. VARIATION OF TRANSLATIONAL STIFFNESS COEFFICIENT WITH FREQUENCY, INTERMEDIATE AND STIFF SOIL PROFILES

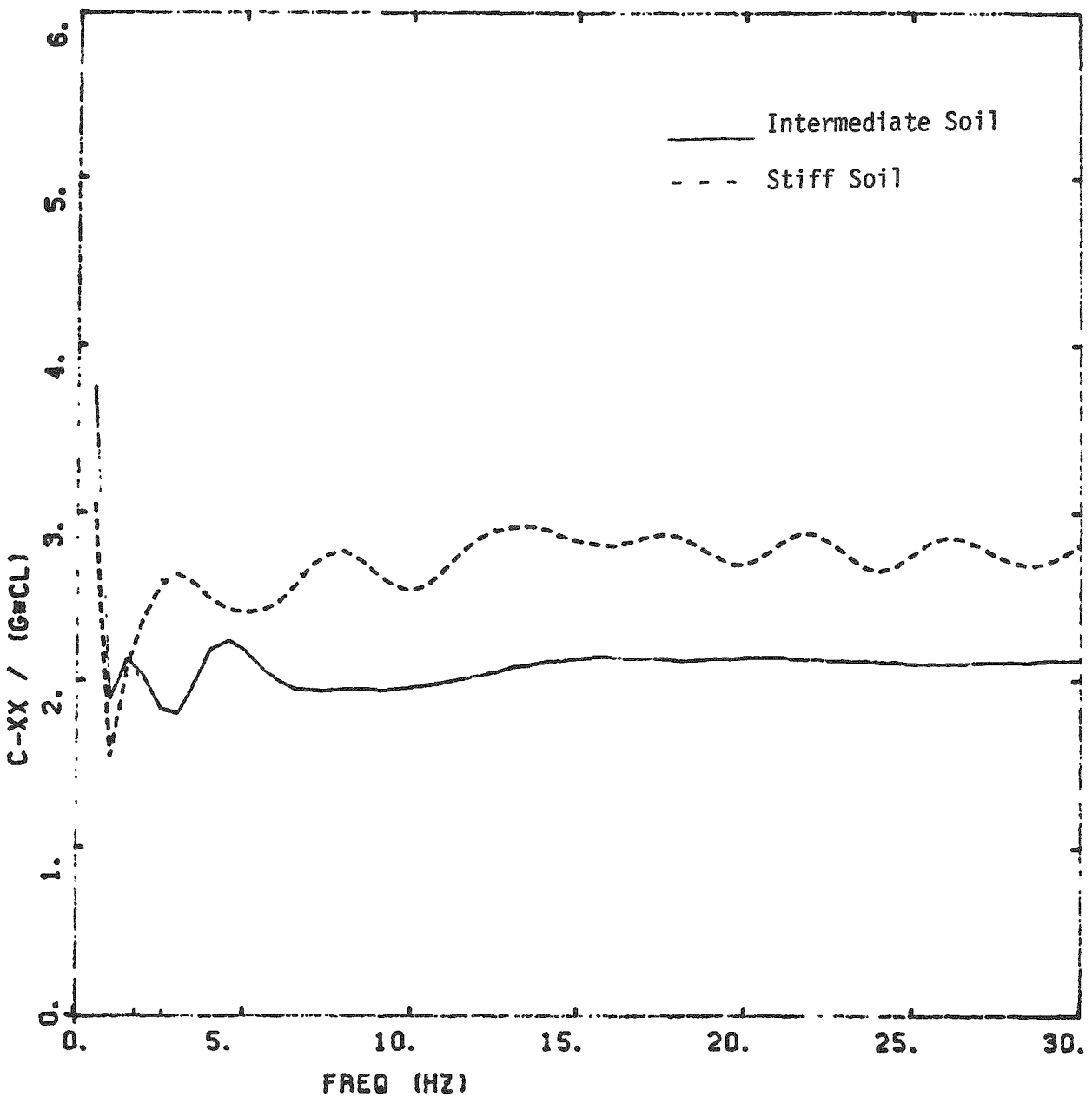

FIGURE A-2. VARIATION OF TRANSLATIONAL DAMPING COEFFICIENT WITH FREQUENCY, INTERMEDIATE AND STIFF SOIL PROFILES

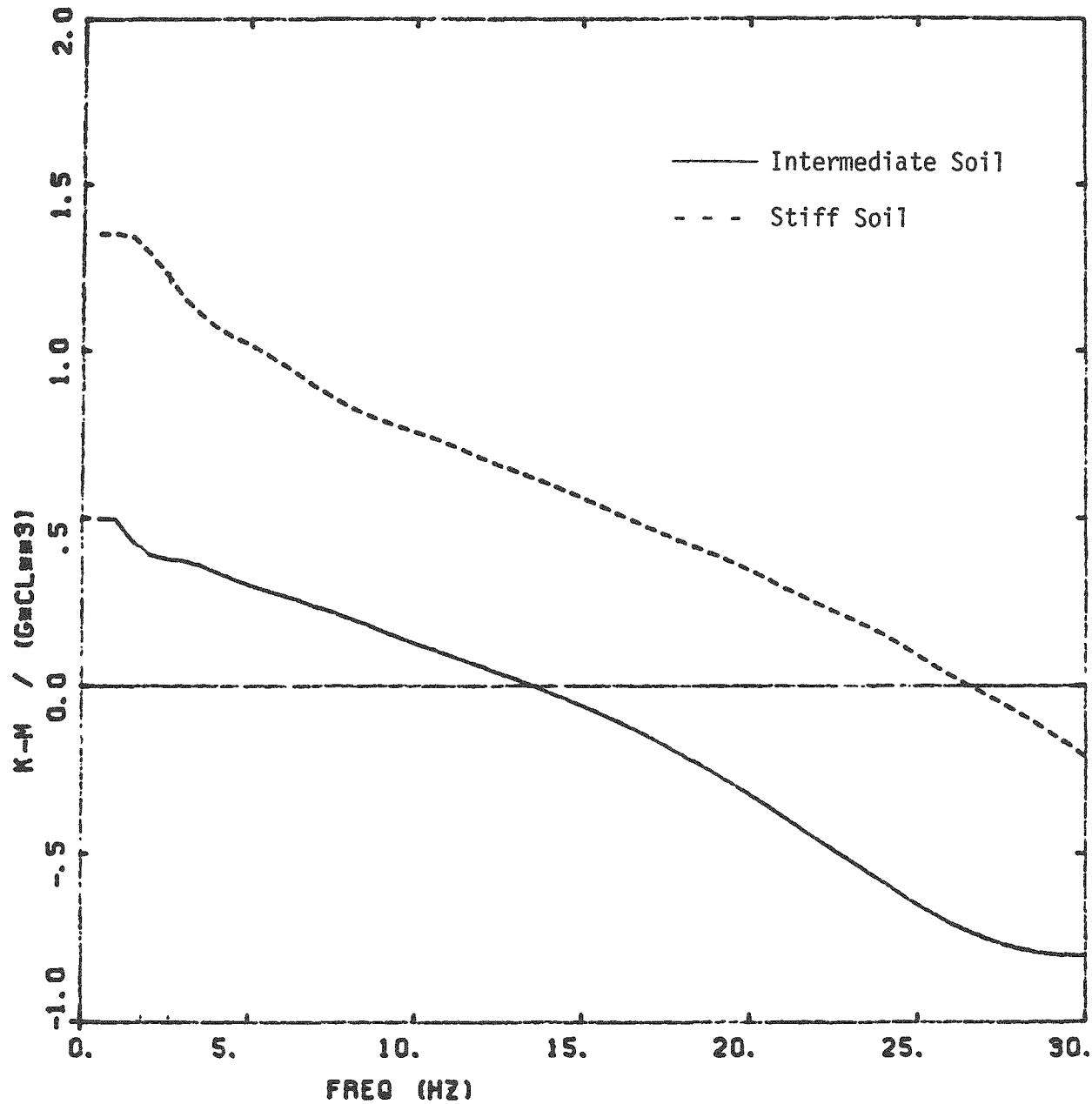

FIGURE A-3. VARIATION OF UNCOUPLED ROCKING STIFFNESS COEFFICIENT WITH FREQUENCY, INTERMEDIATE AND STIFF SOIL PROFILES

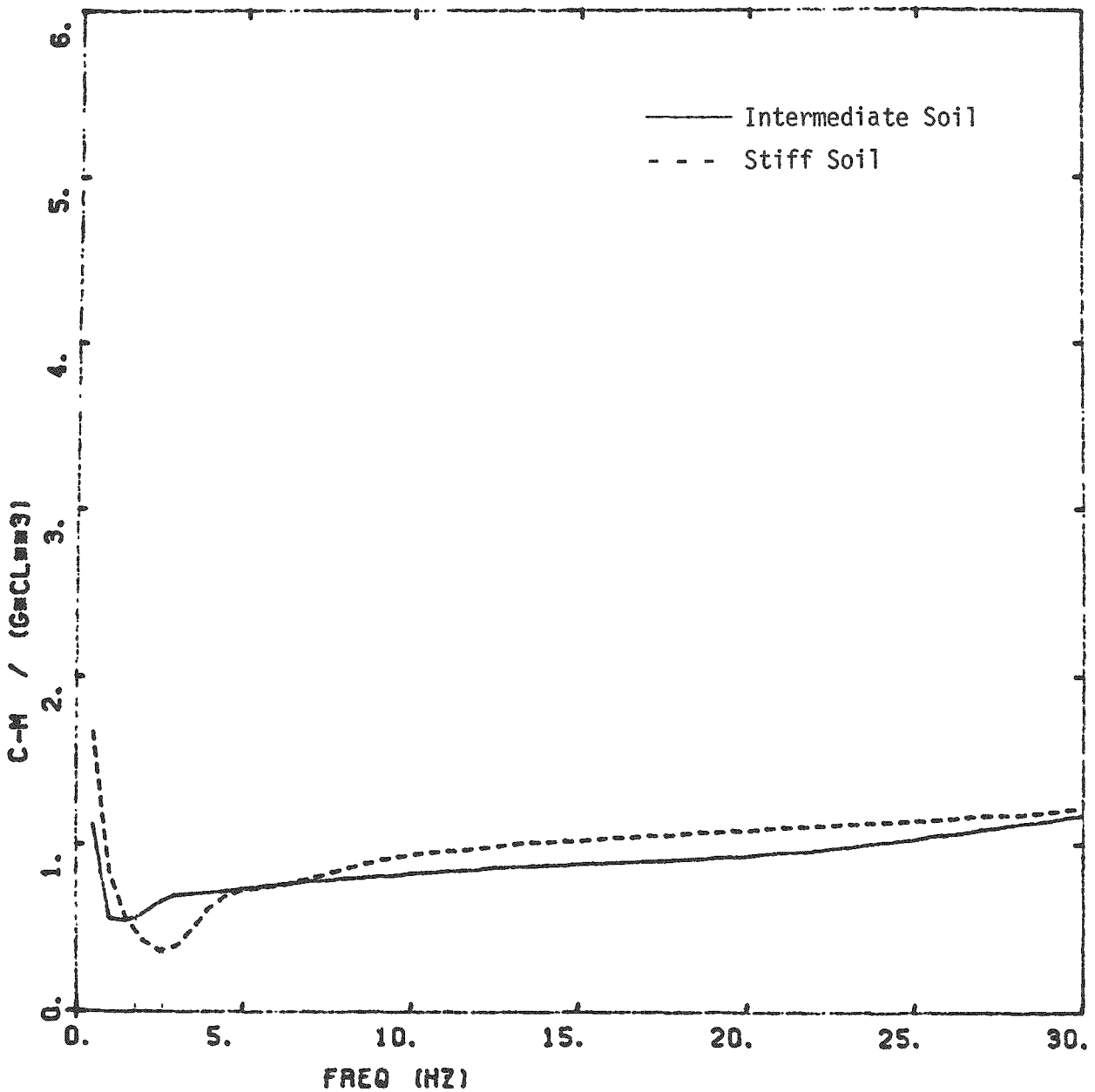

FIGURE A-4. VARIATION OF UNCOUPLED ROCKING DAMPING COEFFICIENT WITH FREQUENCY, INTERMEDIATE AND STIFF SOIL PROFILES

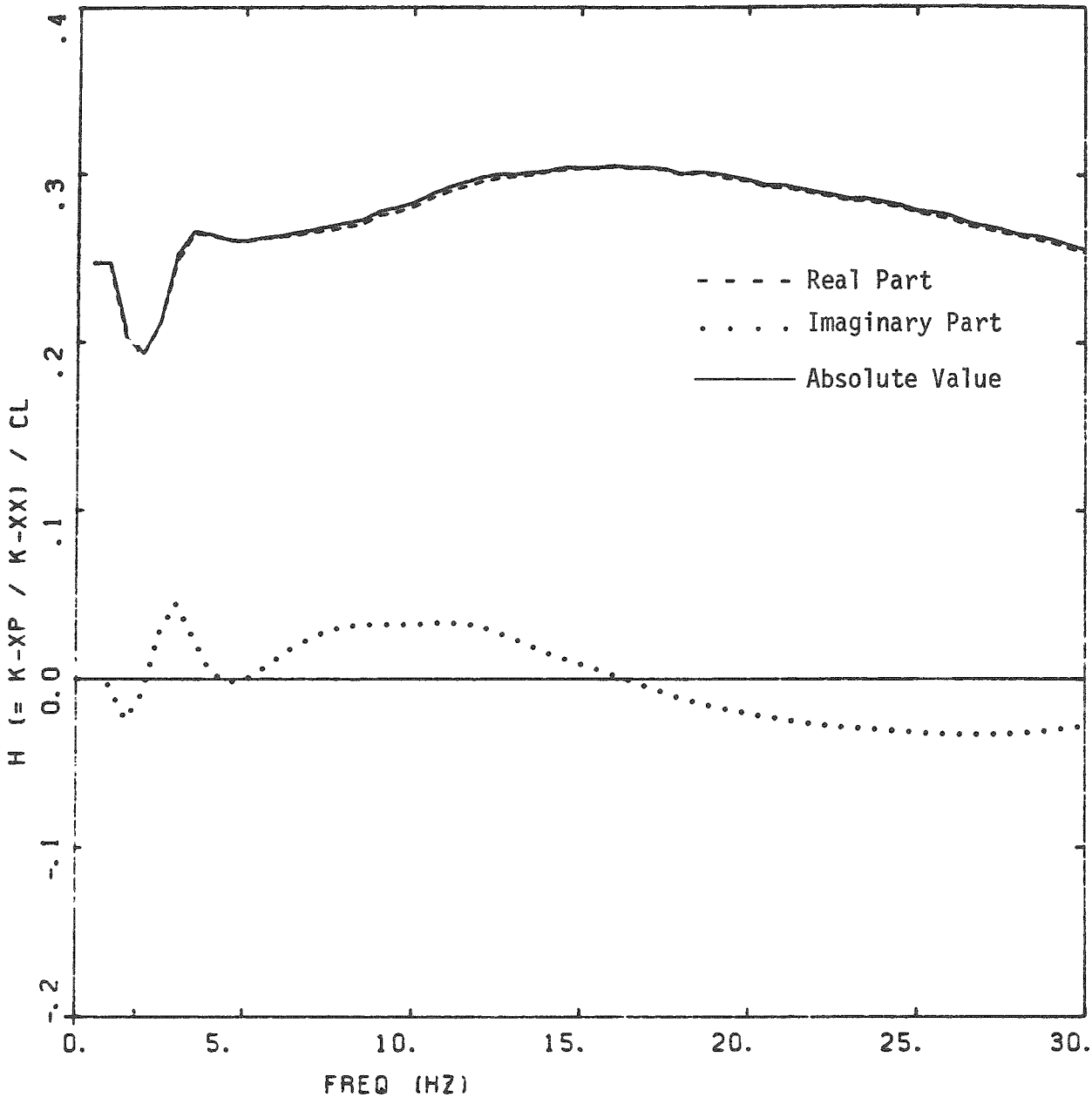

FIGURE A-5. VARIATION OF HEIGHT OF CENTER OF FOUNDATION STIFFNESS, H, WITH FREQUENCY, INTERMEDIATE SOIL PROFILE

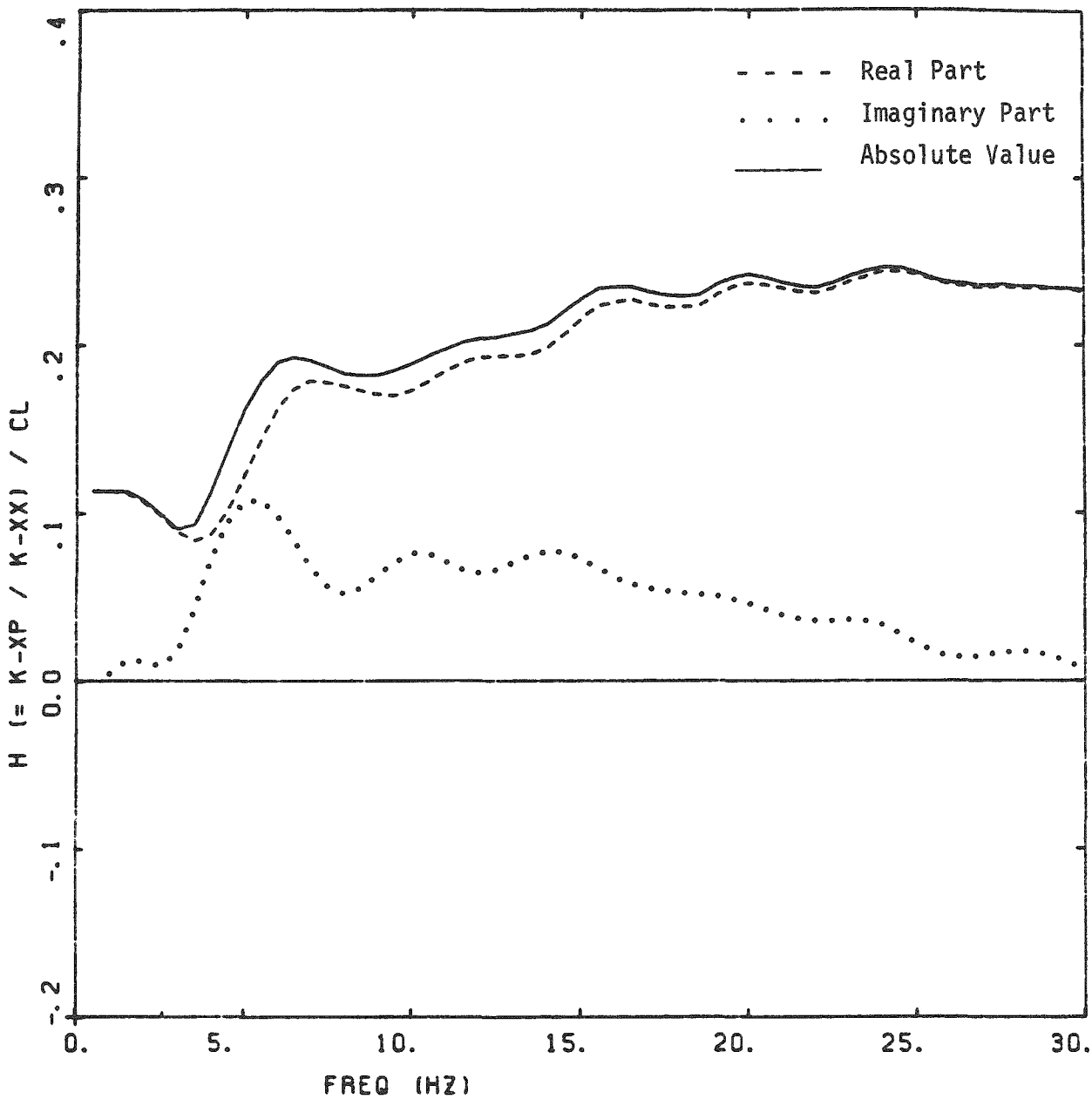

FIGURE A-6. VARIATION OF HEIGHT OF CENTER OF FOUNDATION STIFFNESS, H, WITH FREQUENCY, STIFF SOIL PROFILE

REFERENCES

A-1 Wong, H. L. and Luco, J. E., "Soil Structure Interaction: A Linear Continuum Mechanics Approach (CLASSI)", Report, CE, Department of Civil Engineering, University of Southern California, Los Angeles, California, 1980.

A-2 Powell, G. H., "DRAIN-2D Users Guide", University of California, Berkeley, California, August, 1975.